AN IMPROVED CONTROL STRATEGY FOR A HYBRID SERIES COMPENSATOR

KANNAN KARTHIK

INFORMATION TO USERS

This manuscript has been reproduced from the microfilm master. UMI films the text directly from the original or copy submitted. Thus, some thesis and dissertation copies are in typewriter face, while others may be from any type of computer printer.

The quality of this reproduction is dependent upon the quality of the copy submitted. Broken or indistinct print, colored or poor quality illustrations and photographs, print bleedthrough, substandard margins, and improper alignment can adversely affect reproduction.

In the unlikely event that the author did not send UMI a complete manuscript and there are missing pages, these will be noted. Also, if unauthorized copyright material had to be removed, a note will indicate the deletion.

Oversize materials (e.g., maps, drawings, charts) are reproduced by sectioning the original, beginning at the upper left-hand corner and continuing from left to right in equal sections with small overlaps.

Photographs included in the original manuscript have been reproduced xerographically in this copy. Higher quality 6" x 9" black and white photographic prints are available for any photographs or illustrations appearing in this copy for an additional charge. Contact UMI directly to order.

ProQuest Information and Learning
300 North Zeeb Road, Ann Arbor, MI 48106-1346 USA
800-521-0600

An Improved Control Strategy for a Hybrid Series Compensator

By

© Kannan Karthik, B.E. (Hons.)

A thesis submitted to the School of Graduate
Studies in partial fulfillment of the
Requirements for the degree of
Masters of Engineering

Faculty of Engineering and Applied Science
Memorial University of Newfoundland
July 2001

St.Johns Newfoundland Canada

Abstract

This thesis presents an improved control strategy to ameliorate the load voltage and supply current profiles in a power system. A synchronous d-q-0 based control scheme is developed for a hybrid series compensator topology to cancel the zero, negative and harmonic components from the load voltage and also suppress the supply current harmonics.

The proposed d-q-0 based control scheme combines the decoupling of the current and voltage variables, transformation and filtering to extract the harmonic voltages and currents. In the harmonic current extraction procedure, the zero sequence components (including the fundamental frequency) are removed before applying the required transformations to filter out the harmonics from the supply current. This is done to ensure that the zero sequence components do not produce alternating components in the synchronous frame, which lead to errors in the filtered output. This control approach was developed as an improvement over the instantaneous active and reactive power (IRP) theory based scheme, which assumes a balanced and sinusoidal supply voltage. It is shown that the IRP theory based harmonic extraction procedure does not provide an accurate estimate of the supply current harmonics in the presence of imbalance, voltage distortion and zero sequence components.

The feed-forward control approach based on the synchronous transformations in the d-q-0 frame is susceptible to gain variations which affect both system stability

and the compensation error. Hence, a simplified single phase harmonic equivalent model is developed to carry out stability and distortion analysis of the hybrid series compensator topology. The effect of the controller gain parameters K_V and R_h on the stability limits is investigated with some root-locus plots. The influence of the controller gain parameters on the distortion levels in the load voltage and supply current is examined through a distortion analysis. From the analysis it is shown that limited controller gain margin is one of the drawbacks of the hybrid single-series compensator topology. Moreover, stability constraints on the values of the control parameters limit the range of compensation for wide variations in the supply voltage and load harmonics.

A two-compensator topology is proposed to reduce the interaction between the voltage and current signals by allowing independent control of the two voltage components, thereby increasing the stability limits. A much larger controller gain margin (hence larger compensation range) and suppression of voltage drop across the passive shunt filter are shown to be some of the advantages of the proposed topology.

A simulation model of the overall system with the proposed two-compensator topology is constructed using the SIMULINK toolboxes in MATLAB. The simulation results are used to demonstrate the effectiveness of the proposed d-q-0 based control scheme and the two-compensator topology when applied to load voltage compensation and harmonic isolation of non-linear loads.

Acknowledgements

I would like to thank my supervisor Dr. J. E. Quaicoe for his invaluable guidance, constant understanding, financial support and help in preparing this manuscript. I would also like to extend my sincere thanks to Dr. M. Ramamoorty, Director of Electrical Research and Development Association (ERDA) for his valuable suggestions and insightful comments on our research work.

Appreciation is extended to Dr. R. Seshadri, Dean of the Faculty of Engineering and Applied Science and Dr. M. Haddara, Associate Dean of Engineering for their support during the overall course of my study in Canada. I would like to extend my acknowledgement to Ms. M. Crocker, secretary of the Associate Dean's office for ensuring smooth and efficient operation of the associated administrative tasks of my graduate program. I am also thankful to Messrs Philip van Ulden, T. Pike, D. Guy and D. Johnson for their timely help during the course of the program. In anticipation of any oversight that remains, I wish to thank all those who contributed directly or indirectly to this work.

Finally, I would also like to express my profound gratitude to my parents for their constant encouragement, understanding, guidance and support. I am also grateful to my fellow graduate students for their friendship during my study at Memorial University.

Contents

List of Figures

List of Tables

List of Symbols and Acronyms

a, b, c	Three-phase co-ordinates (first-mention in pg. 9)
α, β	Stationary two co-ordinate system (pg. 31)
e_a, e_b, e_c	Set of three phase voltages (pg. 31)
e_α, e_β	Corresponding α-β co-ordinates of e_a, e_b, e_c (pg. 31)
i_a, i_b, i_c	Set of three phase currents (pg. 31)
i_α, i_β	Corresponding α-β co-ordinates of i_a, i_b, i_c (pg. 31)
p, q	Instantaneous active and reactive powers (pg. 34)
$\overline{p}$, $\overline{q}$	Mean values of instantaneous active and reactive powers (pg. 34)
$\tilde{p}$, $\tilde{q}$	Alternating components of p and q (pg. 34)
p_H, q_H	Contributions to p and q from harmonics(pg. 35)
p_{DC}, q_{DC}	DC components of p and q (pg. 35)
d, q, 0	Synchronously, rotating co-ordinate system (pg. 53)
V_S	Supply voltage
V_{S_h}	Harmonic component of the supply voltage (pg. 94)
i_S	Supply current
i_{S_h}	Harmonic component of supply current (pg. 18)
i_C	Compensator current (pg. 11)
i_{C_h}	Harmonic component of the compensator current (pg. 18)
i_L	Load current
i_{L_h}	Harmonic component of the load current (pg. 11)

V_L	Load voltage (pg. 11)
V_{L_h}	Harmonic component of the load voltage (pg. 96)
ϕ	Power factor angle (pg. 31)
Z_F	Impedance of the shunt passive filter (pg. 97)
Z_t	Line impedance (pg. 96)
Z_L	Load impedance (pg. 96)
R_h	Gain of the harmonic extraction unit (pg. 56)
K_V	Gain of the voltage compensation unit (pg. 56)
$K_{C_{crit}}$	Maximum value of K_V for a stable system
THD_i	Total harmonic distortion in the current
THD_V	Total harmonic distortion in the voltage
V_{F_a}, V_{F_b}, V_{F_c}	Phase voltages at the supply end (pg. 57)
V_{F_α}, V_{F_β}, V_{F_0}	Phase voltages in the α, β and zero co-ordinate system (pg. 57)
V_{F_d}, V_{F_q}, V_{F_0}	Phase voltages in the synchronous d-q-0 frame (pg. 57)
$V_{d_{ref}}$, $V_{q_{ref}}$, $V_{0_{ref}}$	Reference voltages for positive sequence d, q, zero components (pg. 58)
$T_{a-\alpha}$	Transformation matrix: (a-b-c) to (0-α-β) (pg. 57)
$T_{\alpha-d}$	Transformation matrix:(0-α-β) to (0-d-q) (pg. 58)
$T_{d-\alpha}$	Transformation matrix: (0-d-q) to (0-α-β) (pg. 59)
$T_{\alpha-a}$	Transformation matrix: (0-α-β) to (a-b-c) (pg. 59)
KVA_C	KVA rating of the single compensator topology (pg. 111)
KVA_{C1}	KVA rating of the harmonic isolator (pg. 133)
KVA_{C2}	KVA rating of the voltage compensator (pg. 133)

KVL	Kirchoffs voltage law (pg. 96)
CBEMA	Computing Business Equipment Manufacturers Association (pg. 109)
HDF	Harmonic distribution factor (pg. 102)
MA	Moving average (pg. 62)
FIR	Finite impulse response (pg. 62)
THD	Total harmonic distortion (pg. 104)
PLL	Phase locked loop (pg. 55)
PWM	Pulse width modulator (pg. 97)

Chapter 1

Introduction

Growing demands made by the industry on power quality (PQ), as well as the quality diversification imposed by deregulation, point to a need for additional devices that prevent critical loads from failing and causing system downtime. Many automated production line industries cannot tolerate loss of power for even a few tens of milliseconds. This provided the motivation to develop custom power quality control devices to shield the critical loads from the vagaries of nonlinear loads such as arc furnaces and adjustable speed drives (ASDs).

In this chapter a detailed literature review of various power quality problems, custom power devices(CPDs), their topologies, as well as an overview of the underlying control principles are presented. Based on the structure, the CPDs are classified as shunt, series, unified power quality conditioners and hybrid compensators. The hybrid topology is well established as a cost-effective solution to problems concerning load voltage profile and supply current distortion. This topology is discussed in more detail in this and the following chapters. The literature review sets the tone for defin-

ing the objectives of this research and also the detailed control circuit and topological analysis that will follow in the next four chapters.

1.1 Factors Affecting Power Quality

Solid state control of ac power using thyristors and other semiconductor devices is widely employed to feed controlled electric power to electrical loads, such as adjustable speed drives (ASDs), electric arc furnaces and computer power supplies. Since these solid-state converters behave as nonlinear loads, they draw harmonic and reactive currents from the ac mains. In three-phase systems, these nonlinear loads cause imbalance and excessive neutral currents. The excessive harmonics and reactive currents and imbalance in voltages and currents decrease the system efficiency and also reduce the power factor. Other effects of harmonics include winding losses in motors, torque pulsations, load voltage distortion and over-registration of energy meters. Highly reactive loads and single-phase faults cause voltage sags and imbalance. Some of the significant waveform distortions associated with poor power quality are shown in Fig. 1.1.

Voltage sags or swells are a short duration decrease or increase in the voltage magnitude. The typical duration of a sag is between 3 and 30 cycles. Sags or swells lasting more than 2 minutes are classified as under-voltages and over-voltages respectively. In voltage flicker, the amplitude of the voltage is modulated at frequencies less than 25Hz. Flicker is caused by large, rapidly fluctuating loads such as arc furnaces

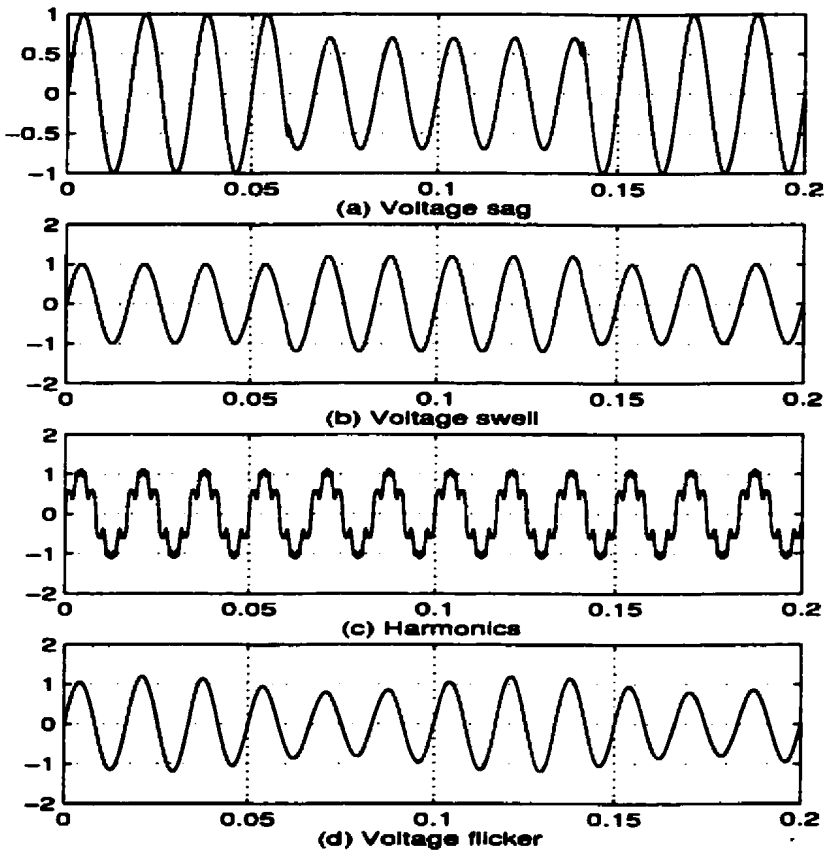

Figure 1.1: The most significant waveform distortions associated with poor power quality

and electric welders.

The influence of such disturbances at the terminals of a load depends on the distance to the origin of the disturbance and the level of interconnection and impedance of the transmission line links. Single-phase to ground, three-phase to ground faults and switching operations such as connection and disconnection of large loads affect the terminal load voltage at certain critical loads. The increased severity of sags, swells and harmonic pollution in power networks has motivated power engineers to develop dynamic and adjustable solutions to power quality problems. Amongst the most severe disturbances endangering power quality are voltage dips and transient power supply interruptions [1].

Power quality is quantified technically on the basis of the following criteria [2]:

- Constant sine-wave shape: no harmonics
- Constant frequency: unchanged nominal value
- Symmetrical three-phase AC power system: three phase voltages with phases shifted by 120°.
- Constant rms value: nominal power system voltage value unchanged over time.
- Fixed voltage: power system voltage unaffected by load changes.
- Reliability: energy in required amounts available at all times.

The following sections discuss some of the custom power quality solutions developed to achieve the above criteria.

1.2 State-of-the-art Custom Power Quality Solutions

Various custom power conditioning devices(CPDs) are widely employed to mitigate the effects of load current harmonics, voltage sags and distortion. Tuned shunt passive filters consisting of LC filters and/or high pass filters were traditionally used to improve the power factor and absorb the harmonics in the power systems. Active filters (as power conditioning devices) have been researched for the past 25-30 years to compensate for harmonics, reactive power, and/or neutral current in ac networks [3], [4], [5]. Active filters are also used to eliminate voltage harmonics, regulate terminal load voltage and to improve voltage balance in the three-phase systems. These objectives are either achieved individually or in combination with one or more compensation devices, depending on the requirements, control strategy and configuration [5].

Custom power quality devices can be classified as shunt compensators, series compensators, combination of series and shunt compensators (referred to as unified power controllers(UPC)) or hybrid compensators.

1.2.1 Shunt compensators

Shunt compensators are used to suppress current harmonics and to provide reactive power compensation and the balancing of unbalanced currents [6], [7]. Shunt compensators used to regulate voltage, control the power factor and stabilize power flow have also been described in the literature [8], [9]. Shunt compensators may be of the active or passive type.

1. Shunt passive filters

Shunt passive filters, primarily due to their simplicity, low cost and high efficiency [10], have traditionally been used to absorb the harmonics generated by large harmonic loads.

The circuit diagram of the shunt passive filter is shown in Fig. 1.2, while Fig. 1.3 shows the corresponding simplified single-phase equivalent model. The nonlinear load is modeled by a harmonic current source in parallel with a linear load. Although not very realistic, the single-phase circuit gives a fair idea of the usefulness of the topology and the control algorithm, and it provides a simple model for carrying out the dynamic response analysis and stability analysis.

The shunt passive filter exhibits a lower impedance than the source impedance at tuned harmonic frequencies to reduce the harmonic currents flowing into the source. In principle, the filtering characteristics of the shunt passive filter are determined by the impedance ratio of the source and shunt passive filter. The shunt passive filter

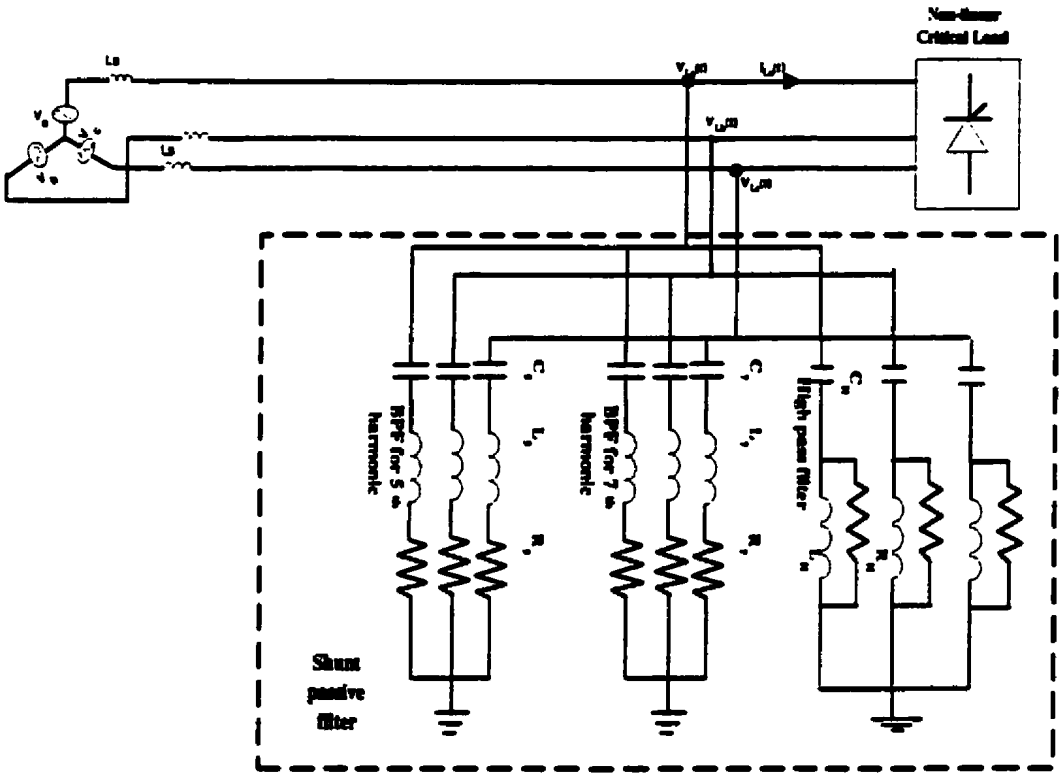

Figure 1.2: System configuration of the shunt passive filter [5]

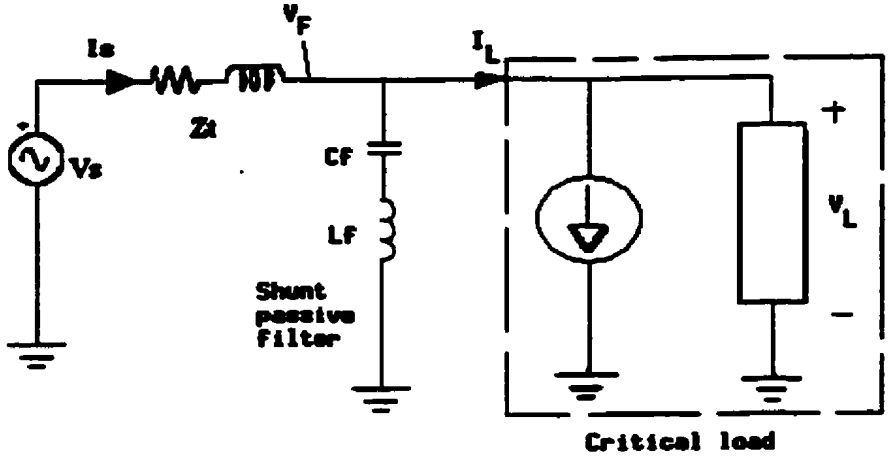

Figure 1.3: Simplified model of the shunt passive filter

has the following drawbacks:

1. The supply impedance strongly influences the compensation characteristics of the passive filter.

2. The filter is highly susceptible to series and parallel resonance with the supply impedance. It is also sensitive to L-C component tolerances. The parallel resonance between the filter and supply impedance results in a harmonic amplifying phenomenon [10].

3. Tuned passive filters have the caveat of attracting harmonic currents from ambient loads and are susceptible to load and line switching transients. Hence passive filters are generally off-tuned with respect to dominant frequencies which defeats their very purpose of installation [11].

To overcome the drawbacks of shunt passive filters, shunt active filters were developed to provide smooth power factor and harmonic current control.

2. Shunt active filters

Shunt active filters are used to eliminate current harmonics, provide reactive power compensation and balance unbalanced currents. Shunt active filters avoid the shortcomings of passive filters by utilizing a switch-mode power electronic inverter to supply the harmonic currents equal to those in the load current. Since the load current harmonics are measured and then supplied by the current-regulated inverter

of the active filter, the performance of the filter is independent of the utility system impedance. The shunt active filter behaves essentially as a harmonic current source. Hence it is not susceptible to resonance at dominant harmonic frequencies.

The shunt active filter can also be used as a static var generator in a power system network for stabilizing and improving the voltage profile. The shunt current injection scheme is suitable for the compensation of voltage fluctuations caused by high reactive current loads such as arc-furnace loads and large motors at startup. In this application mode, the shunt active filter is referred to as a static synchronous condenser (STATCON) [12].

Fig. 1.4 shows an example of a shunt active filter with a neutral wire, which is able to compensate for both current harmonics and power factor. Furthermore, it allows load balancing, eliminating the current in the neutral wire. The power stage which is, basically, a voltage source inverter with only a single capacitor in the DC-side, is controlled as a current source. From the measured values of the phase voltages (V_a, V_b, V_c) and load currents (i_a, i_b, i_c), the controller calculates the reference currents required by the inverter to produce the compensation currents $(i_{ca}, i_{cb}, i_{cc}, i_{cn})$. A simplified single-phase equivalent circuit model of the shunt active filter system is shown in Fig. 1.5 with the shunt filter represented by a controllable current source.

The control strategies employed to generate compensation commands are based on time-domain or frequency-domain correction techniques [5]. Some of the commonly

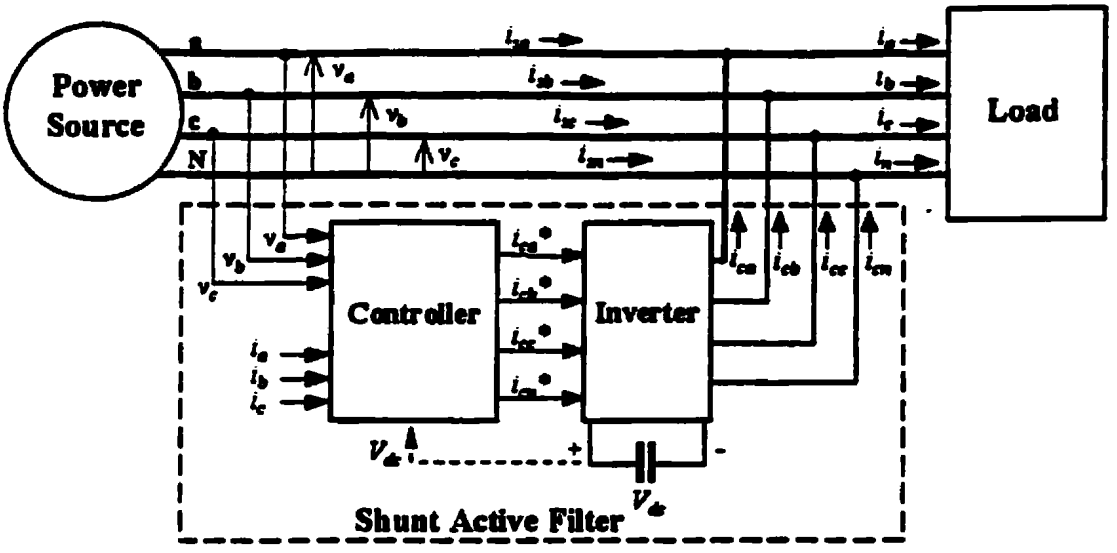

Figure 1.4: System configuration of the shunt active filter [3]

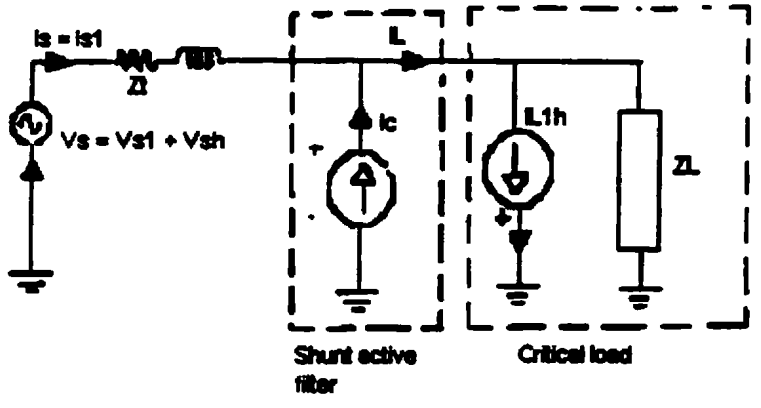

Figure 1.5: Simplified model of the shunt active filter

used control methods for deriving the compensating signals are the instantaneous p-q theory or instantaneous reactive power (IRP) theory [4] and the synchronous d-q reference frame method [11],[12]. Every control scheme has a rudimentary compensation equation which defines its objective. Further, the choice of control strategy such as the d-q or the IRP approach depends on the control objective (e.g. voltage regulation, VAR compensation), the type of controlled parameter (e.g. bus voltage, supply current or real/reactive power) and the controlling parameter (e.g. compensator voltage or current). For instance, to cancel the harmonics in the load current, the shunt active filter is modulated as a harmonic current source, which is forced to track a reference current given by

$$i_C^* = i_{L_h} \tag{1.1}$$

However, if the priority is to regulate and balance the bus voltage, the inverter is controlled as a voltage source. The compensation equation then becomes

$$V_C^* = K_V \cdot (V_L^* - V_F) + V_F \tag{1.2}$$

where K_V is the proportional gain and V_L^* is the nominal load voltage. Finally, to calculate the reference values of the current or voltage, a suitable method based on d-q transformation or IRP theory and filtering may be used. The drawbacks of the shunt active filter can be summarized as follows:

1. Since the device is connected in parallel to the load, the VA rating of the power electronics converter in these active filters is very large because the converter

must withstand the line-frequency utility voltage and supply the harmonic currents. Associated with this large VA rating is higher cost, high electromagnetic interference(EMI), high power losses and hence lower efficiency.

2. The inverter output LC filters provide attenuation of the inverter switching harmonics. However, they are highly susceptible to utility line interactions and require additional active or passive damping.

3. As the short circuit current at the point of common coupling increases, the influence on the phase voltages, which is possible with current injection, decreases. Thus, in such systems, the shunt compensators are less effective for voltage stabilization.

Due to the above drawbacks, series compensators became a preferred choice for improving the load voltage profile.

1.2.2 Series Compensators

The series compensator, which is the dual of the shunt compensator, is used to eliminate voltage harmonics, compensate for voltage dips and swells and regulate the voltage on three-phase systems. It is connected in series with the load between the mains and the load using a matching transformer. It can also be installed by electric utilities to damp out harmonic propagation caused by resonance with line impedance and passive shunt compensators. The basic schematic of a stand-alone series com-

pensator is shown in Fig. 1.6. The simplified model of the series compensator is a controllable voltage source which can inject any voltage waveform into the line to control the bus voltage profile and stem harmonic current flow. This circuit is shown in Fig. 1.7.

The compensator consists of a voltage source inverter operated as a controlled voltage source, which is interfaced with the power system through three single-phase transformers. The series active filter does not compensate for load current harmonics but it acts as a high impedance to the current harmonics from nonlinear loads. When the primary function of the series compensator is load voltage regulation, it is sometimes referred to as the dynamic voltage restorer (DVR) [13]. The voltage compensation equation for the output of the series compensator is given by

$$V_C^* = V_F - V_L^* \tag{1.3}$$

Unlike the shunt compensator, the series compensator is partially rated with respect to the load. Hence the series compensator would be a better choice for voltage regulation due to its relatively lower cost. Some of the drawbacks of the series compensator include its inability to compensate entirely for load current harmonics, suppress neutral currents and balance the load currents.

1.2.3 Unified power quality conditioner

The unified power quality conditioner (UPQC) is a combination of a series compensator and a shunt active filter [14], [15]. If the power conditioner is used for

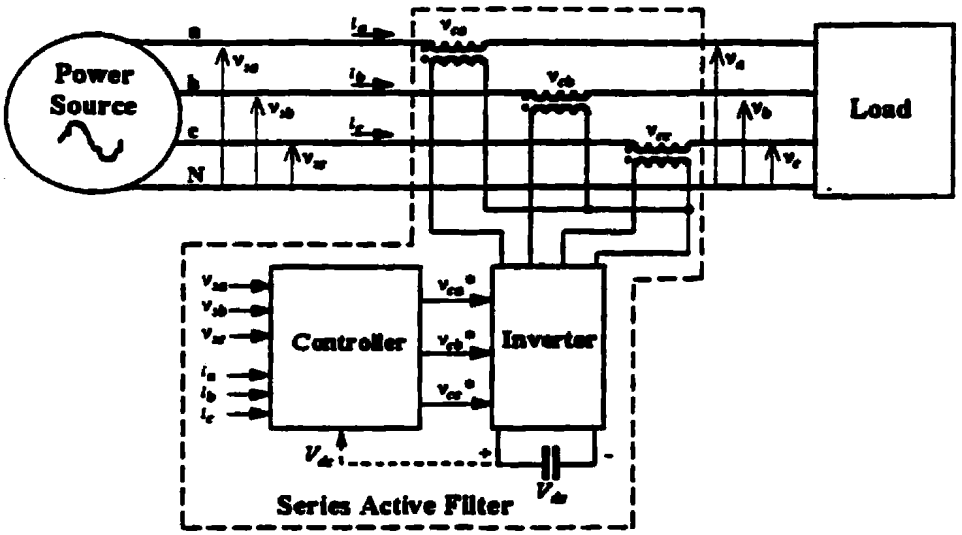

Figure 1.6: System configuration of the series compensator [3]

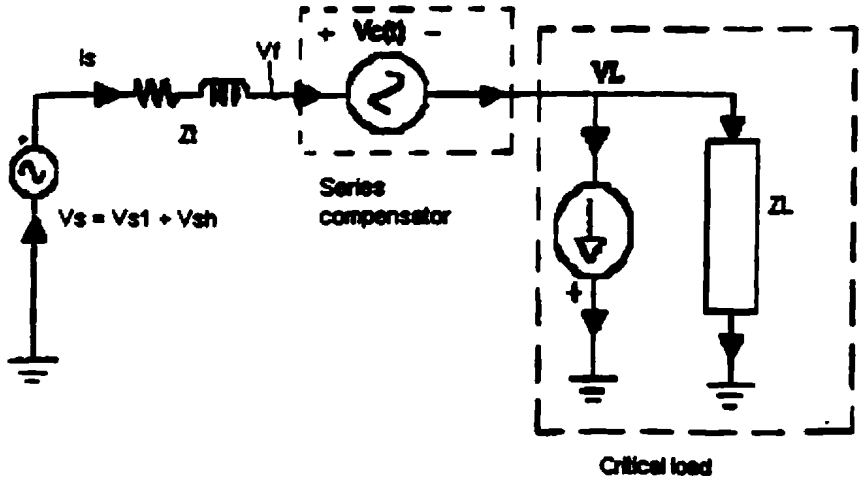

Figure 1.7: Simplified model of the series active filter

fundamental power compensation such as power flow control, the device is called the unified power flow controller (UPFC). The dc link storage element (either inductor or dc bus capacitor) is shared between two current source or voltage source bridges operating as active series and active shunt compensators. The UPQC system can provide fast and simultaneous control of the system terminal voltage and active/reactive power flow. The system is considered as an ideal active filter which eliminates voltage and current harmonics and is capable of providing clean power to critical and harmonic-prone loads such as computers and medical equipment. Figure 1.8 shows the diagram of the UPQC and a simplified circuit model of the same is presented in Fig. 1.9. The series device acts as a controllable voltage source V_C, whereas the shunt device acts as a controllable current source I_C. The UPQC has the cumulative advantages of both the series and shunt compensators.

The shunt device may be controlled to serve the following functions:

1. Regulate the dc link voltage(V_{dc}) by adjusting the amount of active power drawn from the transmission line.

2. Compensate the reactive power of the load.

3. Compensate for line current harmonics, negative and zero sequence components at the fundamental frequency.

Some of the possible functions of the series device are as follows:

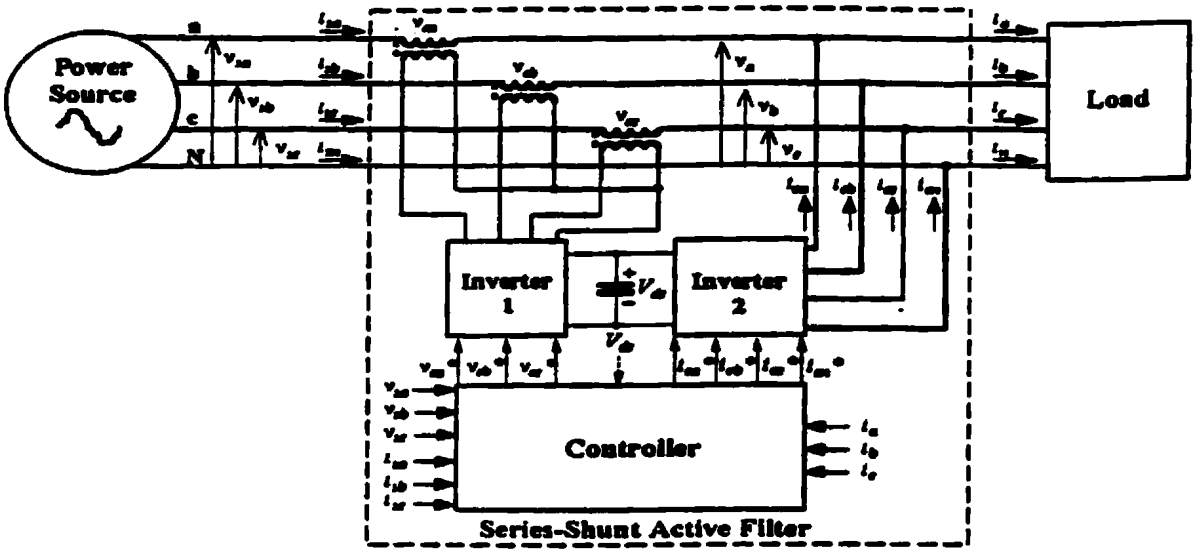

Figure 1.8: System configuration of the unified power quality conditioner [3]

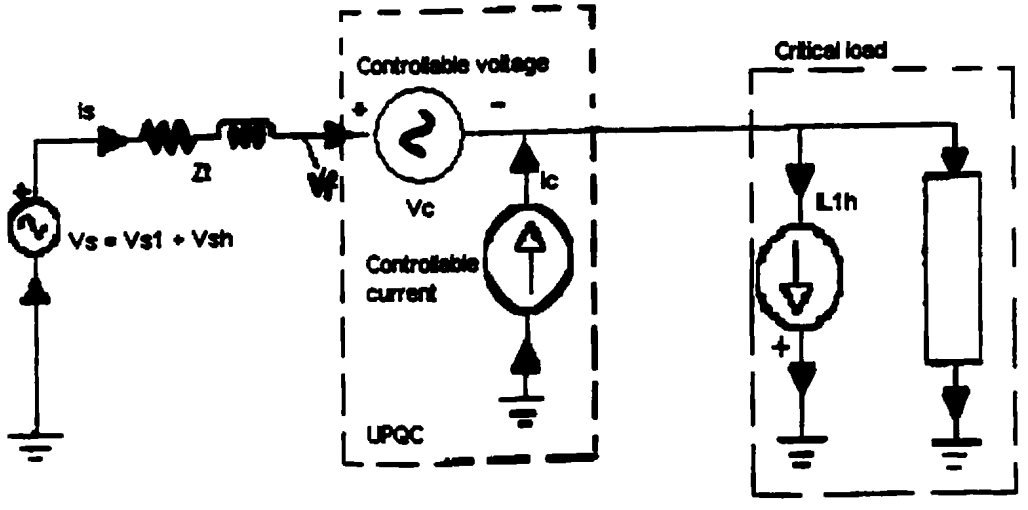

Figure 1.9: Simplified model of the UPQC

1. Compensate for voltage harmonics - including negative and zero sequence components at the fundamental frequency.

2. Suppress the harmonic currents through the power line i.e. provide harmonic isolation.

3. Improve the system stability.

4. Control the active and reactive power flow by controlling the phase and magnitude of the injected voltage with respect to the line current.

One of its main drawbacks is its high cost, low efficiency and control complexity because of the large number of solid state devices involved.

1.2.4 Hybrid filters

Combinations of active series and passive shunt filtering [10],[11],[16] and shunt active and shunt passive filtering [17] are known as hybrid filters. It is a cost-effective solution to voltage distortion and current harmonic suppression. Two hybrid topologies that provide effective solutions to problems concerning both load voltage profile and line and load current harmonics are discussed below.

1. Hybrid shunt filters

Shunt active filters have a high VA rating since the converter has to be rated for the utility voltage. Attempts to reduce the rating of the shunt compensator without compromising its functionality have been proposed in the literature [17]. The line

diagram and the corresponding model of the hybrid shunt topology are shown in Figs 1.10 and 1.11, respectively.

In order to reduce the VA rating of the converter, the fundamental component of the converter current is controlled such that the supply frequency voltage is dropped across the passive filter impedance Z_F. The two equations that influence the operation of the hybrid-shunt filter are:

1. For harmonic cancellation (for sinusoidal supply current,$I_{S_h} = 0$) which means

$$i_{C_h} = i_{L_h}. \tag{1.4}$$

2. The amplitude of the fundamental component of the converter current is controlled so that ($V_{C_1} \approx 0$). Thus

$$V_{F_1} = I_{C_1} * Z_{F_1} = V_{S_1} \tag{1.5}$$

The hybrid shunt filter may not be effective as a VAR compensator due to the high impedance of the passive filter at the fundamental frequency. In such a case, a tradeoff between the voltage rating of the inverter and the range of VAR compensation would be necessary. The hybrid-shunt incurs the same drawbacks as the shunt-active filter with respect to controlling (stabilizing) the bus voltage.

2. The hybrid series compensator

The hybrid series compensator, which comprises a series active and shunt passive filter, is used for terminal voltage regulation, balancing of load voltages and

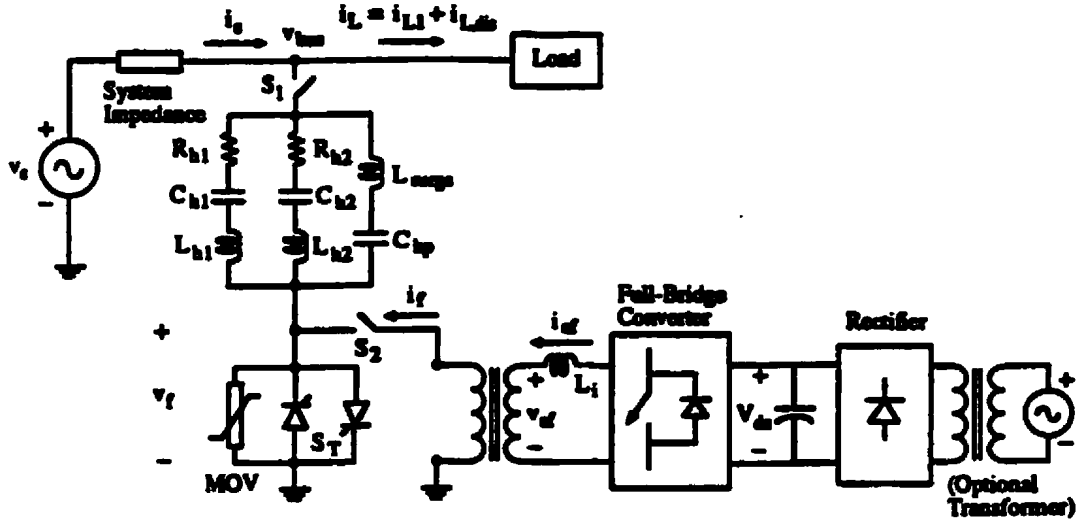

Figure 1.10: System configuration of the hybrid shunt filter [17]

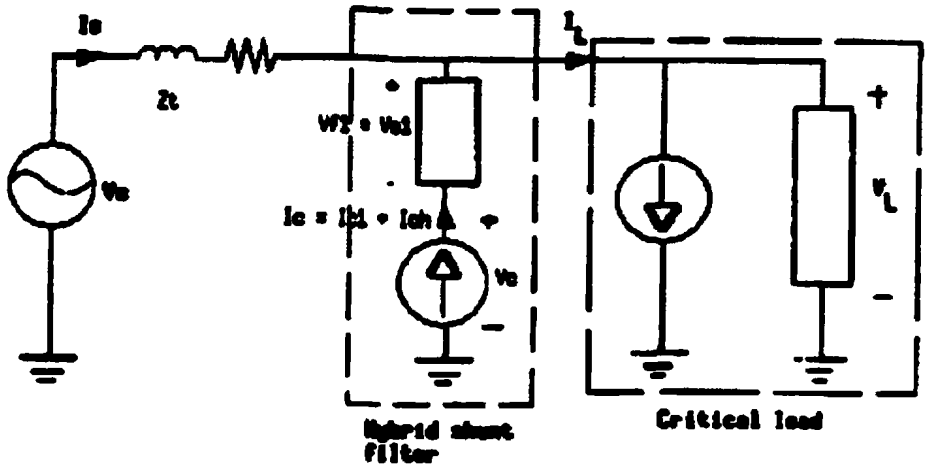

Figure 1.11: Model of the hybrid shunt filter

suppression of line current harmonics.

The system configuration for the hybrid series topology scheme as proposed by Peng et al. [10] is shown in Fig. 1.12. The three-phase hybrid series compensator comprises three single-phase voltage source inverters (labeled A,B,C). An L-C filter at the output of the single-phase inverter is used to filter out the high frequency components in the output voltage of the inverter. The very purpose of using three single-phase inverters is to provide independent phase control. A series transformer is used to match the inverter voltage with the voltage required at the secondary. The single-phase equivalent circuit of the power system is shown in Fig. 1.13. By injecting a voltage in phase with the harmonic component of the supply current, the series compensator simulates a high series resistance. Since the shunt filter has a much lower impedance to harmonics, the load harmonics flow through the shunt filter, thereby isolating the supply and the load. The compensation equation is given by

$$V_C^* = R_h \cdot i_{S_h} \tag{1.6}$$

where, R_h is a constant multiplier that determines the magnitude of the effective (fictitious) resistor. R_h can be made arbitrarily high so as to ensure complete isolation. In this case the series compensator is controlled as a sinusoidal current source [16]. This method of control rids the supply current of any harmonics by bypassing the higher frequencies through the passive shunt filter [11], [16]. However, the method is

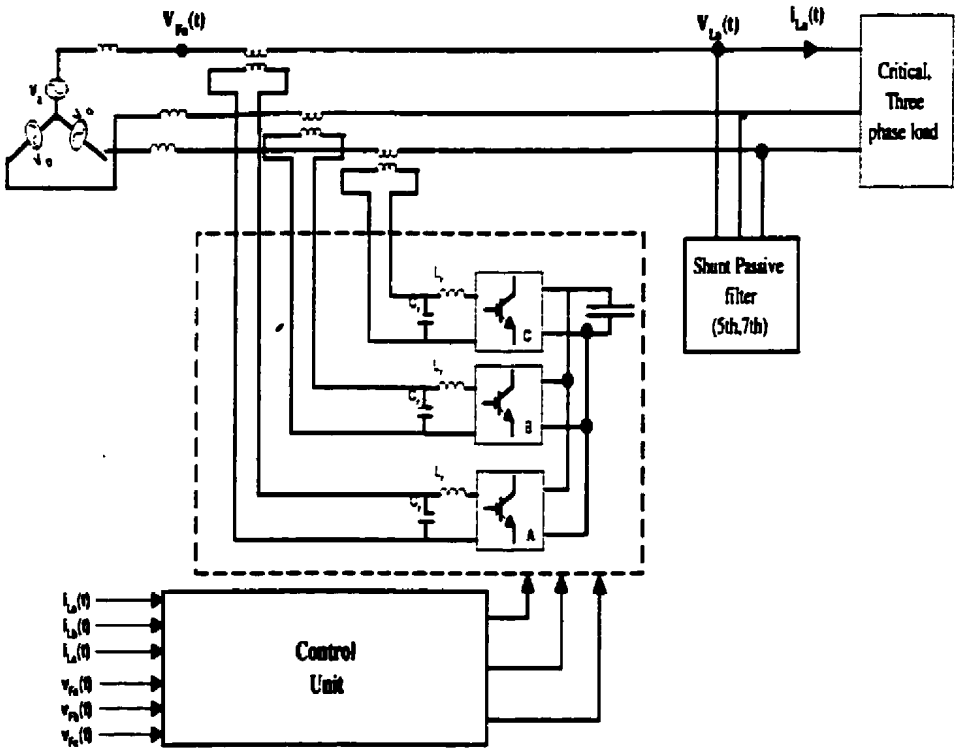

Figure 1.12: System configuration of the hybrid series compensator [10]

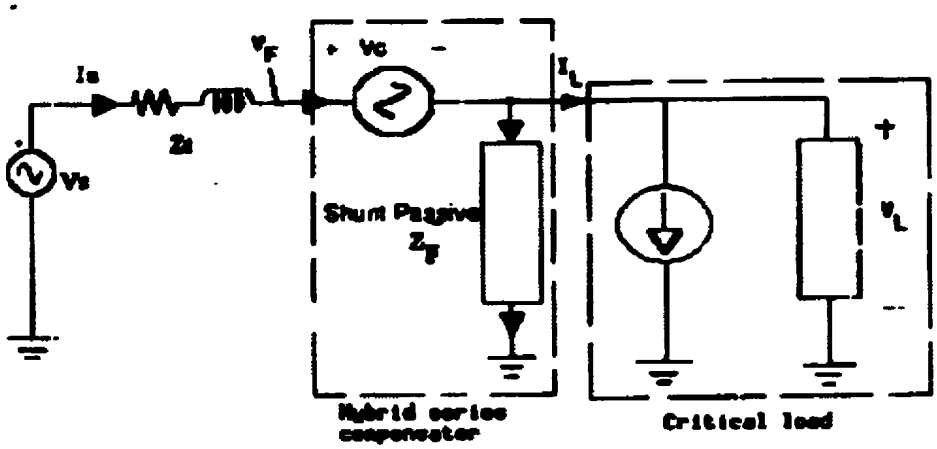

Figure 1.13: Simplified model of the hybrid series compensator

based on the feedback compensation concept which ensures zero steady-state error. However, it does not have as fast a dynamic response as the feed-forward approach. By using a finite value of R_h, the mode of control may be transformed from a feedback type to a feed-forward type.

For effective compensation of voltage sags, swells, flickering, current harmonics, unbalanced loads, and load voltage distortion, the hybrid series compensator is required to perform two major functions,

1. Harmonic isolation: By injecting a harmonic voltage in phase with the harmonic component of the load current, the series compensator behaves as an active impedance in series with the ac source. This active impedance does not cause any appreciable fundamental voltage drop. Rather it serves to constrain all the load current harmonics into the passive filters. It also prevents other nonlinear loads from flooding the critical load with their non-sinusoidal currents. The harmonic isolation feature reduces the need for having precise tuning of the passive filters. This is because the active resistance provides good damping to any resonant current oscillations which may occur between the passive filter and the supply impedance. Thus, the series compensator allows the passive filters to be exactly tuned to the dominant current harmonics thereby improving the compensation characteristics of the passive filter.

2. Voltage compensation: A component of the voltage is injected in series with

the load to eliminate any zero-sequence or harmonic components in the supply voltage and to correct sags and swells.

In order to meet the above requirements, the voltage injected by the compensator can now be expressed as an algebraic sum of two components: a voltage V_{C_1}, which is proportional to the voltage at the supply end of the compensator and a voltage V_{C_2}, which is proportional to the current through the compensator. The basic compensating equation (1.6) can thus be modified and rewritten as

$$V_C^* = V_{C_1} + V_{C_2} = K_v \cdot (V_F - V_L^*) + R_h \cdot i_{S_h} \tag{1.7}$$

V_F represents the voltage at the supply end of the compensator, I_{S_h} represents the harmonic component of the supply (or compensator) current and V_L^* is the nominal load voltage. This modification in the compensation principle, while effective to counter voltage dips and swells, poses some stability constraints on the gains.

Equation (1.7) suggests a need for a precise estimation of I_{S_h}. Akagi et al. [4] proposed a harmonic extraction method based on IRP theory. However, this method fails to provide a good estimate of the harmonic content under unbalanced conditions in the presence of zero sequence components and supply voltage distortion.

The effectiveness of the topologies discussed above in addressing power quality problems are summarized in Table 1.1. The number of stars (scale of 3) indicate the level of preference for a particular topology. The UPQC because of its high cost is selected only for highly polluted environments and only when power flow control

has to be incorporated. It can be seen from the chart that for a combination of problems such as sags, swells, flicker and voltage distortion i.e. row I), the hybrid series compensator is preferred over the UPQC because of its cost-effectiveness. More in depth study of the hybrid series compensator topology is presented in Chapters 4 and 5.

Table 1.1: Summary of compensators and their effectiveness

Problems	Shunt active	Series active	UPQC	Hybrid series active
A) Current harmonics	**		*	*
B) Reactive power	***		*	*
C) Load balancing	*		*	
D) Voltage regulation	*	***	*	**
E) Voltage harmonics			*	**
F) Voltage sags		***	*	**
G) Voltage flicker	***	**	*	**
H) Voltage balancing		***	*	**
I) A + E + F + G			*	**

1.3 Objectives of the thesis

The hybrid topology in general provides a cost-effective solution to voltage compensation and harmonic current suppression since the combined cost of the series compensator and the shunt passive filter is less than the cost of using a shunt active filter alone. The topology is therefore selected for detailed study in this thesis. The goal of the research is to develop a compensation approach that effectively corrects voltage sags, swells, flickering, current harmonics, unbalanced loads and voltage distortion.

To this end the following investigations are undertaken in this research.

1. Development of a robust and more simple harmonic estimation approach that provides an accurate measure of the harmonics in the presence of imbalance, zero-sequence and supply voltage distortion.

2. Extension the compensation to incorporate both voltage compensation and harmonic isolation, as opposed to using the compensator solely as a harmonic isolator.

3. Stability analysis using an approximate single-phase model of the hybrid series compensator, to determine the influence of the controller gain parameters K_V and R_h on the stability of the overall system and to determine the range of values for which the overall system becomes unstable.

4. Development of a topology to increase the gain margin and effectiveness of compensation.

5. Quantitative comparison of the two topologies based on certain key parameters such as compensator ratings, percentage reduction in load voltage distortion, degree of harmonic isolation, compensation error and gain margin.

1.4 Organization of the thesis

Chapter 1 presents the existing power-quality scenario and some custom PQ solutions to critical problems concerning load voltage profile and line current distortion. The custom power devices are classified by their topology with particular interest in the hybrid-series topology due to its flexibility and cost-effectiveness. The objectives and the organization of this thesis are presented in this chapter.

An outline of the control scheme proposed by Peng, et al. [10] is presented in Chapter 2. The IRP theory on which the control scheme is based, is described in detail. The drawbacks of the control scheme in the presence of zero-sequence components and imbalance are highlighted and simulation results are presented to confirm the limitations.

Chapter 3 outlines the development of a new control scheme based on the synchronous d-q-0 transformation. In this scheme, the current and voltage signals are decoupled, to prevent their mutual interaction from affecting the calculation of the reference signals. In order to de-sensitize the effect of unbalanced loading conditions on harmonic extraction, a new current decoupling method is proposed. By deriving a set of balanced currents from each line current, and applying d-q-0 transformation and filtering to each set, the harmonic content of each line current can be precisely determined irrespective of the degree of imbalance. Simulation results are presented in the Chapter to compare the proposed scheme with the IRP based control scheme.

In Chapter 4, the hybrid-series compensator topology is modelled and analyzed. The objective here is to investigate the effect of the controller gain parameters on stability and terminal load voltage distortion. A simplified equivalent circuit is developed to study the effects of the controller gain parameters on the dynamic response and stability of the hybrid-compensator. Finally, it is shown that one of the main drawbacks of applying the single-compensator, hybrid-series topology for both voltage compensation and harmonic isolation is the limited gain margin.

In Chapter 5, a two-compensator topology is proposed to reduce the interaction between the signals from the voltage and current control units thereby increasing the stability range. A quantitative comparison of two topologies is presented by using the load voltage distortion, compensation error, degree of harmonic isolation and compensation ratings as the criteria.

In Chapter 6, a detailed description of the three-phase simulation model is presented. The control scheme accompanying the two-compensator topology is simulated under various loading conditions. Simulation results validating the effectiveness of the proposed scheme and topology are presented in the chapter.

Chapter 7 summarizes the research work. Suggestions are also provided for carrying out future work along the lines of this thesis.

Chapter 2

IRP Based Control Scheme for the Hybrid Series Topology

Introduction

In the previous chapter, the various topologies and their advantages and shortcomings were highlighted. The hybrid topology was described as a cost-effective solution to voltage compensation and harmonic suppression. The control unit that facilitates the harmonic suppression in the voltage and current waveforms is examined in detail in this chapter. This control scheme was first proposed by Peng, et al. [10] in 1990 and is based on the IRP theory.

The principle of operation of the series compensator is discussed along with the IRP theory based scheme. The objective in this chapter is to accentuate the drawbacks of the IRP scheme in order to set the stage for the proposed synchronous d-q-0 based control method discussed in Chapter 3.

2.1 Principle of Operation

As per the scheme proposed by Peng et al. [10], the series active filter is controlled in such a way so as to present zero impedance to the fundamental current and a high impedance to the current harmonics. In this way the series compensator functions primarily as a harmonic isolator, preventing the load harmonics from flowing through the source, and hence improving the supply current and load voltage profile. The reference input for the series filter is described by the equation,

$$V_C^* = R_h \cdot i_{S_h} \tag{2.1}$$

where, i_{S_h} is the harmonic component of the supply current which can be extracted by applying instantaneous real and imaginary power theory [4]. Figure 2.1 shows the system configuration of single compensator topology.

2.2 IRP Theory Based Control Scheme

In 1984, Akagi, et al. [4] proposed the 'Generalized theory of instantaneous reactive power in three phase circuits', also known as instantaneous power theory, or p-q theory. The theory is based on instantaneous voltages and currents in three-phase systems, with or without a neutral wire. The IRP theory is used to determine the instantaneous real and imaginary powers flowing in three-phase circuits (termed as **p** and **q** respectively). The harmonic component of the line current can be estimated by determining precisely the contributions of the line current harmonics to **p** and **q**.

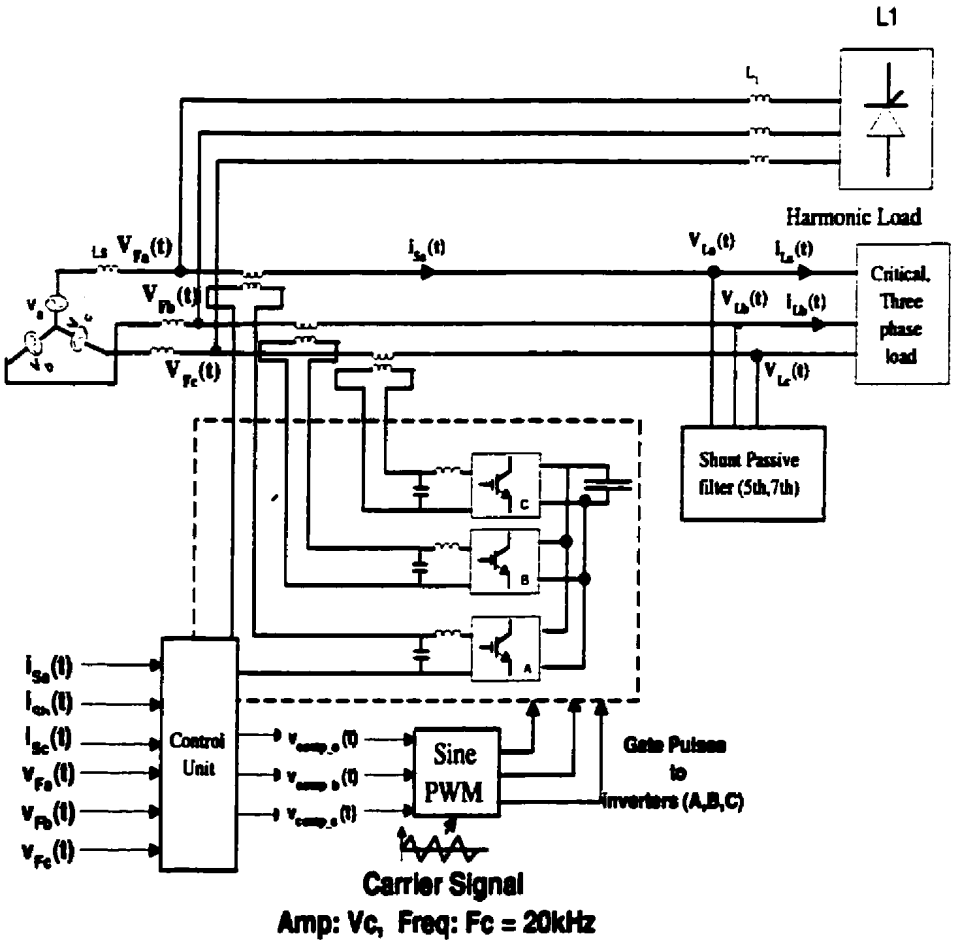

Figure 2.1: Circuit configuration of combined system [10]

2.2.1 Fundamental concepts and equations in IRP theory

In the IRP theory, the instantaneous voltages and currents are expressed as instantaneous space vectors. In $a-b-c$ coordinates, the a, b, c axes are fixed on the same plane and spaced 120 degrees apart from each other. The instantaneous space vectors (e_a, i_a),(e_b, i_b) and (e_c, i_c) are set on the a, b and c-axes, respectively.

The magnitudes and directions of the space vectors are functions of time. These space vectors can be transformed into (α, β) orthogonal co-ordinates, namely (e_α, i_α), along the α-axis and (e_β, i_β) along the β-axis. The transformation equations are:

$$\begin{bmatrix} e_\alpha \\ e_\beta \end{bmatrix} = \sqrt{\frac{2}{3}} \begin{bmatrix} 1 & -1/2 & -1/2 \\ 0 & \sqrt{3}/2 & -\sqrt{3}/2 \end{bmatrix} \cdot \begin{bmatrix} e_a \\ e_b \\ e_c \end{bmatrix} \tag{2.2}$$

$$\begin{bmatrix} i_\alpha \\ i_\beta \end{bmatrix} = \sqrt{\frac{2}{3}} \begin{bmatrix} 1 & -1/2 & -1/2 \\ 0 & \sqrt{3}/2 & -\sqrt{3}/2 \end{bmatrix} \cdot \begin{bmatrix} i_a \\ i_b \\ i_c \end{bmatrix} \tag{2.3}$$

The instantaneous real(**p**) and instantaneous reactive (**q**) powers on a three-phase circuit can now be defined respectively as

$$\mathbf{p} = \mathbf{e}_\alpha \cdot \mathbf{i}_\alpha + \mathbf{e}_\beta \cdot \mathbf{i}_\beta \tag{2.4}$$

$$\mathbf{q} = \mathbf{e}_\alpha \times \mathbf{i}_\beta + \mathbf{e}_\beta \times \mathbf{i}_\alpha \tag{2.5}$$

Figures 2.2 and 2.3 show the two coordinate systems and the space vectors.

2.2.2 Instantaneous real and imaginary powers

In this section the physical significance of the instantaneous powers are explained.

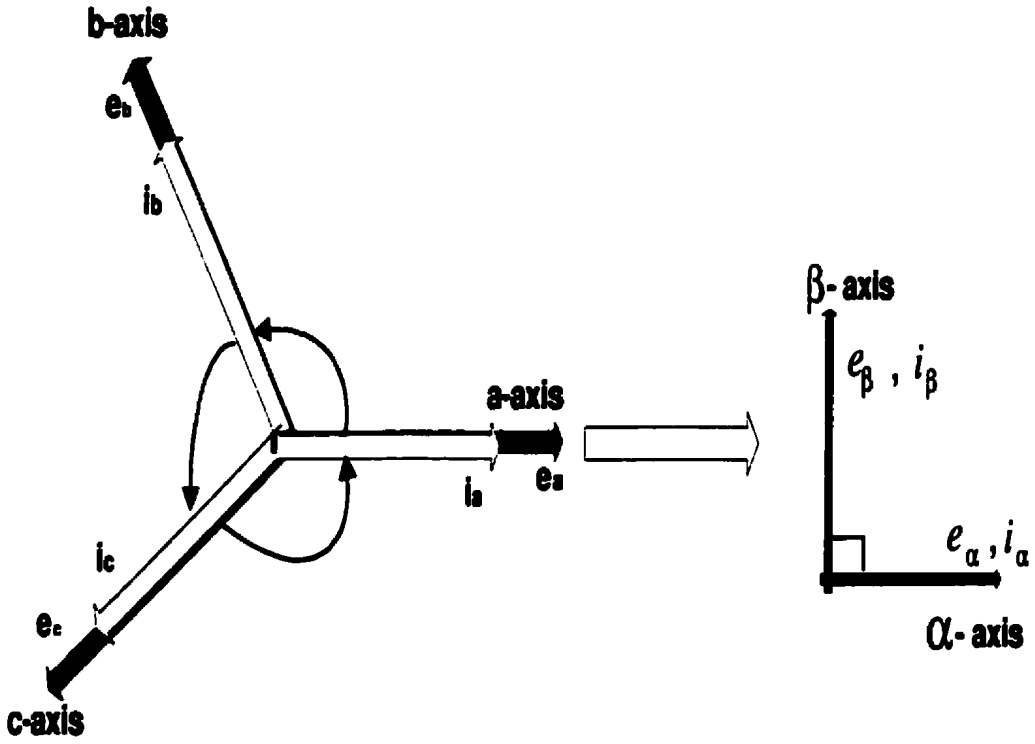

Figure 2.2: Space vectors and coordinate transformation [4]

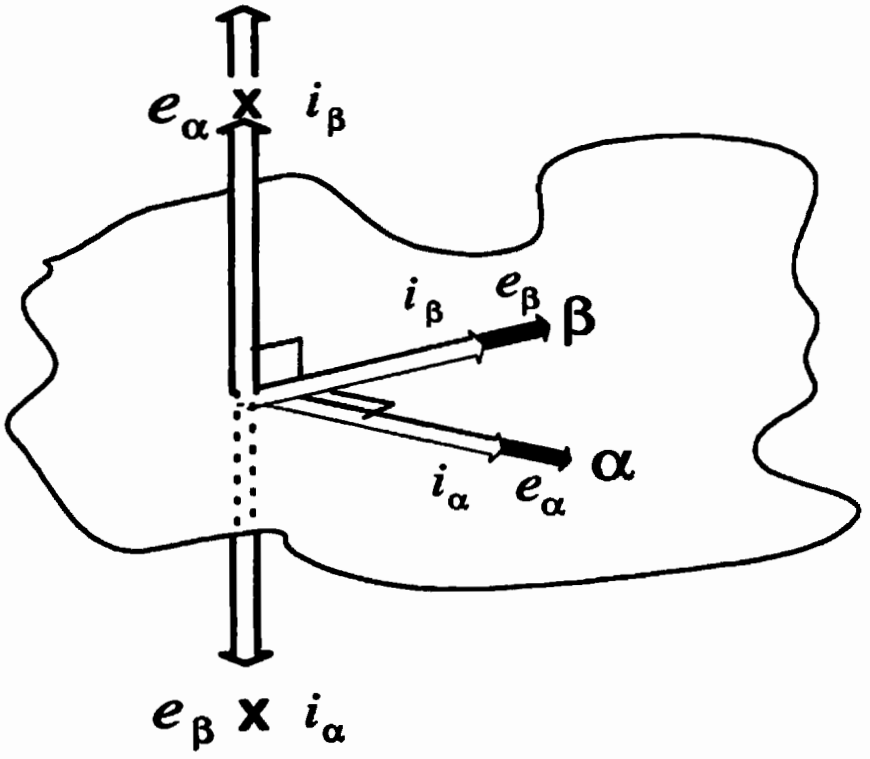

Figure 2.3: Instantaneous space vectors [4]

- The instantaneous real power $p = \bar{p} + \tilde{p}$.

  $\bar{p}$ is the mean value of the real power, which corresponds to the energy per unit time transferred from the power supply to the load. This is the desired power component. For a distortion free load voltage, $\bar{p}$ is equal to the conventional active power flowing in the three-phase circuit.

  $\tilde{p}$ is the alternating value of the instantaneous real power. If the supply voltage and line currents are balanced without any zero sequence components, $p = 0$. Imbalance in fundamental component reflects in the form of a second harmonic component in $\tilde{p}$. Current harmonics also contribute to the higher order harmonics in $\tilde{p}$.

- Instantaneous reactive power q corresponds to the power that is exchanged between the phases of the load. The transfer or exchange of energy between the power supply and the load is not reflected in this component. The instantaneous reactive power is responsible for the existence of undesirable currents that circulate between the system phases. In the case of a balanced sinusoidal voltage supply and a balanced load, with or without harmonics, $\bar{q}$ (the mean value of the instantaneous reactive power) is equal to the conventional reactive power ($\bar{q} = 3 \cdot V \cdot I_1 \cdot \sin(\phi)$).

Calculation of instantaneous powers **p** and **q** is done by recognizing that vector e_α is parallel to i_α and e_β is parallel to i_β and that these vectors are aligned to the

orthogonal axes. The instantaneous powers are obtained as

$$\begin{bmatrix} p \\ q \end{bmatrix} = \begin{bmatrix} e_\alpha & e_\beta \\ -e_\beta & e_\alpha \end{bmatrix} \cdot \begin{bmatrix} i_\alpha \\ i_\beta \end{bmatrix} \tag{2.6}$$

If compensation currents have to be derived based on p-q calculations, (2.6) can be re-written as

$$\begin{bmatrix} i_\alpha \\ i_\beta \end{bmatrix} = \begin{bmatrix} e_\alpha & e_\beta \\ -e_\beta & e_\alpha \end{bmatrix}^{-1} \cdot \begin{bmatrix} p^* \\ q^* \end{bmatrix} \tag{2.7}$$

where p^* and q^* are the desired p and q, respectively. Equation (2.7) can be rewritten as

$$\begin{bmatrix} i_\alpha \\ i_\beta \end{bmatrix} = \frac{1}{[e_\alpha^2 + e_\beta^2]} \begin{bmatrix} e_\alpha & -e_\beta \\ e_\beta & e_\alpha \end{bmatrix} \cdot \begin{bmatrix} p^* \\ q^* \end{bmatrix} \tag{2.8}$$

where e_α and e_β can be termed as reference vectors since they are used to derive the current references from the desired **p** and **q** values. It is important to note that if e_α and e_β are not perfectly sinusoidal, orthogonal and equal in magnitude, the term $\frac{1}{[e_\alpha^2+e_\beta^2]}$ will be time-varying and will distort the compensation currents considerably. Voltage imbalance is likely to distort the ideal characteristics of e_α and e_β thereby rendering the IRP scheme unsuitable for compensation. For harmonic compensation, the reference powers are given by

$$\begin{bmatrix} p^* \\ q^* \end{bmatrix} = \begin{bmatrix} p_H \\ q_H \end{bmatrix} = \begin{bmatrix} p - p_{DC} \\ q - q_{DC} \end{bmatrix} \tag{2.9}$$

where p_{DC} and q_{DC} are the dc-components in p and q, respectively. These components, if present, reflect as a fundamental component in the reference currents (which

is undesirable in the case of harmonic isolation). To ensure that the impedance offered to the fundamental component of the line current is minimal, the dc-component is filtered out using a high-pass filter (preferably a linear phase FIR digital filter).

2.3 Applying IRP Theory to Harmonic Extraction

In the IRP based scheme, the phase voltages $V_{F_a}, V_{F_b}, V_{F_c}$ at the supply end of the compensator and the supply (or compensator) currents $i_{S_a}, i_{S_b}, i_{S_c}$ are transformed into $\alpha - \beta$ orthogonal co-ordinates $V_{F_\alpha}, V_{F_\beta}$ and $i_{S_\alpha}, i_{S_\beta}$ respectively as follows:

$$\begin{bmatrix} V_{F_\alpha} \\ V_{F_\beta} \end{bmatrix} = \sqrt{\frac{2}{3}} \begin{bmatrix} 1 & -1/2 & -1/2 \\ 0 & \sqrt{3}/2 & -\sqrt{3}/2 \end{bmatrix} \cdot \begin{bmatrix} V_{F_a} \\ V_{F_b} \\ V_{F_c} \end{bmatrix} \tag{2.10}$$

$$\begin{bmatrix} i_{S_\alpha} \\ i_{S_\beta} \end{bmatrix} = \sqrt{\frac{2}{3}} \begin{bmatrix} 1 & -1/2 & -1/2 \\ 0 & \sqrt{3}/2 & -\sqrt{3}/2 \end{bmatrix} \cdot \begin{bmatrix} i_{S_a} \\ i_{S_b} \\ i_{S_c} \end{bmatrix} \tag{2.11}$$

From these coordinates the instantaneous active and reactive powers p and q are computed as [4].

$$\begin{bmatrix} p \\ q \end{bmatrix} = \sqrt{\frac{2}{3}} \begin{bmatrix} V_{F_\alpha} & V_{F_\beta} \\ -V_{F_\beta} & V_{F_\alpha} \end{bmatrix} \cdot \begin{bmatrix} i_{S_\alpha} \\ i_{S_\beta} \end{bmatrix} \tag{2.12}$$

The dc components of p and q represent the conventional real and reactive powers respectively. The contribution of the harmonics to p and q (i.e. p_H and q_H) are determined by filtering out the dc component. However, it must be noted that due to the presence of the high pass filter (HPF), a fraction of the real power contained at harmonic frequencies would also be filtered out. This leaves a small portion of the harmonics undetectable. The harmonic component of the compensator current is

calculated from

$$\begin{bmatrix} i_{S_{a_h}} \\ i_{S_{b_h}} \\ i_{S_{c_h}} \end{bmatrix} = \sqrt{\frac{2}{3}} \begin{bmatrix} 1 & 0 \\ -1/2 & \sqrt{\frac{2}{3}} \\ -1/2 & -\sqrt{\frac{2}{3}} \end{bmatrix} \cdot \begin{bmatrix} V_{F_\alpha} & V_{F_\beta} \\ -V_{F_\beta} & V_{F_\alpha} \end{bmatrix}^{-1} \cdot \begin{bmatrix} p_H \\ q_H \end{bmatrix} \tag{2.13}$$

In the presence of voltage imbalance and zero sequence components, the unit reference vectors derived from V_{F_α} and V_{F_β} may no longer be sinusoidal and orthogonal. This redundancy impedes the extraction of all the harmonics, particularly in the presence of zero sequence components.

In the following section, the theory outlined above is illustrated by different examples. To make the theory clear, some examples have been cited to demonstrate the effects of current, voltage distortion and imbalance on the compensation.

2.4 Examples to Highlight the Salient Features of IRP Control Scheme

Since precise harmonic current extraction is a requirement of this scheme, its accuracy is examined by taking up various cases such as voltage and current distortion and imbalance. Here the voltage signals e_a, e_b and e_c, represent the voltages at the supply end of the compensator while the current signals i_{S_a}, i_{S_b} and i_{S_c}, represent the instantaneous supply currents. For ease of calculation, only one dominant harmonic (5^{th}) is considered. The procedure adopted for harmonic extraction using the IRP theory is summarized as follows:

1. The (α, β) coordinates of the phase voltages and currents are computed using

(2.2) and (2.3).

2. The instantaneous reactive and active powers p and q are calculated using $e_\alpha, e_\beta, i_{S_\alpha}, i_{S_\beta}$ from (2.6).

3. The dc component in p and q is calculated by averaging the signal samples. The contribution of the harmonics to p and q are calculated using (2.9).

4. The (α, β) components of the harmonic reference currents $(i_{\alpha_h}, i_{\beta_h})$ are calculated using (2.8) and (2.9).

5. Finally the reference harmonic currents are derived using the transformation (2.13).

The complete control scheme based on the above procedure is depicted in Fig. 2.4.

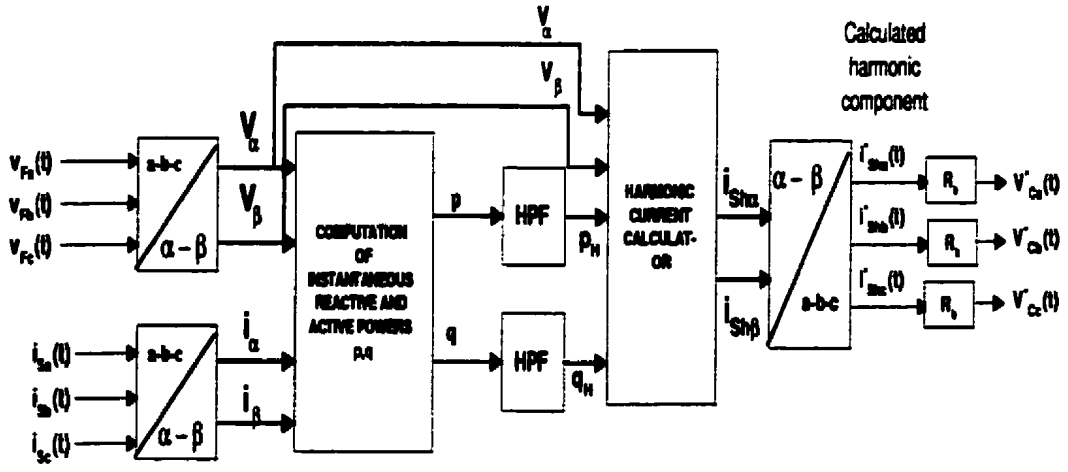

Figure 2.4: Harmonic current extraction based on the IRP theory [10]

2.4.1 IRP theory applied to balanced, sinusoidal voltages and currents

The desired (ideal) case involves balanced, sinusoidal voltages and currents. Although this condition can never be achieved in a power system owing to the presence of numerous nonlinear elements and finite quality factors of the shunt filters, it provides a starting point for illustrating the IRP theory. The balanced voltages and currents are expressed as

$$\begin{bmatrix} e_a \\ e_b \\ e_c \end{bmatrix} = \begin{bmatrix} V_1 \cdot \sin(\omega t) \\ V_1 \cdot \sin(\omega t - \frac{2\pi}{3}) \\ V_1 \cdot \sin(\omega t + \frac{2\pi}{3}) \end{bmatrix} \tag{2.14}$$

$$\begin{bmatrix} i_{S_a} \\ i_{S_b} \\ i_{S_c} \end{bmatrix} = \begin{bmatrix} I_1 \cdot \sin(\omega t - \phi) \\ I_1 \cdot \sin(\omega t - \phi - \frac{2\pi}{3}) \\ I_1 \cdot \sin(\omega t - \phi + \frac{2\pi}{3}) \end{bmatrix} \tag{2.15}$$

where $\cos(\phi)$ is the displacement power factor seen from the supply side. Using (2.2) and (2.3), the α-β components of the supply voltages are obtained as

$$\begin{bmatrix} e_\alpha \\ e_\beta \end{bmatrix} = \begin{bmatrix} \frac{\sqrt{6}}{2} \cdot V_1 \cdot \sin(\omega t) \\ -\frac{\sqrt{6}}{2} \cdot V_1 \cdot \cos(\omega t) \end{bmatrix} \tag{2.16}$$

Similarly the α-β components of the line currents are obtained as

$$\begin{bmatrix} i_{S_\alpha} \\ i_{S_\beta} \end{bmatrix} = \begin{bmatrix} \frac{\sqrt{6}}{2} \cdot I_1 \cdot \sin(\omega t - \phi) \\ -\frac{\sqrt{6}}{2} \cdot I_1 \cdot \cos(\omega t - \phi) \end{bmatrix} \tag{2.17}$$

Equations (2.16) and (2.17) show that the $\alpha-\beta$ components of the supply voltages and the line currents are sinusoidal and orthogonal. From (2.6), the instantaneous powers are obtained as

$$\begin{bmatrix} p \\ q \end{bmatrix} = \begin{bmatrix} \frac{3}{2} \cdot V_1 \cdot I_1 \cdot \cos(\phi) \\ -\frac{3}{2} \cdot V_1 \cdot I_1 \cdot \sin(\phi) \end{bmatrix} \tag{2.18}$$

and from (2.9),

$$\begin{bmatrix} p_H \\ q_H \end{bmatrix} = \begin{bmatrix} 0 \\ 0 \end{bmatrix} \tag{2.19}$$

Hence from (2.13)

$$\begin{bmatrix} i_{S_{a_h}} \\ i_{S_{b_h}} \\ i_{S_{c_h}} \end{bmatrix} = \begin{bmatrix} 0 \\ 0 \\ 0 \end{bmatrix} \tag{2.20}$$

As expected, no harmonic components are reflected in the calculations.

2.4.2 IRP theory applied to balanced sinusoidal voltages, non-sinusoidal currents

The THD in the line currents of DC drive supplies may range from 5% to as high as 30%. In switch mode power supplies (SMPS), the currents drawn are concentrated in short bursts of 2-3ms in each half-cycle. In an SMPS the odd-harmonics are dominant. To simplify the calculations only the fifth harmonic is considered for the analysis, and it is assumed that the THD is 30% (i.e. $I_5 = 0.3I_1$). The balanced voltages are given by

$$\begin{bmatrix} e_a \\ e_b \\ e_c \end{bmatrix} = \begin{bmatrix} V_1 \cdot \sin(\omega t) \\ V_1 \cdot \sin(\omega t - \frac{2\pi}{3}) \ ] \\ V_1 \cdot \sin(\omega t + \frac{2\pi}{3}) \end{bmatrix} \tag{2.21}$$

The non-sinusoidal currents are expressed as

$$\begin{bmatrix} i_{S_a} \\ i_{S_b} \\ i_{S_c} \end{bmatrix} = \begin{bmatrix} I_1 \cdot \sin(\omega t - \phi) + 0.3I_1 \cdot \sin(5\omega t - 5\phi) \\ I_1 \cdot \sin(\omega t - \phi - \frac{2\pi}{3}) + 0.3I_1 \cdot \sin(5\omega t - 5\phi - 5 \cdot \frac{2\pi}{3}) \\ I_1 \cdot \sin(\omega t - \phi + \frac{2\pi}{3}) + 0.3I_1 \cdot \sin(5\omega t - 5\phi + 5 \cdot \frac{2\pi}{3}) \end{bmatrix} \tag{2.22}$$

Since the supply voltage is sinusoidal and balanced, e_α and e_β are the same as obtained in (2.16). However i_{S_α} and i_{S_β} are obtained as

$$\begin{bmatrix} i_{S_\alpha} \\ i_{S_\beta} \end{bmatrix} = \begin{bmatrix} 1.224I_1 \cdot \sin(\omega t - \phi) + 0.367I_1 \cdot \sin(5\omega t - 5\phi) \\ -1.224I_1 \cdot \cos(\omega t - \phi) + 0.367I_1 \cdot \cos(5\omega t - 5\phi) \end{bmatrix} \tag{2.23}$$

and the instantaneous powers are calculated as

$$\begin{bmatrix} p \\ q \end{bmatrix} = \begin{bmatrix} 1.5V_1I_1\cos(\phi) - 0.45V_1I_1\cos(6\omega t - 5\phi) \\ -1.5V_1I_1\sin(\phi) + 0.45V_1I_1\sin(6\omega t - 5\phi) \end{bmatrix} \tag{2.24}$$

$$\begin{bmatrix} p_H \\ q_H \end{bmatrix} = \begin{bmatrix} -0.45V_1I_1\cos(6\omega t - 5\phi) \\ 0.45V_1I_1\sin(6\omega t - 5\phi) \end{bmatrix} \tag{2.25}$$

The reference currents are obtained as

$$\begin{bmatrix} i_{S_{a_h}} \\ i_{S_{b_h}} \\ i_{S_{c_h}} \end{bmatrix} = \begin{bmatrix} 0.3I_1 \cdot \sin(5\omega t - 5\phi) \\ 0.3I_1 \cdot \sin(5\omega t - 5\phi - 5 \cdot \frac{2\pi}{3}) \\ 0.3I_1 \cdot \sin(5\omega t - 5\phi + 5 \cdot \frac{2\pi}{3}) \end{bmatrix} \tag{2.26}$$

Equation 2.26 shows that for balanced sinusoidal voltages and non-sinusoidal currents the IRP theory accurately determines the harmonic currents.

2.4.3 IRP theory applied to non-sinusoidal voltages and currents (No zero sequence components)

Acceptable terminal voltage distortion levels are in the range 1-2% for most process control systems. However, in the presence of large nonlinear loads and relatively high line impedances, the distortion levels may rise to 10% or higher. In this case a more practical scenario in which a 10% voltage distortion($V_5 = 0.1V_1$) and a 30% current distortion ($I_5 = 0.3I_1$) are assumed in the following analysis. The non-sinusoidal voltages are expressed as

$$\begin{bmatrix} e_a \\ e_b \\ e_c \end{bmatrix} = \begin{bmatrix} V_1 \cdot \sin(\omega t) + 0.1V_1 \cdot \sin(5\omega t) \\ V_1 \cdot \sin(\omega t - \frac{2\pi}{3}) + 0.1V_1 \cdot \sin(5\omega t - 5 \cdot \frac{2\pi}{3}) \\ V_1 \cdot \sin(\omega t + \frac{2\pi}{3}) + 0.1V_1 \cdot \sin(5\omega t + 5 \cdot \frac{2\pi}{3}) \end{bmatrix} \tag{2.27}$$

and the non-sinusoidal currents are given by

$$\begin{bmatrix} i_{S_a} \\ i_{S_b} \\ i_{S_c} \end{bmatrix} = \begin{bmatrix} I_1 \cdot \sin(\omega t - \phi) + 0.3I_1 \cdot \sin(5\omega t - 5\phi) \\ I_1 \cdot \sin(\omega t - \phi - \frac{2\pi}{3}) + 0.3I_1 \cdot \sin(5\omega t - 5\phi - 5 \cdot \frac{2\pi}{3}) \\ I_1 \cdot \sin(\omega t - \phi + \frac{2\pi}{3}) + 0.3I_1 \cdot \sin(5\omega t - 5\phi + 5 \cdot \frac{2\pi}{3}) \end{bmatrix} \tag{2.28}$$

The α, β components of the supply voltages are obtained as

$$\begin{bmatrix} e_\alpha \\ e_\beta \end{bmatrix} = \begin{bmatrix} 1.224V_1 \cdot \sin(\omega t) + 0.1225V_1 \cdot \sin(5\omega t) \\ -1.224V_1 \cdot \cos(\omega t) + 0.1225V_1 \cdot \cos(5\omega t) \end{bmatrix} \tag{2.29}$$

Both e_α and e_β are non-sinusoidal but orthogonal and this will not impede the extraction of harmonics from the calculated values of p_H and q_H. However, as shall be shown later this introduces some additional harmonics. Similarly, the α-β components of the line currents are obtained as

$$\begin{bmatrix} i_{S_\alpha} \\ i_{S_\beta} \end{bmatrix} = \begin{bmatrix} 1.224I_1 \cdot \sin(\omega t - \phi) + 0.367I_1 \cdot \sin(5\omega t - 5\phi) \\ -1.224I_1 \cdot \cos(\omega t - \phi) + 0.367I_1 \cdot \cos(5\omega t - 5\phi) \end{bmatrix} \tag{2.30}$$

Simplifying and neglecting the sine terms that are very small the instantaneous powers are obtained as

$$\begin{bmatrix} p \\ q \end{bmatrix} = \begin{bmatrix} 1.5V_1I_1\cos(\phi) + 0.045V_1I_1\cos(5\phi) - 0.45V_1I_1\cos(6\omega t - 5\phi) \\ -0.15V_1I_1\cos(6\omega t - \phi) \\ -1.5V_1I_1\sin(\phi) + 0.045V_1I_1\sin(5\phi) + 0.45V_1I_1\sin(6\omega t - 5\phi) \\ -0.15V_1I_1\sin(6\omega t - \phi) \end{bmatrix} \tag{2.31}$$

The first two terms in (2.31) correspond to the dc-components which are suppressed by the high pass filter. As can be seen from (2.31) an additional dc-term is contributed by the fifth harmonic. This dc component will be suppressed through the HP filtering. This loss of information leads to some inaccuracy in the detection of the fifth-harmonic.

$$\begin{bmatrix} p_H \\ q_H \end{bmatrix} = \begin{bmatrix} -0.45V_1I_1\cos(6\omega t - 5\phi) - 0.15V_1I_1\cos(6\omega t - \phi) \\ 0.45V_1I_1\sin(6\omega t - 5\phi) - 0.15V_1I_1\sin(6\omega t - \phi) \end{bmatrix} \tag{2.32}$$

The reference currents should contain the fifth harmonic alone but instead they contain higher order harmonics. A small fundamental component is also present due

to the mixing of the 5^{th} harmonic from the voltage and 6^{th} harmonic from p and q. The extracted harmonic currents are obtained as

$$\begin{bmatrix} i_{S_{a_h}} \\ i_{S_{b_h}} \\ i_{S_{c_h}} \end{bmatrix} = \begin{bmatrix} \frac{f_{a_1}}{f_{a_2}} \\ \frac{f_{b_1}}{f_{b_2}} \\ \frac{f_{c_1}}{f_{c_2}} \end{bmatrix} \tag{2.33}$$

where

$$\left.\begin{aligned} f_{a_1} &= 0.298I_1\sin(5\omega t - 5\phi) + 0.01I_1\sin(\omega t - \phi) - 0.1I_1\sin(7\omega t - \phi) \\ &\quad -0.29I_1\sin(7\omega t - 5\phi) \\ f_{b_1} &= 0.298I_1\sin(5\omega t - 5\phi - 5\cdot\tfrac{2\pi}{3}) + 0.01I_1\sin(\omega t - \phi - \tfrac{2\pi}{3}) \\ &\quad -0.1I_1\sin(7\omega t - \phi - 7\cdot\tfrac{2\pi}{3}) - 0.29I_1\sin(7\omega t - 5\phi - 7\cdot\tfrac{2\pi}{3}) \\ f_{c_1} &= 0.298I_1\sin(5\omega t - 5\phi + 5\cdot\tfrac{2\pi}{3}) + 0.01I_1\sin(\omega t - \phi + \tfrac{2\pi}{3}) \\ &\quad -0.1I_1\sin(7\omega t - \phi + 7\cdot\tfrac{2\pi}{3}) - 0.29I_1\sin(7\omega t - 5\phi + 7\cdot\tfrac{2\pi}{3}) \\ f_{a_2} &= f_{b_2} = f_{c_2} = 1 - 0.05\cos(6\omega t) \end{aligned}\right\} \tag{2.34}$$

Due to the complexity of the current equations, an FFT of the current in phase-a is presented in Fig. 2.5. It can been seen from the plot that although there is no seventh harmonic originally in the current signal, the spectrum of the extracted current contains the 7^{th} harmonic (10%). The presence of the time-varying term in the denominator in (2.33) results in higher order harmonics. Hence it is imperative that the voltage signals e_α and e_β be properly filtered before being used to derive the current references.

2.4.4 IRP theory applied to unbalanced voltages and distorted currents

Voltage imbalance results in zero and negative sequence components. In this case a 25% single-phase sag in phase A (due to a possible ground fault) is considered.

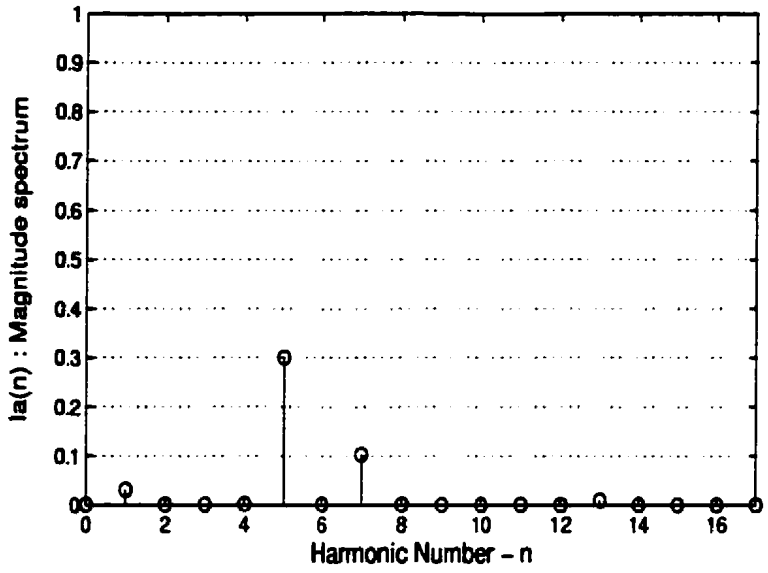

Figure 2.5: Frequency spectrum of the extracted harmonic components (phase-a) for non-voltages and currents

The unbalanced voltages are represented by

$$\begin{bmatrix} e_a \\ e_b \\ e_c \end{bmatrix} = \begin{bmatrix} 0.75V_1 \cdot \sin(\omega t) \\ V_1 \cdot \sin(\omega t - \frac{2\pi}{3}) \\ V_1 \cdot \sin(\omega t + \frac{2\pi}{3}) \end{bmatrix} \quad (2.35)$$

As before a 30% THD in the current is assumed, and the non-sinusoidal currents are expressed as

$$\begin{bmatrix} i_{S_a} \\ i_{S_b} \\ i_{S_c} \end{bmatrix} = \begin{bmatrix} I_1 \cdot \sin(\omega t - \phi) + 0.3I_1 \cdot \sin(5\omega t - 5\phi) \\ I_1 \cdot \sin(\omega t - \phi - \frac{2\pi}{3}) + 0.3I_1 \cdot \sin(5\omega t - 5\phi - 5 \cdot \frac{2\pi}{3}) \\ I_1 \cdot \sin(\omega t - \phi + \frac{2\pi}{3}) + 0.3I_1 \cdot \sin(5\omega t - 5\phi + 5 \cdot \frac{2\pi}{3}) \end{bmatrix} \quad (2.36)$$

The α, β components of the supply voltages and line currents are obtained as

$$\begin{bmatrix} e_\alpha \\ e_\beta \end{bmatrix} = \begin{bmatrix} 1.021V_1 \cdot \sin(\omega t) \\ -1.200V_1 \cdot \cos(\omega t) \end{bmatrix} \quad (2.37)$$

$$\begin{bmatrix} i_{S_\alpha} \\ i_{S_\beta} \end{bmatrix} = \begin{bmatrix} 1.224I_1 \cdot \sin(\omega t - \phi) + 0.367I_1 \cdot \sin(5\omega t - 5\phi) \\ -1.224I_1 \cdot \cos(\omega t - \phi) + 0.367I_1 \cdot \cos(5\omega t - 5\phi) \end{bmatrix} \quad (2.38)$$

The instantaneous powers are determined as

$$\begin{bmatrix} p \\ q \end{bmatrix} = \begin{bmatrix} 1.38V_1I_1\cos(\phi) + 0.125V_1I_1\cos(2\omega t - \phi) \\ -0.038V_1I_1\cos(4\omega t - 5\phi) - 0.413V_1I_1\cos(6\omega t - 5\phi) \\ \\ -1.38V_1I_1\sin(\phi) + 0.125V_1I_1\sin(2\omega t - \phi) \\ -0.038V_1I_1\sin(4\omega t - 5\phi) - 0.413V_1I_1\sin(6\omega t - 5\phi) \end{bmatrix} \tag{2.39}$$

$$\begin{bmatrix} p_H \\ q_H \end{bmatrix} = \begin{bmatrix} 0.125V_1I_1\cos(2\omega t - \phi) - 0.0375V_1I_1\cos(4\omega t - 5\phi) \\ -0.4125V_1I_1\cos(6\omega t - 5\phi) \\ \\ 0.125V_1I_1\sin(2\omega t - \phi) - 0.0375V_1I_1\sin(4\omega t - 5\phi) \\ -0.4125V_1I_1\sin(6\omega t - 5\phi) \end{bmatrix} \tag{2.40}$$

The extracted currents are obtained as

$$\begin{bmatrix} i_{S_{a_h}} \\ i_{S_{b_h}} \\ i_{S_{c_h}} \end{bmatrix} = \begin{bmatrix} \frac{f_{a_1}}{f_{a_2}} \\ \frac{f_{b_1}}{f_{b_2}} \\ \frac{f_{c_1}}{f_{c_2}} \end{bmatrix} \tag{2.41}$$

where

$$\left.\begin{aligned} f_{a_1} &= 0.29I_1\sin(5\omega t - 5\phi) - 0.09I_1\sin(3\omega t - \phi) \\ &\quad +0.0178I_1\sin(\omega t - \phi) - 0.0345I_1\sin(3\omega t - 5\phi) \\ &\quad -0.028I_1\sin(7\omega t - 5\phi) \\ \\ f_{b_1} &= 0.29I_1\sin(5\omega t - 5\phi - 5\cdot\tfrac{2\pi}{3}) - 0.09I_1\sin(3\omega t - 3\cdot\tfrac{2\pi}{3} - \phi) \\ &\quad -0.035I_1\sin(3\omega t - 3\cdot\tfrac{2\pi}{3} - 5\phi) - 0.0283I_1\sin(7\omega t - 7\cdot\tfrac{2\pi}{3} - 5\phi) \\ &\quad +0.0178I_1\sin(\omega t - \phi - \tfrac{2\pi}{3}) \\ \\ f_{c_1} &= 0.29I_1\sin(5\omega t - 5\phi - 5\cdot\tfrac{2\pi}{3}) - 0.09I_1\sin(3\omega t + 3\cdot\tfrac{2\pi}{3} - \phi) \\ &\quad -0.035I_1\sin(3\omega t + 3\cdot\tfrac{2\pi}{3} - 5\phi) - 0.0283I_1\sin(7\omega t + 7\cdot\tfrac{2\pi}{3} - 5\phi) \\ &\quad +0.0178I_1\sin(\omega t - \phi + \tfrac{2\pi}{3}) \\ \\ f_{a_2} &= f_{b_2} = f_{c_2} = 1 + 0.18I_1\cos(2\omega t) - 0.197I_1\cos(6\omega t) \end{aligned}\right\} \tag{2.42}$$

An FFT of the extracted currents is presented in Fig. 2.6. The presence of sidebands about the fifth harmonic indicates the nonlinearity introduced by the algorithm.

The sinusoidal terms in the denominator of (2.41) contribute to higher order harmonics. From the analysis presented, it can be inferred that the IRP based control

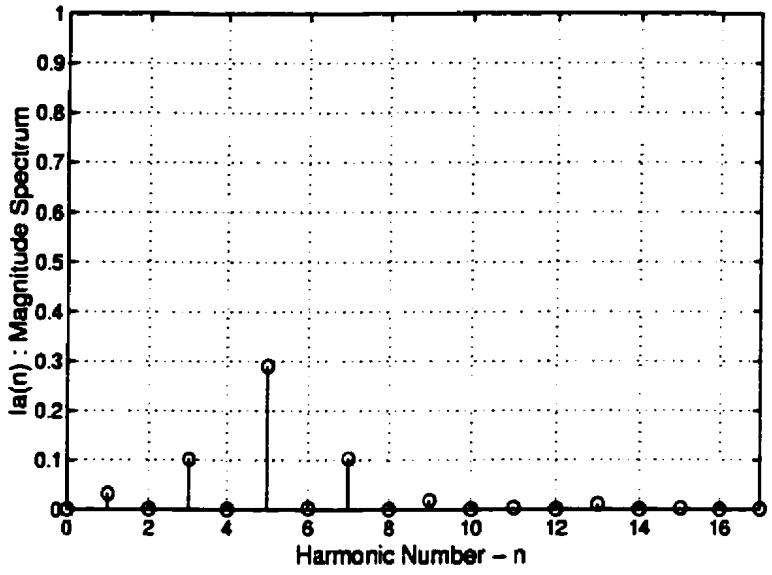

Figure 2.6: Frequency spectrum of the extracted harmonic currents (phase a) for unbalanced voltages and distorted currents

scheme will provide the worst case performance for unbalanced and distorted voltages and currents. This is because distorted voltages and currents as mentioned earlier will contribute to the dc component in p, which will be filtered by the HPF. Voltage imbalance results in zero and negative sequence components at the fundamental frequency which go undetected . Hence, the extracted harmonic estimate may contain an undesired fundamental component. Simulation results are presented to confirm the analysis.

2.5 Simulation Results and Analysis

A SIMULINK model of the harmonic extraction procedure shown in Fig. 2.4 was constructed to test the effectiveness of the algorithms in the presence of imbalance

and zero sequence components. The details of the SIMULINK models are given in Appendix A. Predetermined distorted signals emulating the measured voltages, V_{F_a}, V_{F_b} and V_{F_c} at the supply end of the compensator and the supply currents, i_{S_a}, i_{S_b} and i_{S_c}, were fed to the control block. The internal details of the IRP scheme are presented in Fig. 2.4. The effectiveness of the filtering algorithm is determined by subtracting the extracted harmonics from the unfiltered supply currents. A Fast Fourier Transform (FFT) presents the frequency decomposition of the filtered currents i_{FIL_a}, i_{FIL_b}, i_{FIL_c}. The load and supply current distortion parameters are listed in Table 2.1 and the line current components in Table 2.2. The setup is shown in Fig. 2.7.

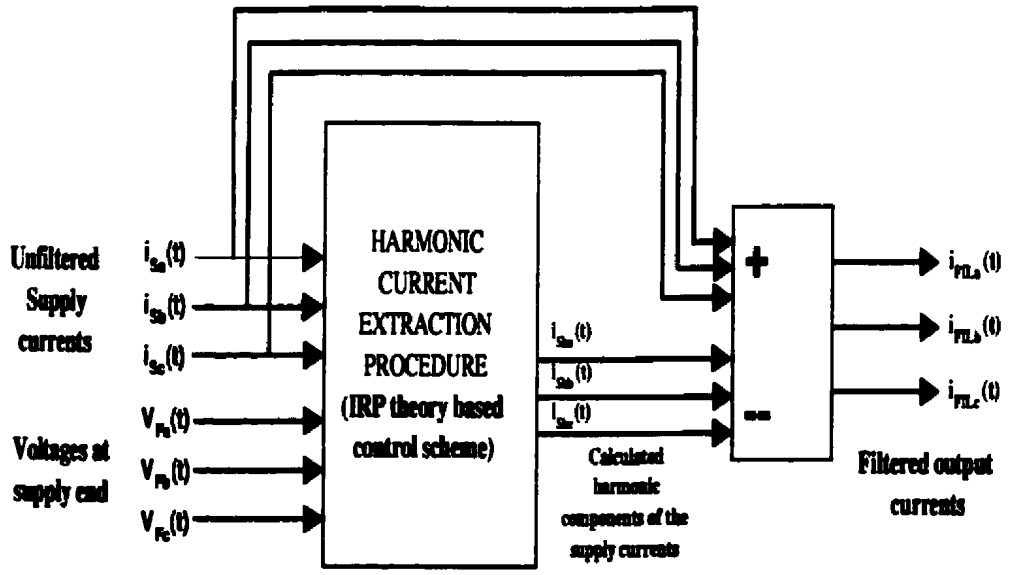

Figure 2.7: Controller test setup

Simulation is carried out for the worst case condition of unbalanced, non-sinusoidal supply voltages and currents with zero sequence to illustrate the implementation of

Table 2.1: Parameters for testing the algorithm

Line Voltage	$THD_V = 6\%$ Single-ph-sag= 25% (ph-a)
Supply-current	$THD_I = 25\%$ Zero-seq(3rd)=5%

Table 2.2: Harmonic components of the supply current (THD = 25%)

Harmonic Number - n	$\frac{I_{S_n}}{I_{S_1}} X100$
3	5%
5	20%
7	14.3%
11	9.1%

the scheme in SIMULINK. The SIMULINK results shown in Fig. 2.8 confirm the analysis presented in this chapter. The results confirm that the IRP based control scheme provides the worst performance for unbalanced and distorted voltages and currents.

2.6 Drawbacks of the IRP Based Scheme

From the theoretical point of view supported by examples and simulation results shown in Fig. 2.8, the following general statements can be made about the drawbacks of the Instantaneous Reactive Power(IRP) theory based compensator:

1. In the presence of voltage distortion, the harmonic voltages and currents result in non-zero real power, which reflects as a dc component in p and q. This dc component is filtered out by the high pass filter. This non-detection of real

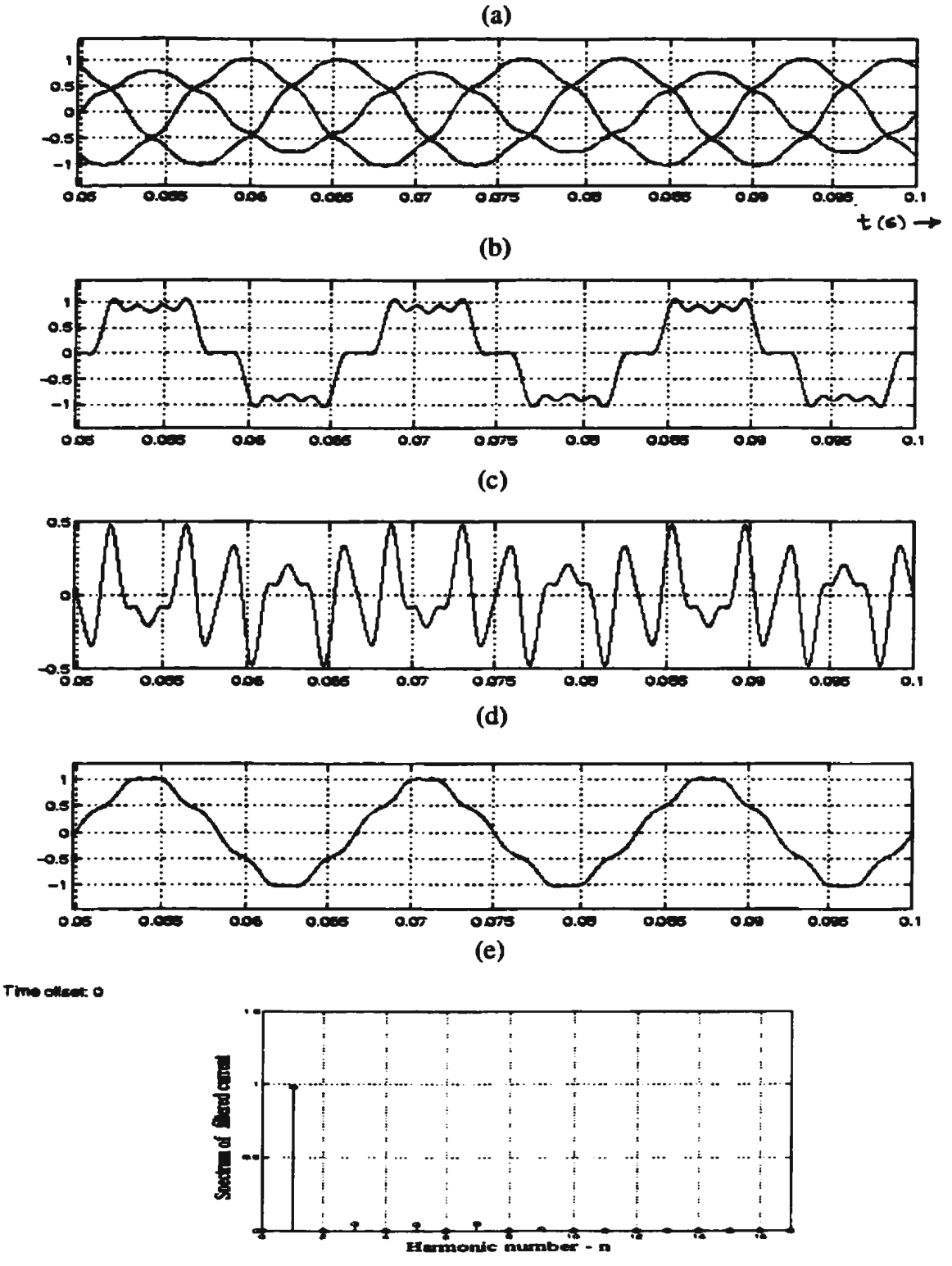

Figure 2.8: Results for unbalanced non-sinusoidal voltage (%Sag (phase-a) = 25, THD = 6%), non-sinusoidal supply current (THD = 25%) with zero sequence: (a) Supply voltage, (b) Supply current, (c) Extracted harmonic component of (b), (d) Filtered output current (phase-a) (e) Frequency spectrum of filtered output, (d) (THD = 11%)

power at harmonic frequencies prevents extraction of all the harmonics in the supply current.

2. Due to the passive filter terminal voltage distortion, unit vectors derived from real and reactive power definitions may not be sinusoidal and orthogonal. This will impede the extraction of all harmonics and will not allow true decoupling between the supply and the load.

3. Due to the absence of one degree of freedom in the $\alpha - \beta$ frame of reference, imbalance and the presence of zero sequence components impede effective harmonic extraction.

4. This control scheme can be employed only for the purpose of enforcing harmonic isolation. This provided the motivation to extend the compensation principle to incorporate additional functions such as voltage compensation.

2.7 Summary

The performance of the IRP theory based control scheme for suppressing the supply current harmonics was investigated in this chapter. After reiterating some fundamental concepts in IRP theory, the effects of voltage imbalance, zero sequence and harmonic components on the IRP based harmonic extraction procedure was verified through simulation.

The IRP based scheme was analyzed for five different cases which illustrated the

cumulative effects of voltage distortion, zero sequence and imbalance on the extraction of supply current harmonics. It is shown that the application of IRP theory assumes a balanced and sinusoidal input voltage.

In the presence of voltage distortion, the harmonic voltages and currents will result in non-zero real power, which reflects as a dc component in p and q. This dc component is filtered out by the high pass filter. This non-detection of real power at harmonic frequencies does not permit complete extraction of all the harmonics in the supply current. These drawbacks of the IRP scheme provide the motivation and set up the stage for the development of a more robust control scheme for harmonic extraction.

Chapter 3

Synchronous Frame Based Control Scheme For The Hybrid Series Topology

Introduction

The operation of the hybrid series compensator system is strongly dependent on the filtering algorithm involved. The salient features of the IRP based control scheme for the hybrid series topology was discussed in the previous chapter. Some of the problems can be avoided by slightly modifying the control scheme. Zero sequence current components can be eliminated by averaging the load currents and subtracting the averaged current from each of the phase currents before performing the transformations. The effects of load voltage distortion can be mitigated by deriving the unit reference vectors V_{F_α} and V_{F_β} through a phase locked loop(PLL). However, if immunity to imbalance is to be incorporated, the scheme will have to extract the positive and negative sequence components and determine their contributions to **p** and **q**. In most cases, VAR compensation is not the prime objective, and so, there is no need to

compute **p** and **q**. Harmonic current extraction can be carried out without knowledge of **p** and **q** through synchronous d-q transformation and filtering or through selective harmonic filtering.

In order to incorporate voltage compensation along with harmonic isolation, decoupling of the voltages and currents is essential. This chapter proposes a control scheme based on d-q-0 transformation to facilitate voltage compensation and harmonic isolation. It is shown that the synchronous d-q-0 based controller achieves significant performance improvement without any assumptions regarding supply waveform quality. The development of the controller along with various simulation results and examples to illustrate the performance of the proposed scheme provide the focus of this chapter.

3.1 Proposed Modification to the Compensation Principle Proposed by Peng, et al.

As noted in the previous chapter, the compensation scheme proposed by Peng et al. [10] primarily provides harmonic isolation. Since the series compensator is required to balance the three-phase voltages and also overcome sags, swells and flicker, there arises a need to extend the functionality of the compensator. A compensation equation which incorporates these additional functions may be described by the equation

$$V_c^* = R_h \cdot I_{S_h} + K_v \cdot (V_F - V_{F_{ref}}) \tag{3.1}$$

where, V_F is the voltage measured at the supply end of the compensator; $V_{F_{REF}}$ is the desired voltage; and K_V and R_h are voltage and current gains of the controller. The second term in the compensation equation allows for the compensation of voltage sags, swells, flicker and independent phase voltage balancing. Thus, the proposed compensation principle provides two functions: harmonic isolation and voltage compensation.

3.2 Development of the Controller for the Proposed Compensation Principle

The controller for the proposed compensation principle can be realized as two independent functional units. This is important, since one of the problems with the IRP scheme is the mutual coupling between the voltage and current signals. The IRP based scheme was proposed for three-phase balanced systems with no zero sequence components. In order to extract zero sequence voltages or currents, the third degree of freedom (the 0-axis) in the d-q-0 reference frame is exploited.

The major considerations for the choice of d-q-0 transformation are highlighted below.

- In a synchronously rotating d-q-0 reference frame, the components at the fundamental frequency (under balanced conditions) are transformed to dc and harmonics to non-dc quantities with a frequency shift corresponding to the fundamental frequency in the spectrum. The removal of the dc component to extract

the harmonics can be easily done using a digital FIR filter (linear phase). Also, reference voltages and currents in the d-q frame are dc quantities which eliminate the need for sine-cosine lookup tables. Moreover, since harmonic extraction is the objective of this approach, the d-q-0 based scheme is the appropriate choice.

- If feedback control is to be employed in regulating the fundamental component of the voltage, proportional integral (PI) regulators can be employed in the d-q-0 domain. PI controllers are employed effectively in systems which have a fairly low bandwidth. Stability becomes a critical issue otherwise. Since the fundamental component reflects as a dc in the d-q-0 axis, the error signal would be slowly varying and would suit the PI implementation for a feedback control scheme involving fundamental voltage/current regulation.

- A phase locked loop provides synchronization between the injected inverter voltage and the supply voltage in one of the three phases. In-phase synchronization minimizes the magnitude of the voltage that will have to be injected with respect to one of the three phases. The synchronization can be easily realized in the d-q-0 reference frame.

As indicated earlier, the controller is realized in two sub-units, as shown in Fig. 3.1. The functions of the two units are:

- The Voltage Compensation Unit(VCU), extracts the zero sequence components and harmonics in the faulted voltage.

- The Harmonic Current Extraction Unit(HCEU), extracts the harmonic component of the supply current and uses it to simulate a harmonic resistor to facilitate harmonic isolation.

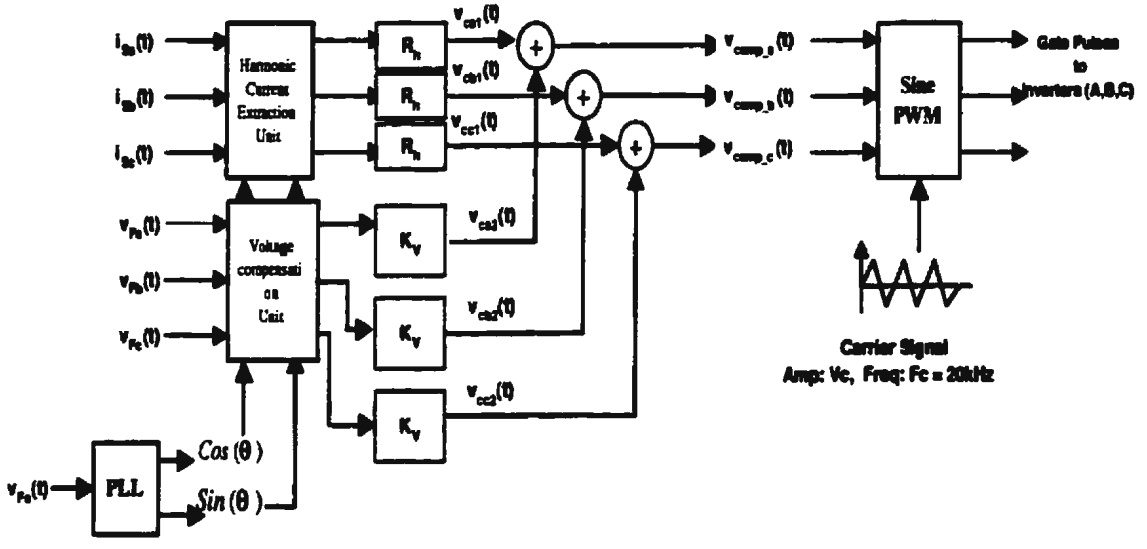

Figure 3.1: Control Unit

The controller gains K_V and R_h associated with the units are used for tuning the controller to obtain the desired response. The realization of the two units are discussed in the following sections.

3.2.1 Voltage Compensation Unit(VCU)

Single-phase or three-phase faults may cause magnitude and phase imbalance leading to the generation of zero and negative sequence components. Voltage harmonics are the result of harmonic voltage drop across the line impedance. In order to provide most sensitive and critical loads with a balanced and sinusoidal load voltage, the VCU must cancel out the undesired zero and negative sequence voltage components and harmonics. These components are obtained by taking the difference between the desired positive sequence components and the measured phase voltages.

The unit reference vectors are derived from the load voltage in phase-a using a PLL. The PLL helps in synchronizing the faulted voltage $V_{F(a,b,c)}$, i.e. the voltages at the supply end of the series compensator with the voltage injected by the inverter.

The three-phase voltages V_{F_a}, V_{F_b} and V_{F_c} are first transformed to stationary coordinates $V_{F_0}, V_{F_\alpha}, V_{F_\beta}$ and finally to synchronous frame values V_{F_0}, V_{F_d} and V_{F_q}, respectively. The two level transformation simplifies the controller implementation, compared to a direct transformation from a-b-c to d-q-0. The transformation matrices for the two level transformation are as follows:

$$\left[T_{a-\alpha} \right] = \frac{2}{3} \begin{bmatrix} 1/2 & 1/2 & 1/2 \\ 1 & -1/2 & -1/2 \\ 0 & \frac{\sqrt{3}}{2} & \frac{\sqrt{3}}{2} \end{bmatrix} \tag{3.2}$$

$$\left[T_{a-d} \right] = \begin{bmatrix} 1 & 0 & 0 \\ 0 & \cos(\theta) & \sin(\theta) \\ 0 & \sin(\theta) & -\cos(\theta) \end{bmatrix} \tag{3.3}$$

where $\theta = \omega t$ is the phase of the unit vector locked in with the phase-a voltage.

The reference voltages $V_{0_{ref}}$,$V_{d_{ref}}$ and $V_{q_{ref}}$ are obtained by determining the d-q-0 values under normal conditions (i.e. in the absence of any voltage disturbances). Since phase-a is chosen as the reference, the 0,d,q co-ordinates are (0,0,1). Thus the balanced and sinusoidal voltage set, $v_a(t) = V_1 \sin(\omega t), v_b(t) = V_1$ $sin(\omega t - \frac{2\pi}{3})$ and $v_c(t) = V_1 \sin(\omega t + \frac{2\pi}{3})$ corresponds to (0,0,1) in the 0-d-q domain. The equation for co-ordinate transformation is given by

$$\left[V_{F_0} \;\; V_{F_d} \;\; V_{F_q} \right]^T = \left[T_{a-d} \right] \cdot \left[T_{a-a} \right] \cdot \left[V_{F_a} \;\; V_{F_b} \;\; V_{F_c} \right]^T \tag{3.4}$$

The transformed voltages are subtracted from the reference values to obtain the error signal for cancelling out the zero-sequence and harmonic components in the voltage. Hence the corresponding error voltages are obtained as

$$\begin{bmatrix} V_{error-0} \\ V_{error-d} \\ V_{error-q} \end{bmatrix} = \begin{bmatrix} V_{0_{ref}} - V_{F_0} \\ V_{d_{ref}} - V_{F_d} \\ V_{q_{ref}} - V_{F_q} \end{bmatrix} \tag{3.5}$$

Finally the desired compensator reference voltage signals are obtained through inverse transformation to the a-b-c domain as follows:

$$\left[V_{C_{a2}} \;\; V_{C_{b2}} \;\; V_{C_{c2}} \right]^T = \left[T_{a-a} \right] \cdot \left[T_{d-a} \right] \cdot \left[V_{error_0} \;\; V_{error_d} \;\; V_{error_q} \right]^T \cdot K_V \tag{3.6}$$

where K_V is the gain of the VCU. The transformation matrices are given by

$$\left[T_{d-a} \right] = \left[T_{d-a} \right]^{-1} = \left[T_{a-d} \right] \tag{3.7}$$

$$\left[T_{a-a} \right] = \frac{3}{2} \begin{bmatrix} 2/3 & 2/3 & 0 \\ 2/3 & -1/3 & \frac{1}{\sqrt{3}} \\ 2/3 & -1/3 & -\frac{1}{\sqrt{3}} \end{bmatrix}. \tag{3.8}$$

The internal block diagram of the voltage compensation unit representing the procedure described above is shown in Fig. 3.2.

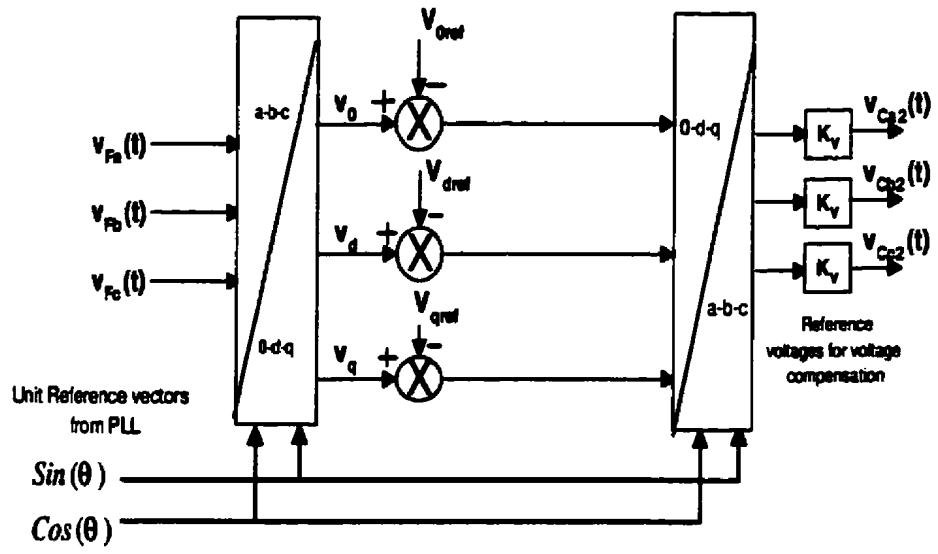

Figure 3.2: Voltage compensation unit

3.2.2 Harmonic Current Extraction Unit(HCEU)

The function of the harmonic current extraction unit, as the name suggests, is to extract the harmonic component of the supply current(or compensator current).

This current, scaled by R_h, combined with the voltage signals derived by the voltage compensation unit, forms the voltage reference for the inverter.

Several harmonic extraction schemes have been developed such as IRP based schemes proposed by Peng et al. [10] and Watanabe et al. [14], the synchronous frame based scheme by Divan et al. [11], notch filter based schemes [12] and schemes based on current feedback [16]. The IRP based scheme and the notch filter schemes are feed-forward control schemes that extract the harmonic component of the supply currents and use that information to simulate a series harmonic resistor. Dixon's scheme [16] is based on current feedback in which the supply current is forced to track a desired sinusoidal reference thereby emulating a sinusoidal current source.

The advantages of feed-forward schemes are fast-response and fewer sensor requirements as compared to a feedback control scheme. The down-side is that they are highly sensitive to gain inaccuracies due to nonlinearities in the filter impulse response and quantization errors. The feedback control scheme on the other hand is self regulatory (zero steady state error) but suffers from a relatively slow dynamic response. Quick response time is crucial in a power system environment in the proximity of fluctuating loads such as arc furnaces and adjustable speed drives.

The d-q-0 based harmonic estimation scheme was developed as a simple solution to the estimation problem to primarily overcome the drawbacks of the IRP based harmonic extraction scheme. The development of the proposed scheme is discussed

in two stages, the second stage being a more robust and effective version of the previous one.

1. Harmonic current extraction scheme based on synchronous d-q-0 transformation: Method 1

This method takes a step in the direction of making an improvement in Peng's [10] method of harmonic extraction. The currents are decoupled from the voltages, so that voltage imbalance does not affect the extraction procedure. The block diagram representing the extraction procedure is shown in Fig. 3.3.

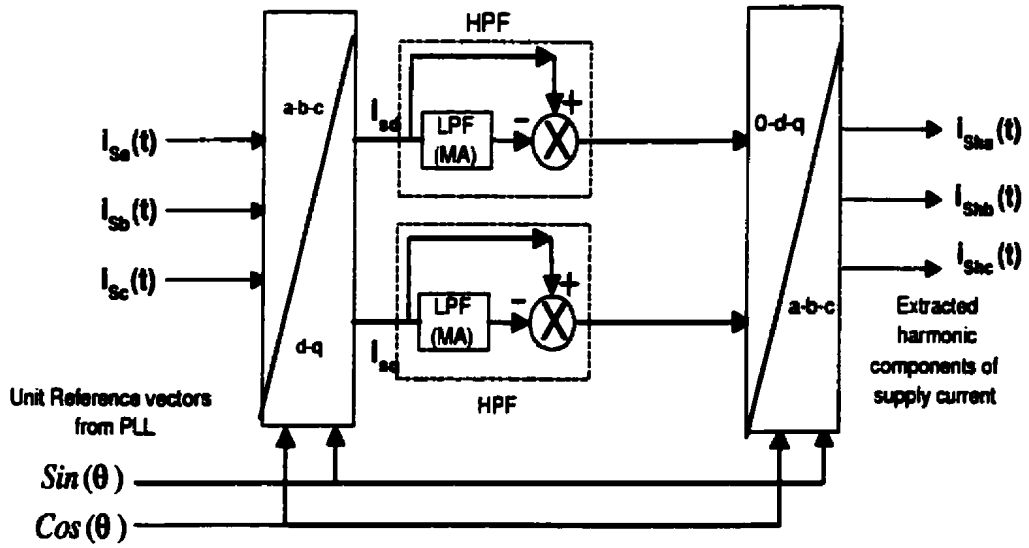

Figure 3.3: A scheme for extracting current harmonics: Method 1

The supply (compensator) currents are measured and synchronously transformed into d-q-0 coordinates through a PLL (locked to one of the phase voltages, i.e. phase-a). The dc components corresponding to the fundamental frequencies are eliminated

using a moving average (MA), finite impulse response (FIR) filter and a summer. The order of the moving average filter is decided by the sampling frequency, since, in order to average the samples over a fundamental period T_1, the sampling period T_s, is related to the fundamental period T_1 by $T_1 = N_s \cdot T_s$ where N_s is the total number of samples per cycle. The moving average filter extracts the dc component alone (provided the sampling times are properly adjusted). The dc signal is then subtracted from the original signal to give the harmonic component. The spectral shifts associated with the transformation under balanced and unbalanced loading conditions are illustrated below.

a) Shift in frequency spectra for balanced currents

If all the supply currents are balanced (may be non-sinusoidal but do not contain zero or negative sequence components), the components at the fundamental frequency are transformed to dc quantities. Also, all the harmonics are transformed to non-dc quantities and undergo a frequency shift of 60Hz in the spectrum.

The transformed signals in the d-q domain are represented by the subscript 'dq'.

$$i(f_n t) \longrightarrow i_{dq}(f_{n-1} t) \ , \ n \geq 1 \tag{3.9}$$

where, $i(f_n t)$ represents the n^{th} harmonic of the current signal entering the d-q transformation block. Also note that $i(f_0 t)$ and $i(f_1 t)$ represent the dc current component and the fundamental component respectively. Under balanced conditions, the linearity of the transformation is retained (i.e one frequency component in the a-b-c frame

gives rise to only one component (although the frequency may be translated) in the d-q frame. This results in a one-sided spectral shift.

b) Shift in frequency spectra for unbalanced currents

With unbalanced currents, each component translates to two sidebands. Consider the example shown in Fig. 3.4. The first part of the figure shows the corresponding d-q components of current signals comprising the first, third and fifth harmonics, $i(f_1 t)$, $i(f_3 t)$ and $i(f_5 t)$, respectively. The fundamental component translates to a dc component and a second harmonic component. The inverse transformation produces undesired fundamental sequence in the harmonic estimate as shown in the second part of Fig. 3.4.

The reference signal to the PWM inverter must not contain any traces of the fundamental component. If there is a fundamental component, the compensator will tend to offer some resistance to the component, thereby affecting the power flow. The magnitude of the fundamental component reflected in the extracted currents is heavily dependent on the degree of imbalance in the three phases. The performance of the harmonic extraction procedure outlined above is studied for the following cases:

i) Balanced three-phase loads with harmonics and no zero sequence components;

ii) Balanced three-phase currents with harmonics and zero sequence components;

iii) Unbalanced three-phase currents with harmonics and zero sequence components;

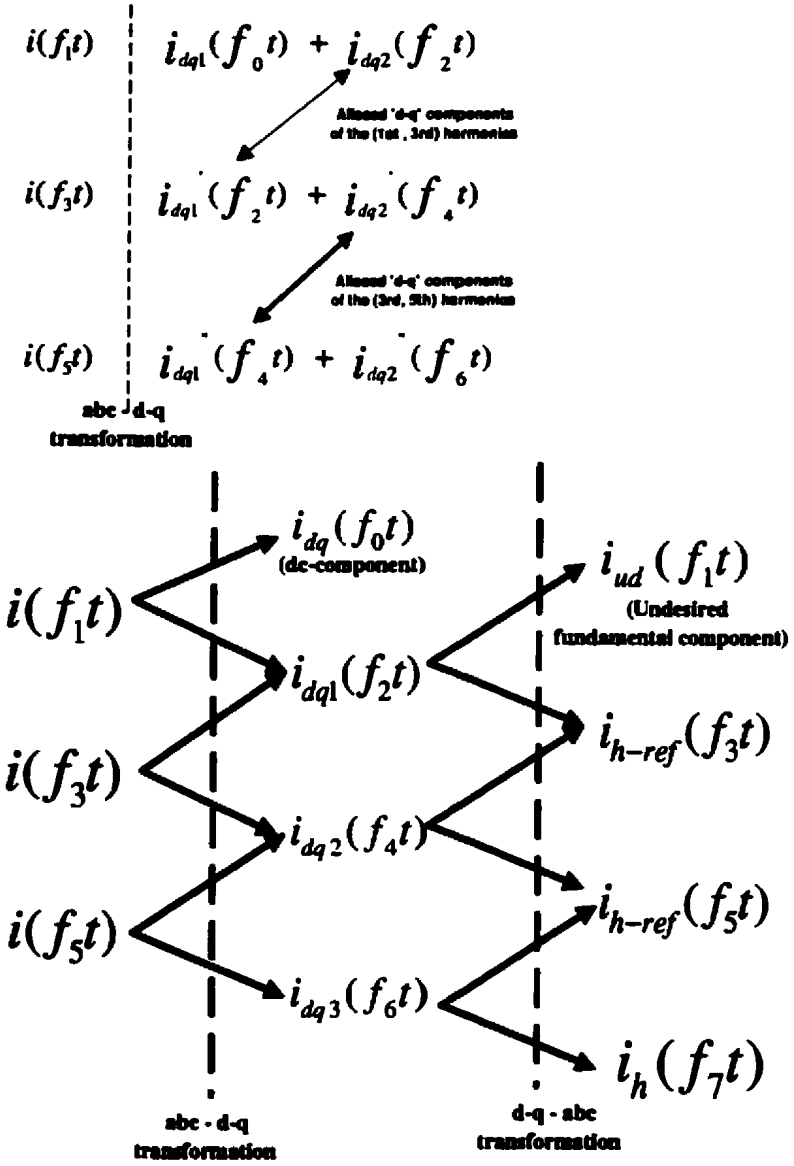

Figure 3.4: Aliasing in the d-q domain due to unbalanced currents

It is assumed that the supply current has a total harmonic distortion (THD_i) of 26%. The algorithm was tested using the SIMULINK toolbox in MATLAB [18]. The setup is shown in Fig. 3.5 and the details of the SIMULINK blocks and models are given in Appendix A.

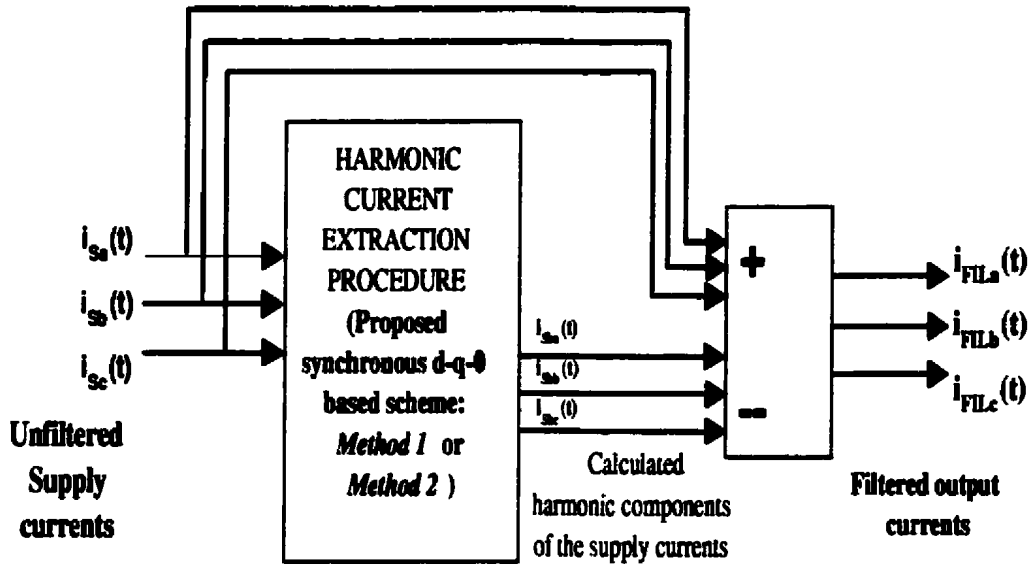

Figure 3.5: Controller test setup

i) Performance under balanced load conditions

In the balanced case there are no zero sequence components. The individual contributions of the harmonics is summarized in Table 3.1. Fig. 3.6, shows the waveforms for the balanced case. The corresponding frequency spectra are shown in Fig. 3.7.

As can be seen from Fig. 3.7, the filtered current $i_{FIL_a}(t)$ does not contain any harmonics. The extracted harmonic current, $i_{S_{h_a}}(t)$, is devoid of the fundamental

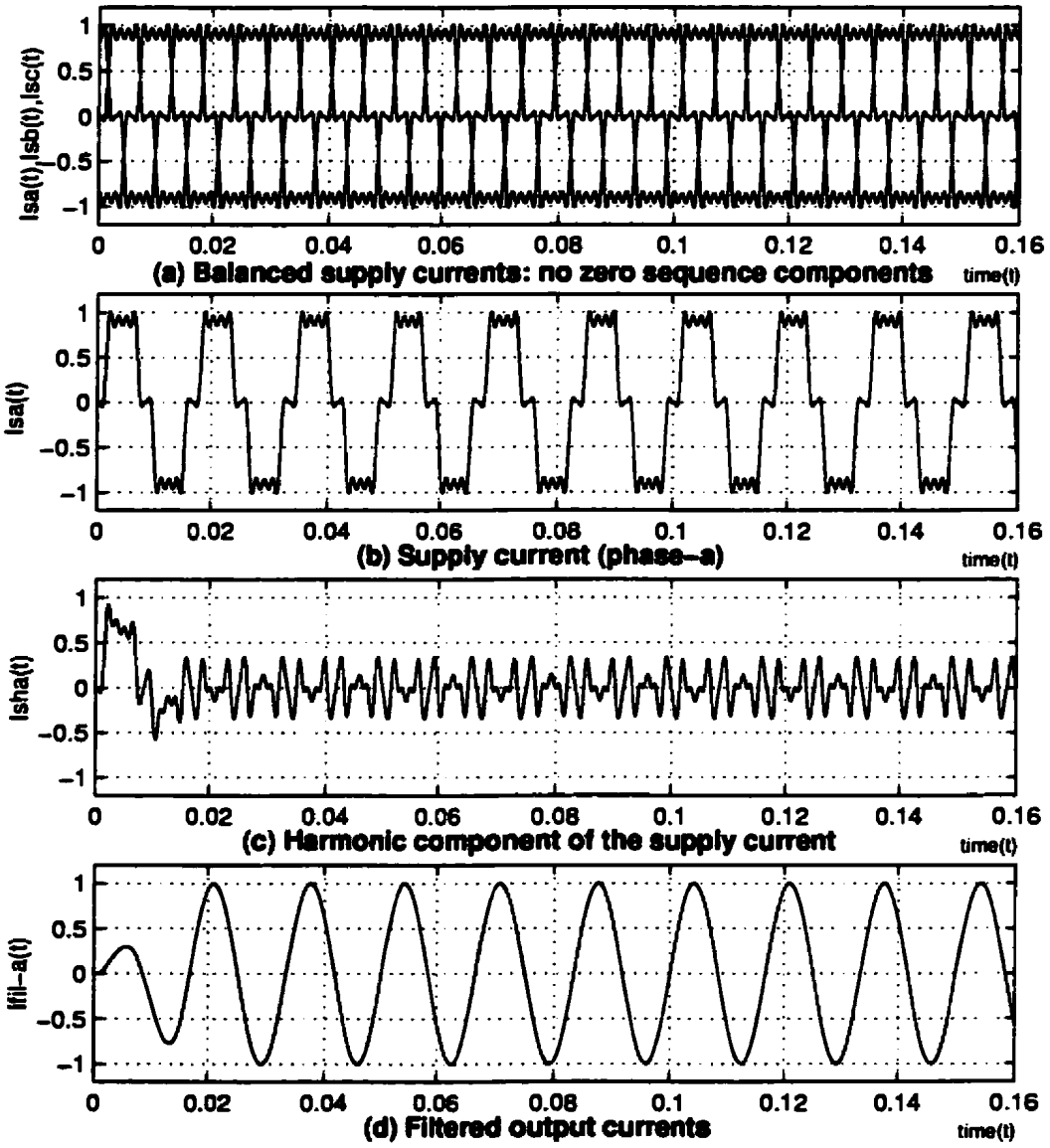

Figure 3.6: Case-1: Current waveforms for balanced supply currents: Method 1

Table 3.1: Harmonic components of the supply currents (THD = 25%) for a balanced set

Harmonic Number(n)	$\frac{I_{S_n}}{I_{S_1}} X100$
3	0
5	20
7	14.3
11	9.1

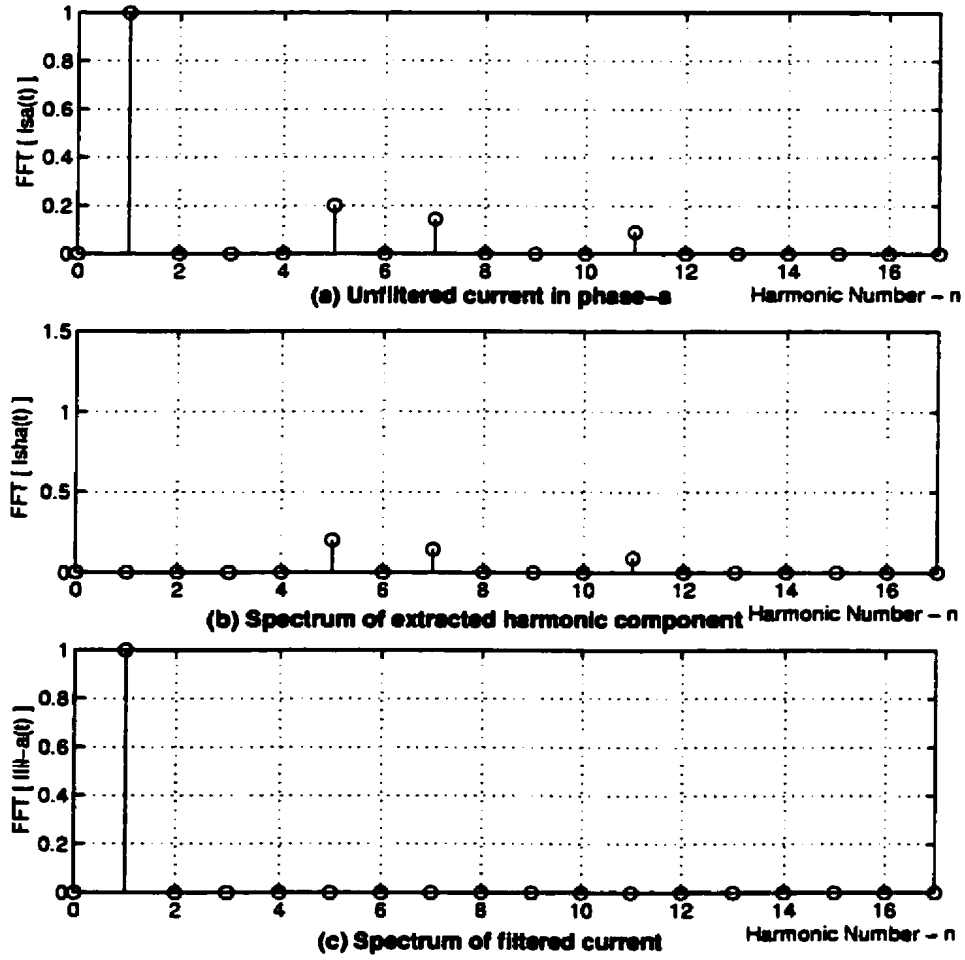

Figure 3.7: Case-1: Frequency spectra of the unfiltered and filtered currents: Method 1

component. Thus, the control scheme works fine in the balanced case.

ii) Performance in the presence of zero-sequence components

A third harmonic is introduced as a zero sequence component in addition to the other harmonics. The individual contributions of the harmonics is summarized in Table 3.2. Fig. 3.8, shows the waveforms for the unfiltered and filtered currents

Table 3.2: Harmonic components of the supply currents (THD = 25%) with zero sequence

Harmonic Number(n)	$\frac{I_{S_n}}{I_{S_1}} X100$
3	10
5	20
7	14.3
11	9.1

when a zero sequence component is introduced. The corresponding frequency spectra are shown in Fig. 3.9. The spectrum of the extracted harmonics, $i_{S_{h_a}}(t)$ shown in Fig. 3.9(b) indicates that the third harmonic zero sequence component is not detected in the extracted harmonic current. Hence, the filtered current has a third harmonic component.

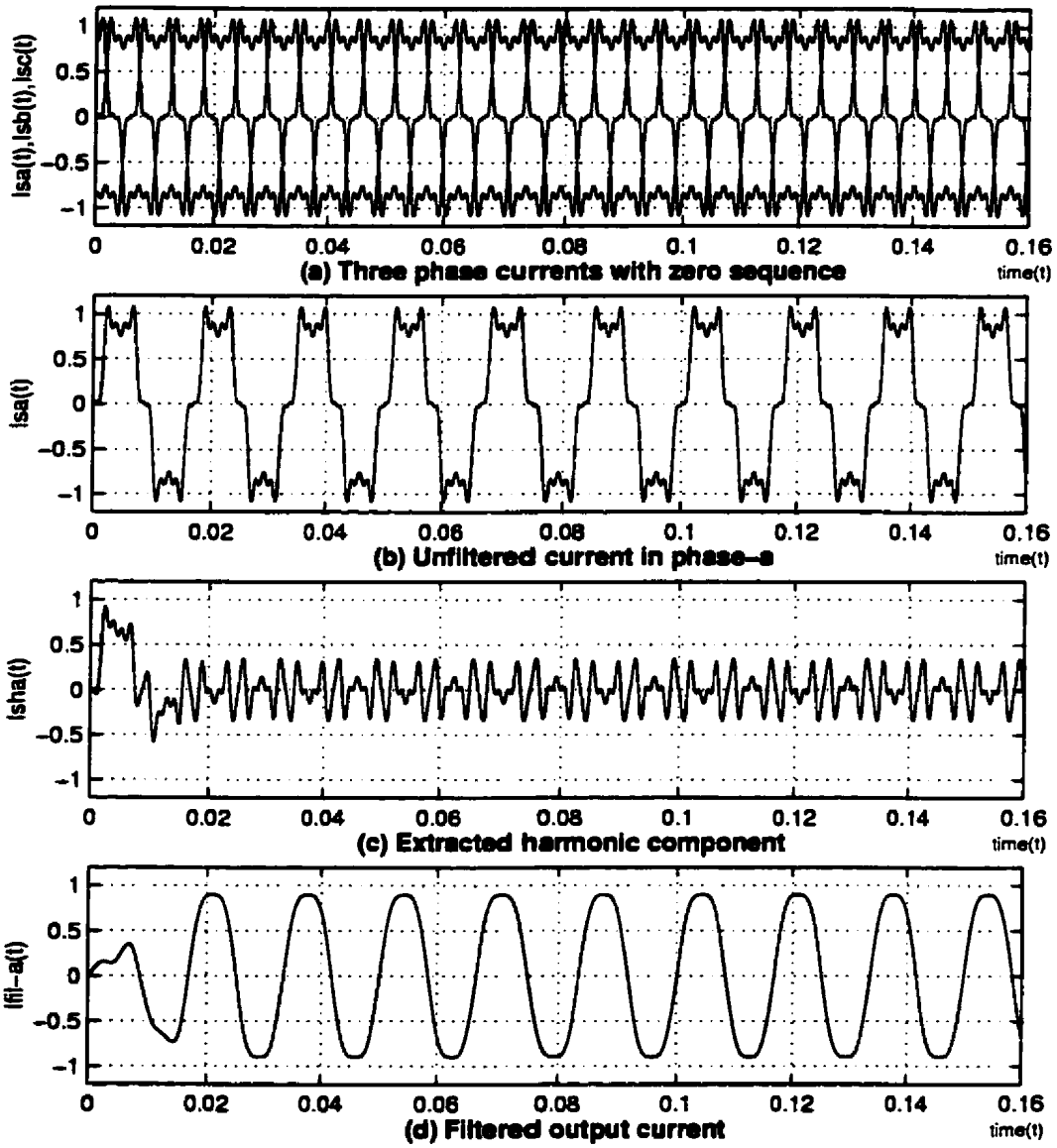

Figure 3.8: Case-2: Current waveforms for balanced supply currents with zero sequence components: Method 1

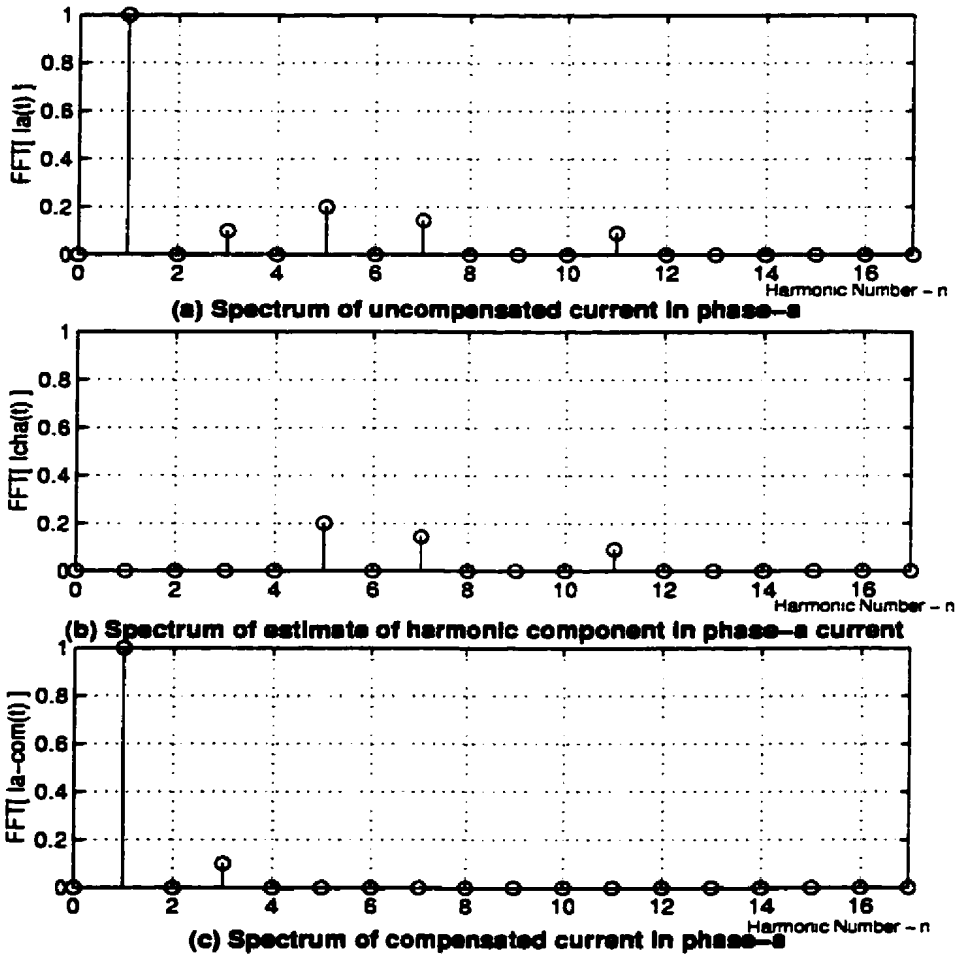

Figure 3.9: Case-2: Frequency spectra of the supply and filtered currents: Method 1

iii) Performance in the presence of unbalanced currents

A significant imbalance is introduced to illustrate the ineffectiveness of this method when the loads are not balanced. The degree of imbalance in phase-a is (50%), while that in phase-b is (30%). The individual contributions of the harmonics is summarized in Table 3.3. Fig. 3.10, shows the waveforms for the unfiltered and

Table 3.3: Harmonic components of supply current (THD = 25%) for an unbalanced set

Harmonic Number(n)	$\frac{I_{S_n}}{I_{S_1}} X100$		
	$I_{a_n}(\%)$	$I_{b_n}(\%)$	$I_{c_n}(\%)$
3	5	7	10
5	10	14	20
7	7.15	9.9	14.3
11	4.55	6.3	9.1

filtered currents. The corresponding frequency spectra are shown in Fig. 3.11.

As described earlier in the d-q theory, the imbalance in the load currents leads to the translation of a base frequency current signal $i(f_n t)$ into sidebands, $i'(f_{n-1}t) + i''(f_{n+1}t)$ in the d-q domain. As a result, the fundamental component translates into a dc and a second harmonic. The second harmonic component passes through the HPF unfiltered thereby reflecting as an undesired fundamental component in the estimated harmonic current, $i_{S_{h_a}}(t)$ shown in Fig. 3.11(b). Imbalance also contributes to the zero sequence which in turn is not detected. The consequence of these problems is the evident distortion in the filtered current $i_{FIL_a}(t)$ shown in Fig. 3.11(c)).

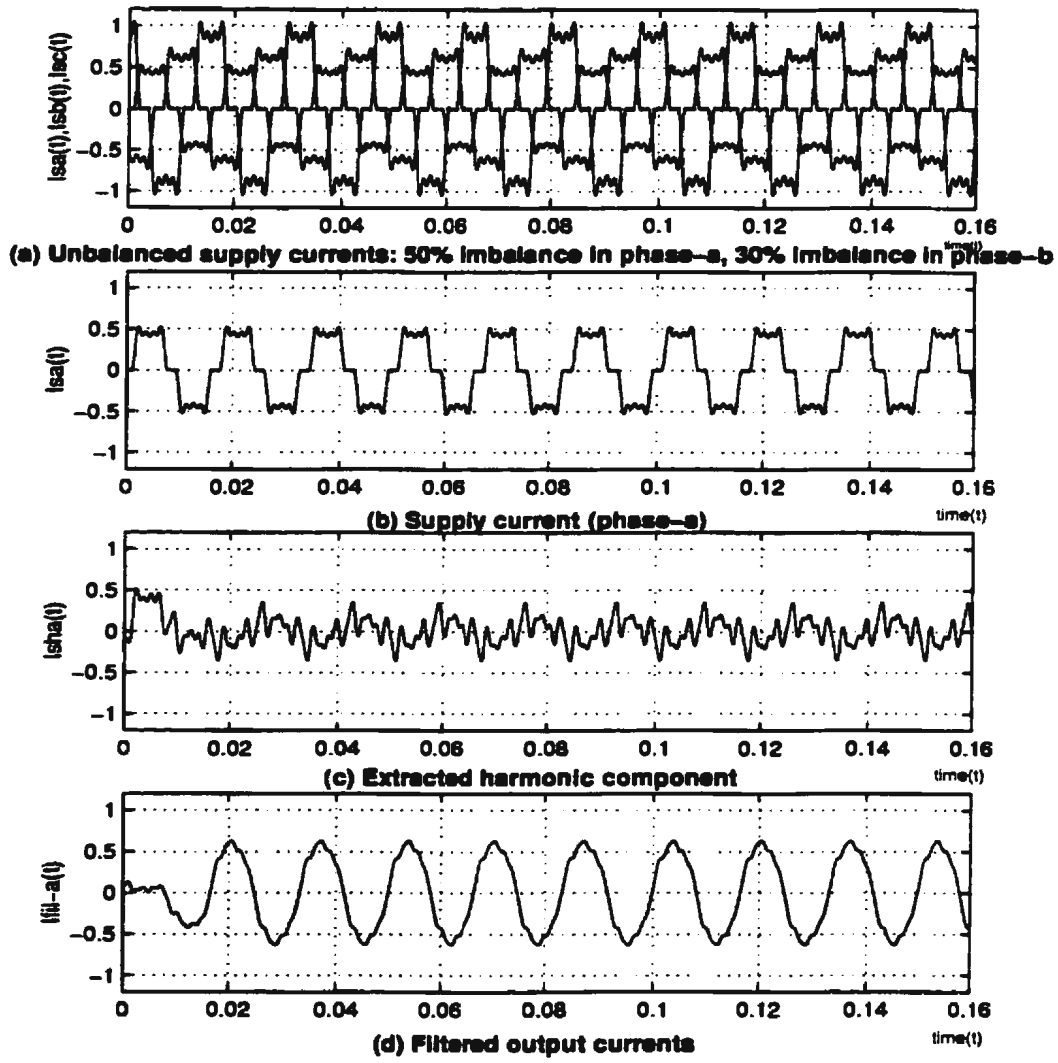

Figure 3.10: Case-3: Current waveforms for unbalanced supply currents: Method 1

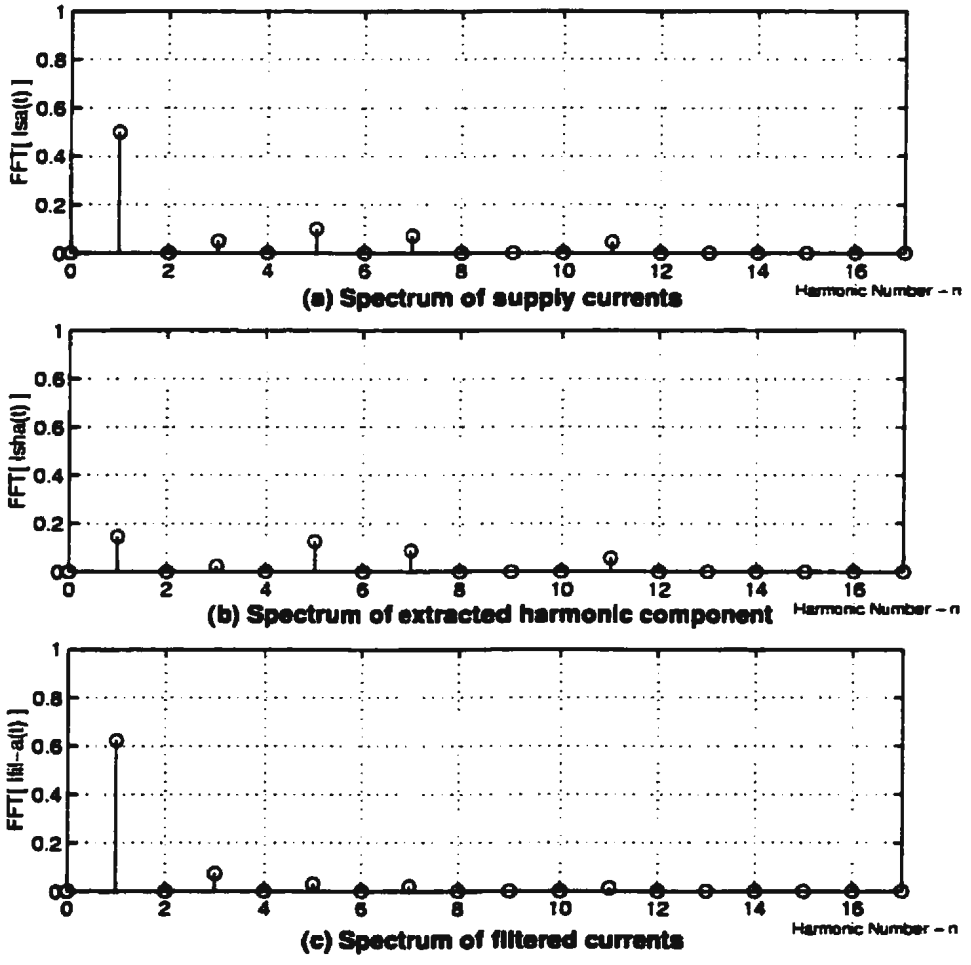

Figure 3.11: Case-3: Frequency spectrum of supply and filtered currents: Method 1

The scheme proposed above is much simpler as far as computational complexity is concerned. However, as illustrated above, this method cannot be applied to unbalanced currents or to currents that contain zero sequence components. A further improvement in the direction of a more robust scheme is described in the next section.

2. Harmonic current extraction scheme based on synchronous d-q-0 transformation with decoupling - Method 2

As was discussed in the previous section, the control scheme based on d-q transformation and filtering proves ineffective for unbalanced load currents. This provided the motivation to develop a new harmonic extraction procedure to overcome this limitation.

Decoupling the individual phase currents removes the aliasing in the d-q components described in Method 1. A notch filter can be used for each phase to block the fundamental component and pass all harmonics. However, the design of a notch filter is difficult and suffers from phase distortion and tuning problems, especially if the order of the filter is high, i.e has an extremely small reject band. Phase distortion is unacceptable for harmonic isolation. Starting with the basic extraction procedure for balanced currents shown in Fig. 3.3, the following modifications are made to increase the robustness of the scheme.

- For each phase current, say phase-a current i_{S_a}(t), a set of delayed signals $i_{S_{a1}}(\omega t) = i_{S_a}(\omega t - \frac{2\pi}{3})$ and $i_{S_{a2}}(\omega t) = i_{S_a}(\omega t - \frac{4\pi}{3})$ are generated from the phase

current, $i_{S_a}(t)$ and processed independently as shown in Fig. 3.12. The delays can be implemented through a set of phase-shifters or linear phase digital filters. If the current set is generated in the discrete domain, the delay times have to be calculated based on the sampling frequency and filter order. By delaying the signals, the zero and negative sequence components at the fundamental frequency can be eliminated before the synchronous d-q-0 is transformation is applied. This ensures that the harmonic estimate does not contain any trace of the fundamental frequency component.

- The set of currents, $i_{S_a}, i_{S_{a1}}$ and $i_{S_{a2}}$, is free from zero or negative sequence components at the fundamental frequency. This initial removal of zero sequence is repeated for the other two phases. Figure 3.12 shows the details of the proposed harmonic current extraction procedure for a three-phase system. The modification in this circuit over that of Fig. 3.3 is the decoupling and pre-filtering of the zero sequence component. The idea of removing the zero sequence components (including the fundamental component) before applying the required transformations is done to ensure that the zero sequence current will not give rise to alternating components in the synchronous frame causing error in the filtered output.

There are three similar units for the three-phase currents. The high pass filter removes the dc component. An inverse [d-q-0 to a-b-c] transformation yields the

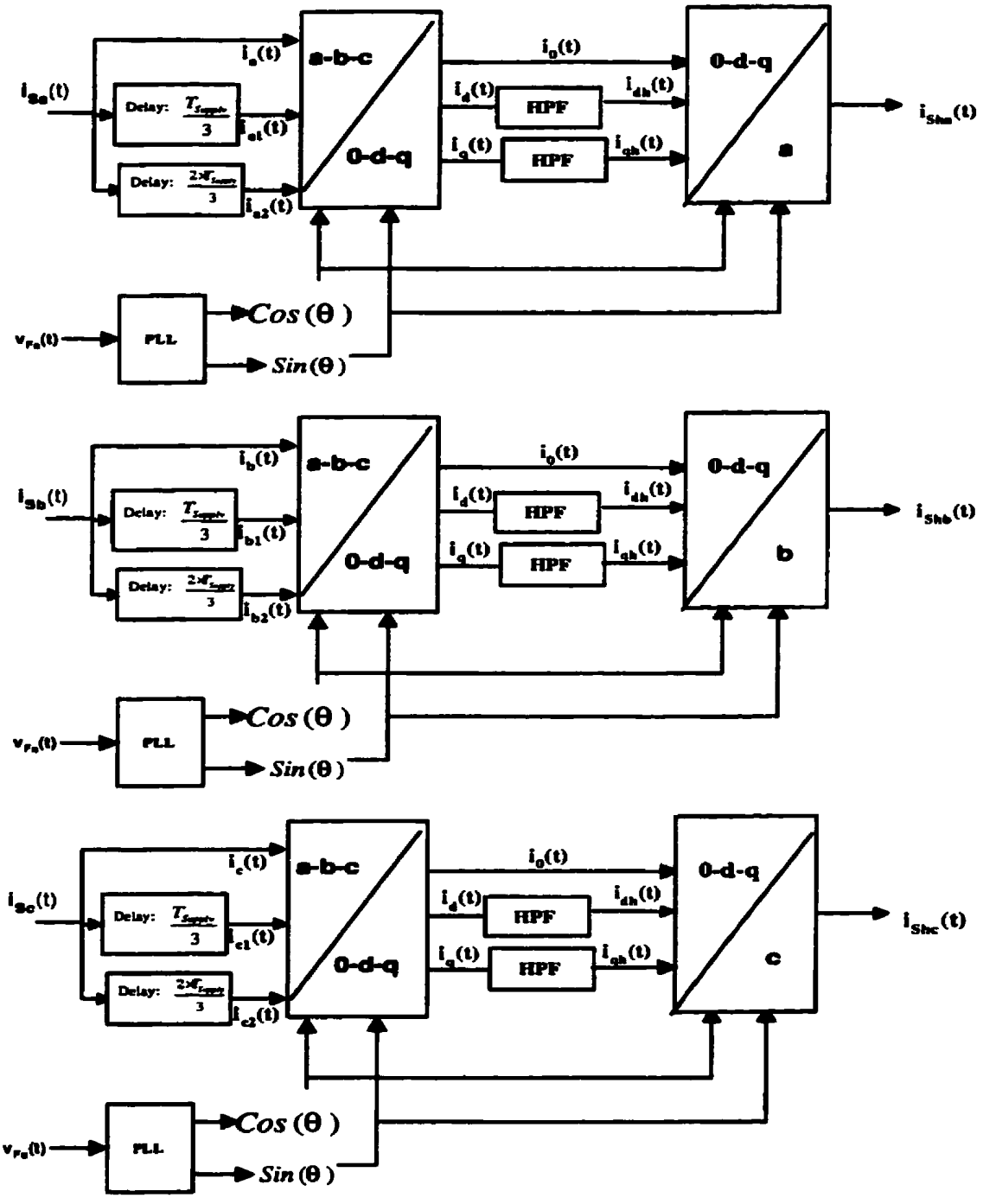

Figure 3.12: Decoupled harmonic current extraction unit (DHCEU) for a three-phase system

harmonic component of the supply current $i_{S_{h_a}}(t)$.

$$i_{S_{h_a}} = \begin{bmatrix} 1 & \cos(\theta) & \sin(\theta) \end{bmatrix} \cdot \begin{bmatrix} i_0 \\ i_{d_h} \\ i_{q_h} \end{bmatrix} \tag{3.10}$$

The harmonic current extraction procedure in the proposed scheme thus involves decoupling, transformation and filtering. Current decoupling is instrumental in overcoming problems associated with load current imbalance.

The decoupled harmonic current extraction (DHCE) scheme is tested for the same three conditions as the earlier proposed non-decoupled d-q based scheme. Test cases to illustrate the effect of imbalance and zero-sequence on extraction are discussed below. The details of the SIMULINK blocks and models are given in Appendix A.

i) Performance of the DHCE scheme under balanced load conditions

Fig. 3.13 shows the waveforms for the balanced case. The corresponding frequency spectra are shown in Fig. 3.14. Filtering is effective as in Method 1. Figure 3.14(c) shows the FFT of the filtered current $i_{FIL_a}(t)$, which indicates that it is clear from all harmonics.

ii) Performance of the DHCE scheme in the presence of zero-sequence components

Figures 3.15 and 3.16 show the accuracy of the decoupled scheme in estimating the harmonic component in spite of the zero-sequence component. The change from three-to-two co-ordinate transformation to three-to-three co-ordinate transformation preserves information pertaining to the zero sequence component. The filtered

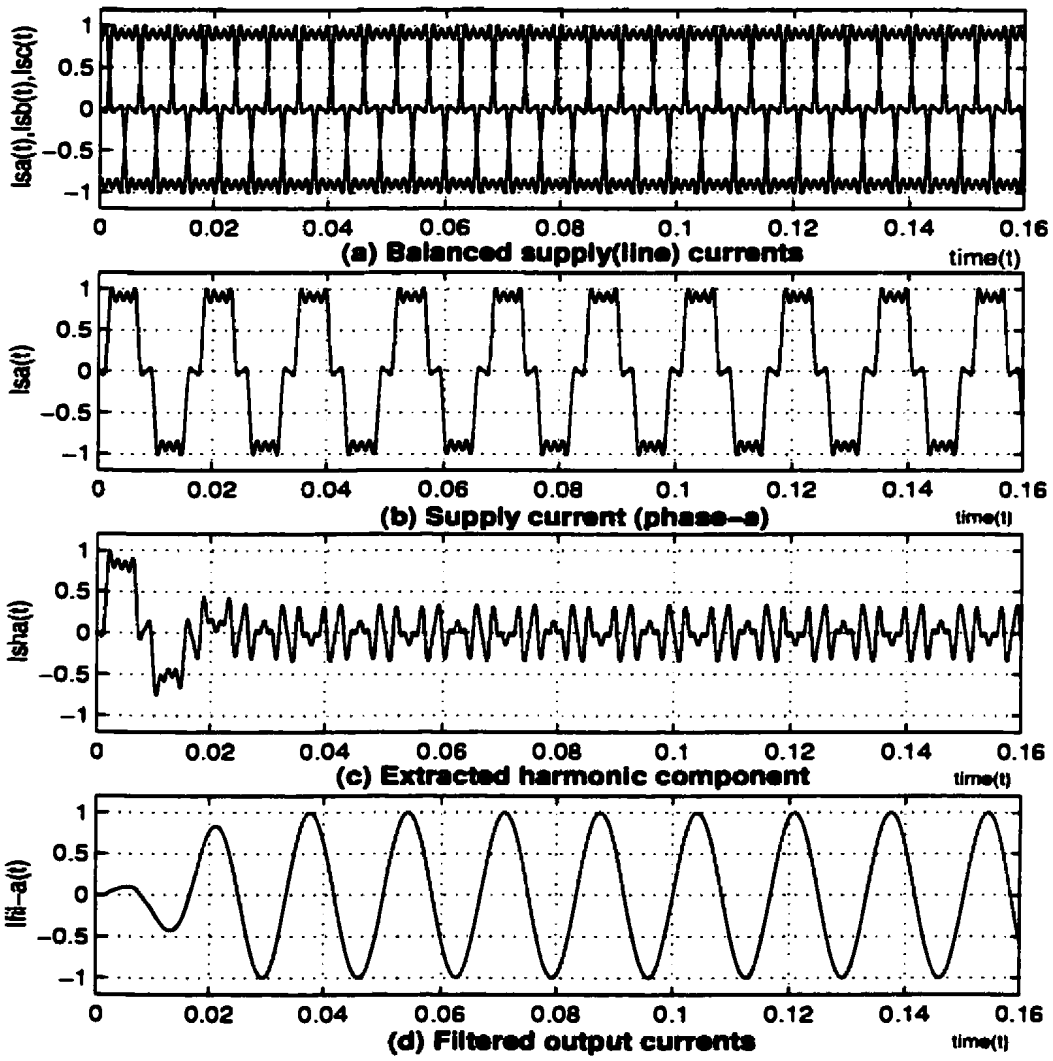

Figure 3.13: Case-1: Currents for balanced supply (line) currents : Method 2

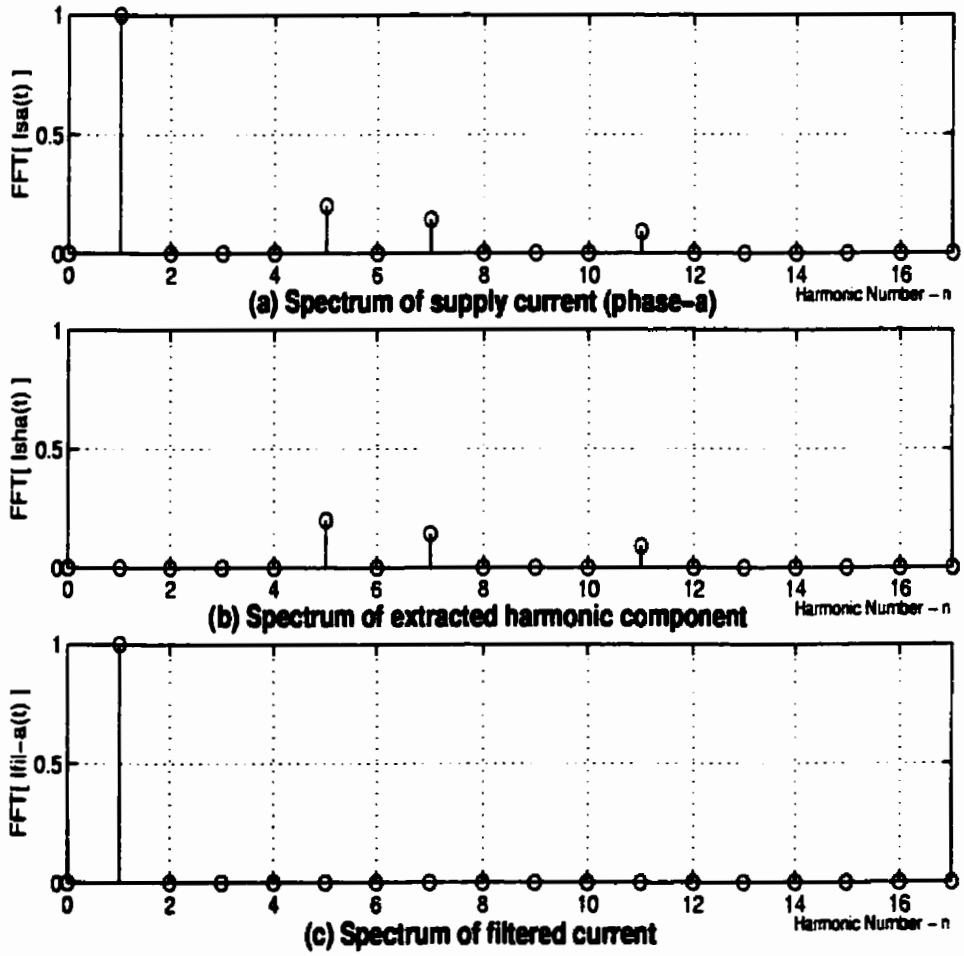

Figure 3.14: Case-1: Frequency spectra of supply and filtered currents : Method 2

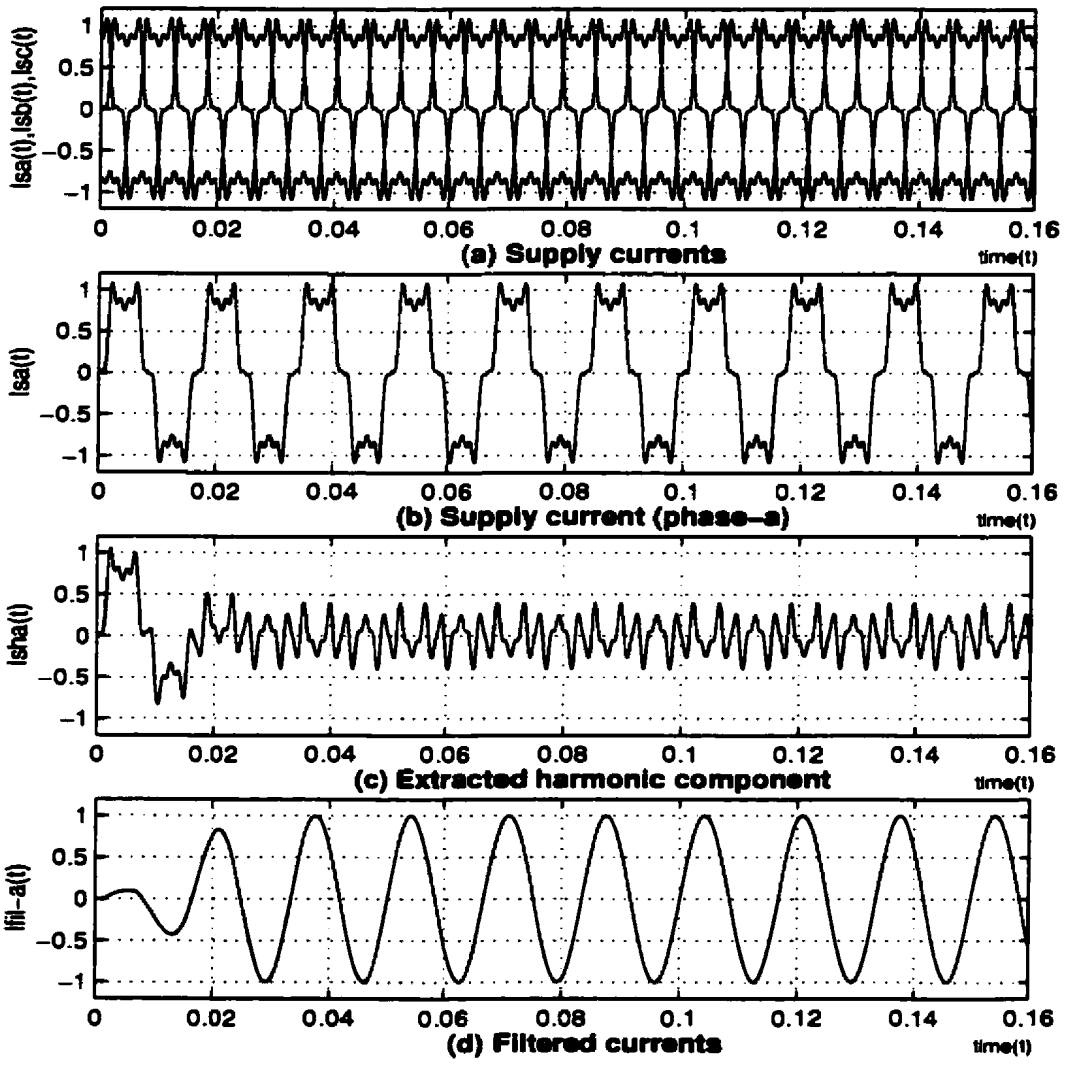

Figure 3.15: Case-2: Current waveforms for balanced supply currents with zero sequence components: Method 2

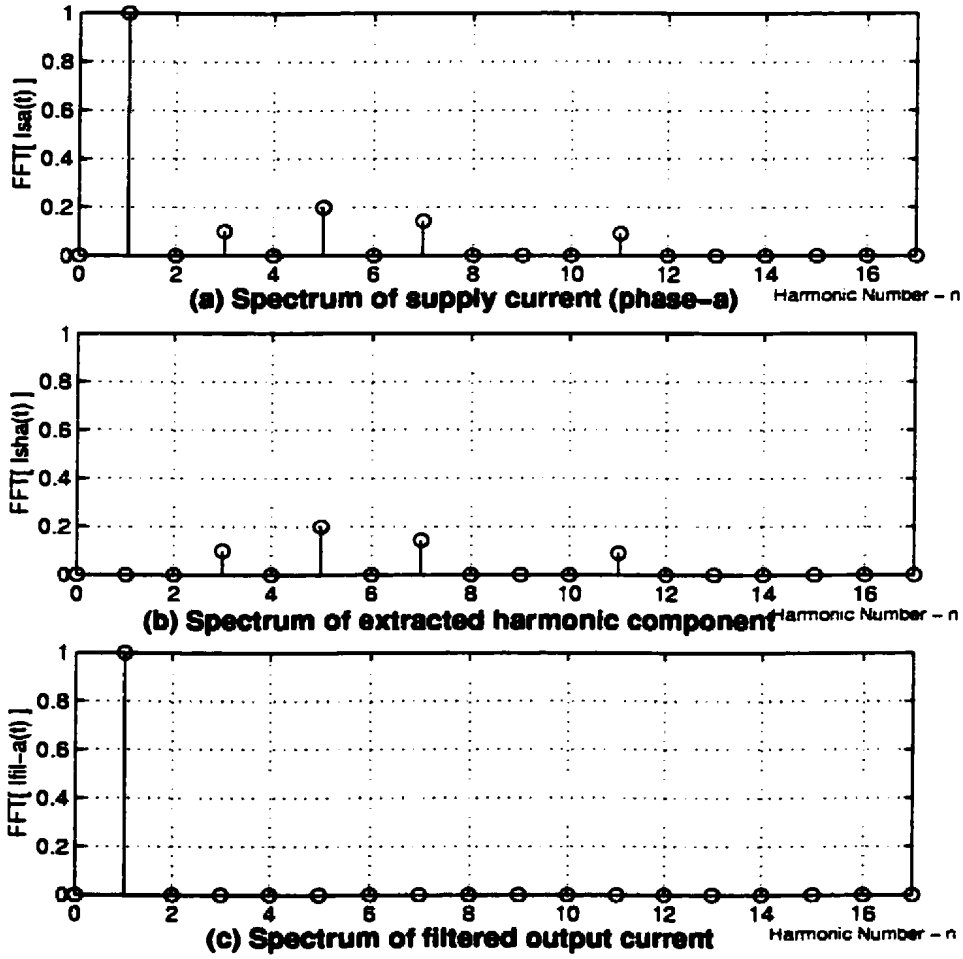

Figure 3.16: Case-2: Frequency spectra of supply and filtered currents : Method 2

current $i_{FIL_a}(t)$ is almost sinusoidal, as can be seen from the nature of the waveforms in Fig. 3.15(d) and the FFT results shown in Fig. 3.16(c).

iii) Performance of the DHCE scheme in the presence of unbalanced currents

The same degree of imbalance as given in Table 3.3 for Method 1 is considered in this case. Figure 3.17 shows the waveforms for the unfiltered and filtered currents. The corresponding frequency spectra are shown in Fig. 3.18.

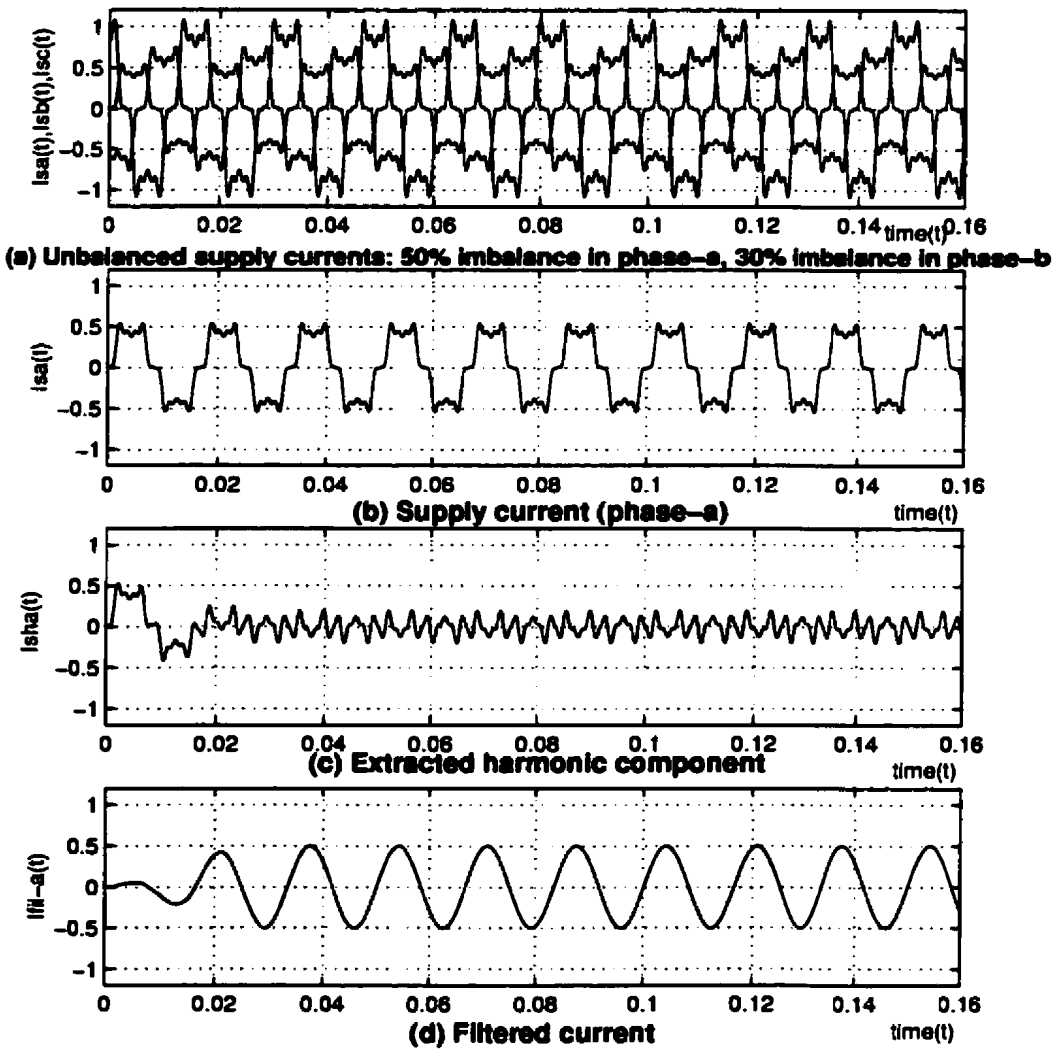

Figure 3.17: Case-3: Current waveforms for unbalanced supply currents: Method 2

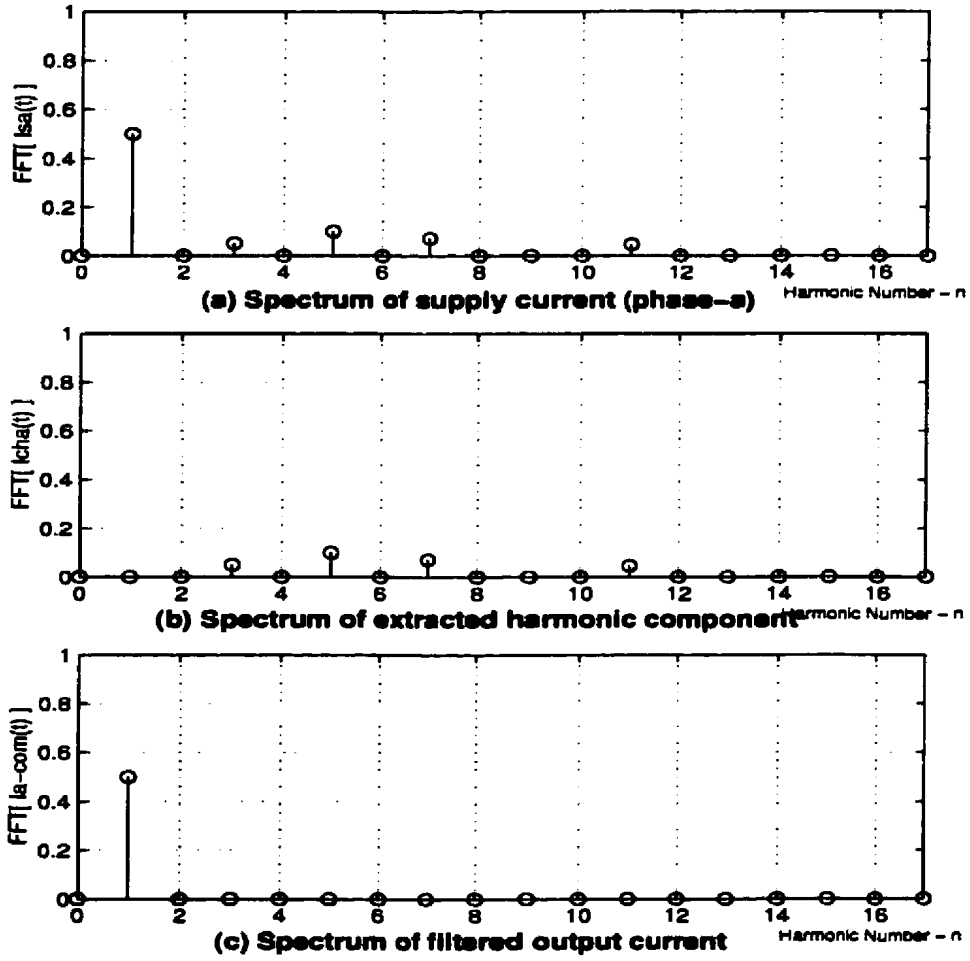

Figure 3.18: Case-3: Frequency spectra of supply and filtered currents: Method 2

As can be seen the decoupling helps in precise estimation of the harmonics. The removal of zero sequence components before applying the synchronous d-q-0 transformation and filtering helps in eliminating the aliasing shown in Fig. 3.4. Hence the proposed DHCE method is shown to be much more robust than the IRP based scheme. The problem however is in the computation complexity which is relatively higher than the other two harmonic extraction schemes (IRP-based method and the synchronous d-q transformation based on Method 1). The computational complexity is evaluated in terms of the number of floating point/integer multiplications, additions and divisions that must be performed to determine the harmonic components in the supply current. Table 3.4 presents a comparative study of the computation complexity of the three extraction procedures. It can be seen that the DHCE scheme is computationally more intensive than the other two schemes although the most accurate. Since accuracy of harmonic detection and quick response time are equally important parameters, the computation time of the DHCE scheme can be decreased by using faster and more hardware.

Table 3.4: Order of computation for IRP, d-q Method 1 and DHCE schemes

Harmonic extraction method	ADDs	MULs	DIVs	Total(operations)
IRP	15	50	2	67
d-q, Method 1	15	20	-	35
d-q-0, Method 2 (DHCE)	45	60	-	105

3.3 Simulation Results and Comparison with the IRP Based Scheme

The proposed DHCE algorithm is compared with the IRP-based scheme. Predetermined distorted signals (emulating the measured load voltages and compensator currents) were fed to the voltage and current control units. The parameters listed in Table 3.5 are used to simulate the two control schemes. The worst case operation was simulated for supply voltage imbalance, load voltage distortion of THD_v= 6% and supply current distortion (THD_i = 25%).

Table 3.5: Parameters for comparison between the IRP and DHCE extraction procedures

Line Voltage	$THD_v = 6\%$ Single-ph-sag= 25% (ph-a)
Supply-current	$THD_i = 25\%$ Zero-seq(3rd)=5%

Figure. 3.19 shows the simulation waveforms for the proposed DHCE scheme. The THD_i of the filtered output current is nearly zero, which indicates that the proposed extraction scheme works effectively even in the presence of imbalance and zero sequence components. The simulation waveforms for the same set of parameters for the IRP-based scheme are shown in Fig. 3.20. The THD_i of the filtered output current for the IRP based scheme is 11%. Thus the proposed DHCE scheme proved to be more effective and robust harmonic extraction scheme than the IRP based control scheme.

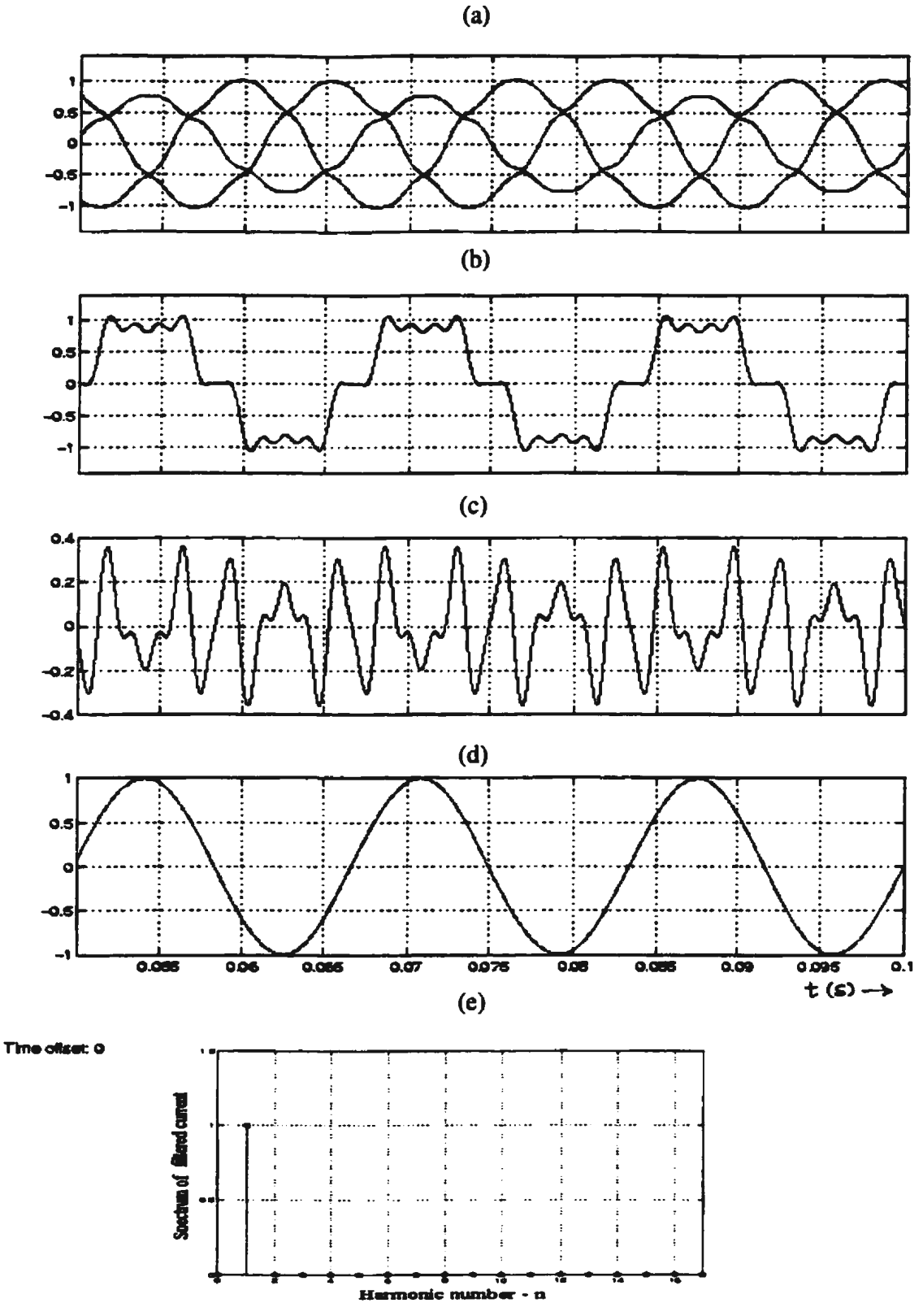

Figure 3.19: Simulation results using the proposed DHCE scheme, for unbalanced non-sinusoidal voltage (%Sag (phase-a) = 25, THD = 6%), non-sinusoidal supply current (THD = 25%) with zero sequence: (a) Supply voltage, (b) Supply current, (c) Extracted harmonic component of (b), (d) Filtered output current (phase-a) (e) Frequency spectrum of filtered output, (d) (THD ≈ 0%)

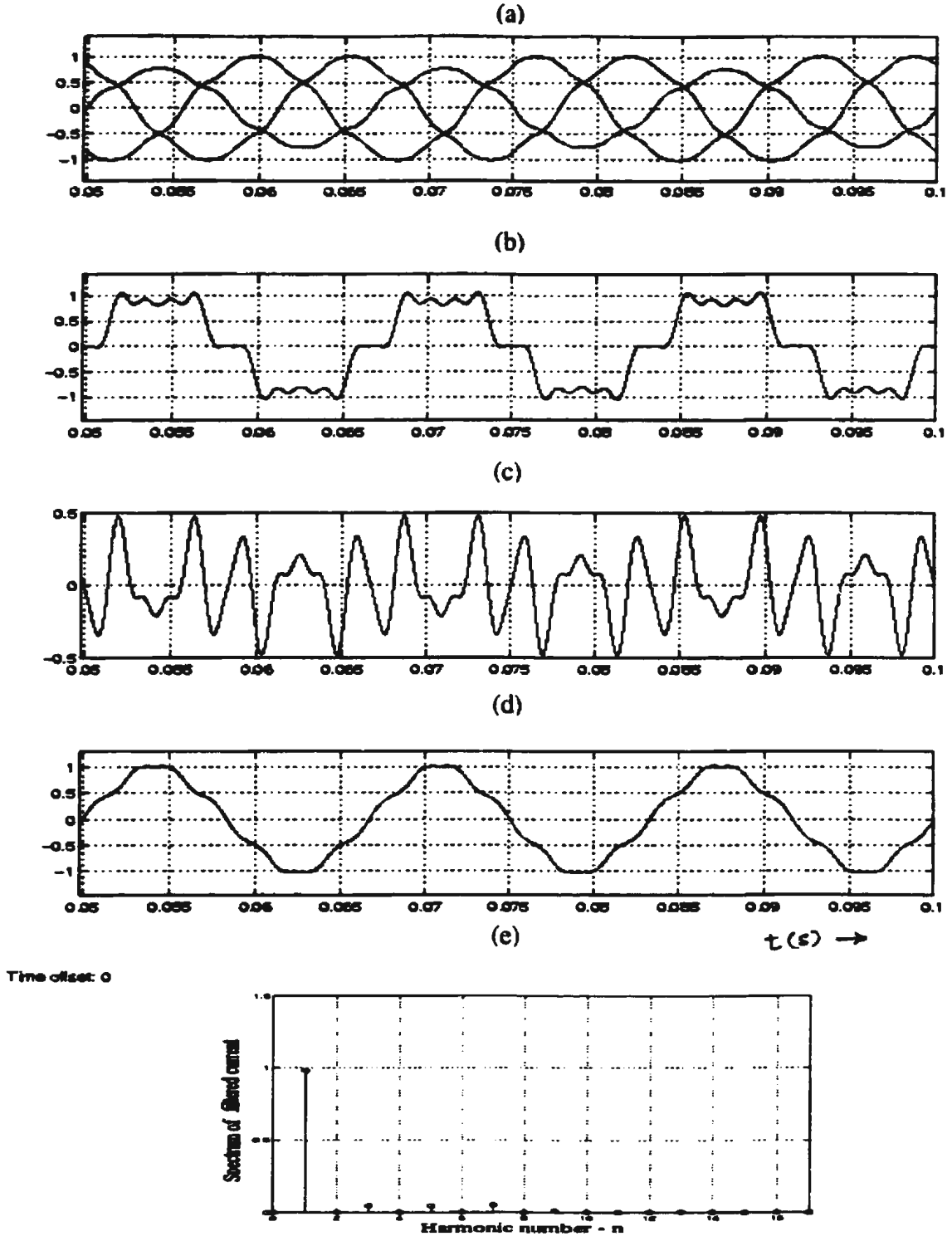

Figure 3.20: Simulation results using the IRP theory based control scheme, for unbalanced non-sinusoidal voltage (%Sag (phase-a) = 25, THD = 6%), non-sinusoidal supply current (THD = 25%) with zero sequence: (a) Supply voltage, (b) Supply current, (c) Extracted harmonic component of (b), (d) Filtered output current (phase-a) (e) Frequency spectrum of filtered output, (d) (THD = 11%)

3.4 Summary

This chapter has focused on the development of a control scheme based on synchronous d-q-0 transformation that facilitates voltage compensation and harmonic isolation in hybrid series compensators. It was shown that the current-decoupling technique followed by synchronous transformation and filtering helps in immunizing the harmonic extraction technique to zero-sequence components and imbalance.

Examples and simulation results were presented in the chapter to demonstrate the performance of the proposed scheme. For the same parameters, simulation results were also provided for both the decoupled harmonic extraction scheme and the instantaneous reactive power extraction scheme. The results showed that the decoupled harmonic extraction scheme was more effective even in the presence of imbalance and zero sequence components but was more computationally intensive by a factor of about 60%.

Chapter 4

Modelling And Analysis Of the Hybrid Series Compensators

Introduction

The control scheme for the hybrid series compensator was proposed and discussed in Chapter 3. Due to quantization errors, nonlinearity in the phase and magnitude response in the sensors and filters, fluctuations in the dc-link voltage, the loop gains, K_V and R_h, of the two control units, the voltage compensation unit (VCU) and the harmonic current extraction unit (HCEU), may not remain constant. The variations in K_V and R_h affect the stability of the compensator.

Demonstration of the filtering characteristics and controller implementation using the IRP theory was the main focus of Peng et al. [10]. Stability analysis was one aspect which was not investigated. When Peng's harmonic suppression principle is extended to voltage compensation, stability becomes a key issue. The effect of R_h and K_V on the system stability and the degree of voltage and current suppression are investigated in this chapter through single-phase circuit modelling and analysis.

4.1 Model of the Hybrid Series Compensator

The main components of the hybrid series compensator are shown in Fig. 4.1. The series compensator comprises three single-phase inverters, labelled as A, B, and C. A shunt passive filter, tuned to the dominant harmonics, is connected across the load to bypass the dominant harmonics. Two loads are connected to the load bus: A nonlinear load, which is an approximate model of a dc-drive, and a critical harmonic sensitive load.

Fig. 4.2 shows the single-phase phasor equivalent model of the hybrid system. The cumulative effect of the various nonlinear loads connected at the point of common coupling (PCC), the source voltage, which may contain harmonics (e.g. during faults), is represented by the Thevenin equivalent circuit, consisting of a fundamental voltage source V_{S_1} and a harmonic voltage source V_{S_h} in series with the impedance $\mathbf{Z_t}$. The series inverter, the output filter and the transformer are represented as a controlled voltage source V_C while the nonlinear load is approximated by a constant current source.

4.2 Analysis of the Hybrid Series Compensators

Single-phase analysis was the choice due to its simplicity, further justified by the following:

- The results of the single-phase analysis can be used for choosing the initial

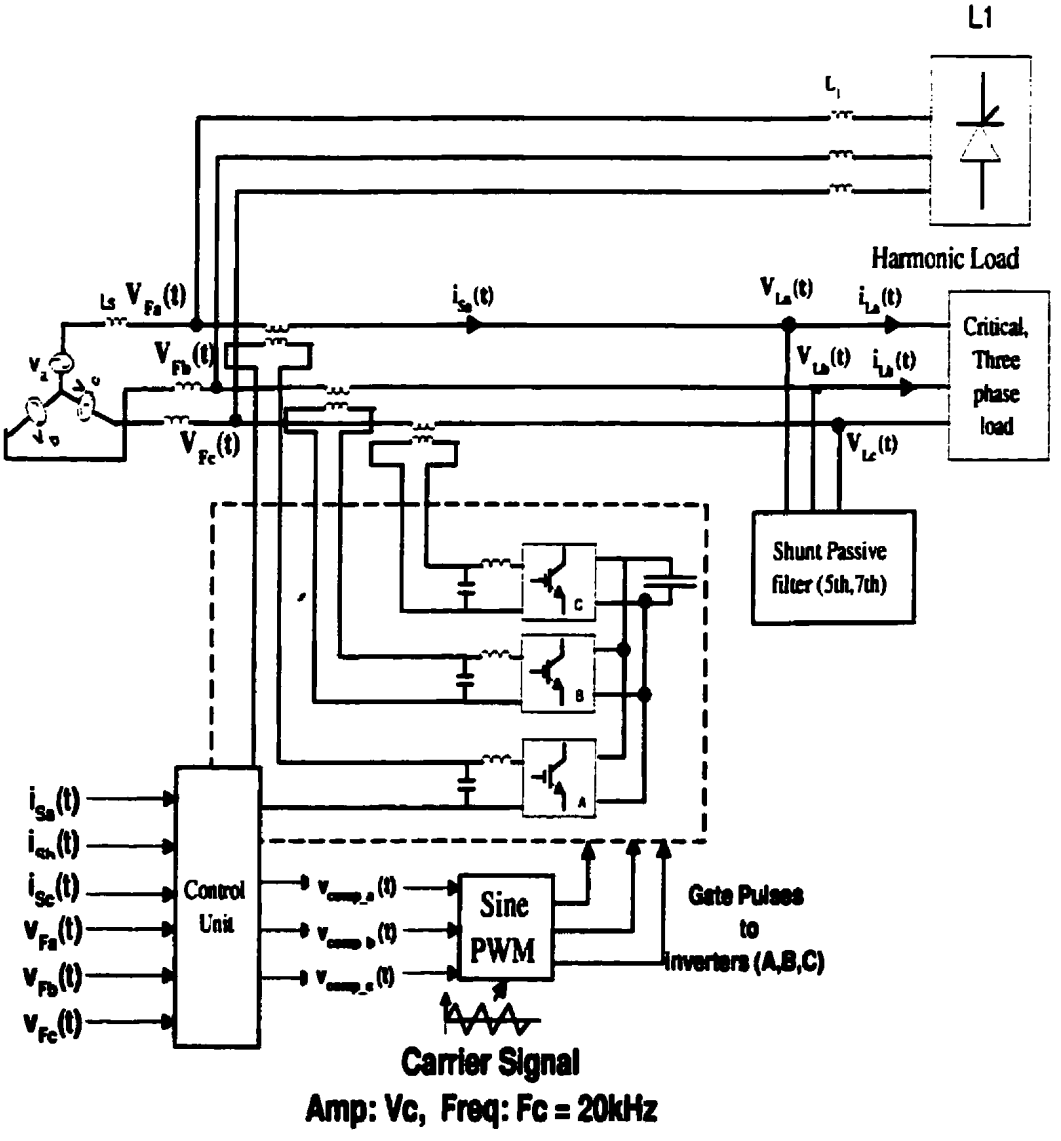

Figure 4.1: Basic hybrid single compensator topology

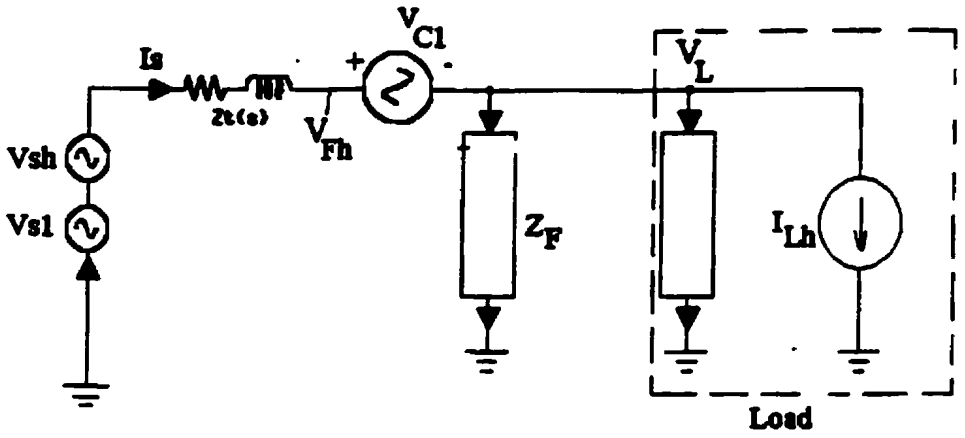

Figure 4.2: Single-phase phasor equivalent model of the hybrid system.

values for the controller gain parameters.

- The proposed d-q-0 based extraction procedure is linear and is used to generate the individual phase voltage corrections as opposed to correcting the line to line voltages.

The analysis is carried out in two parts:

1. Harmonic equivalent circuit analysis is used to study the effects of the controller parameters on stability, suppression of terminal voltage distortion and harmonic isolation.

2. Fundamental frequency analysis is used to arrive at the compensator ratings and the effects of controller parameters on the steady state error.

As mentioned in Chapter 3, the equation which governs the compensation in the hybrid system is described by

$$V_c^* = R_h \cdot I_{S_h} + K_v \cdot (V_F - V_{F_{ref}}) \tag{4.1}$$

For the harmonic analysis, $V_{F_{ref}}$ is set to zero and the compensation equation reduces to

$$V_c = R_h \cdot I_{S_h} + K_v \cdot V_{F_h} \tag{4.2}$$

where, I_{S_h} is the harmonic component of the supply current, while V_{F_h} is the voltage at the supply end of the compensator.

With reference to the phasor equivalent circuit shown in Fig. 4.2, the load voltage distortion can be expressed as a superposition of the two harmonic sources in the model: the distortion at the source end (cumulatively represented as V_{S_h}) and the nonlinear load modeled as a current source, I_{L_h}. In order to clarify the harmonic analysis procedure, the model is redrawn in Fig. 4.2. From the proposed compensation scheme of equation (4.2), it can be seen that the compensator in the harmonic-domain can be modelled as a controlled voltage source $K_V \cdot \mathbf{V_{F_h}}$ in series with a resistance R_h. The basic model and the derived circuits for the cases when the harmonic source voltage is set to zero and the harmonic current of the nonlinear load is set to zero and circuits for $\mathbf{V_{S_h}} = \mathbf{0}$ and $\mathbf{I_{L_h}} = \mathbf{0}$ are shown in Figs 4.2(b) and (c), respectively.

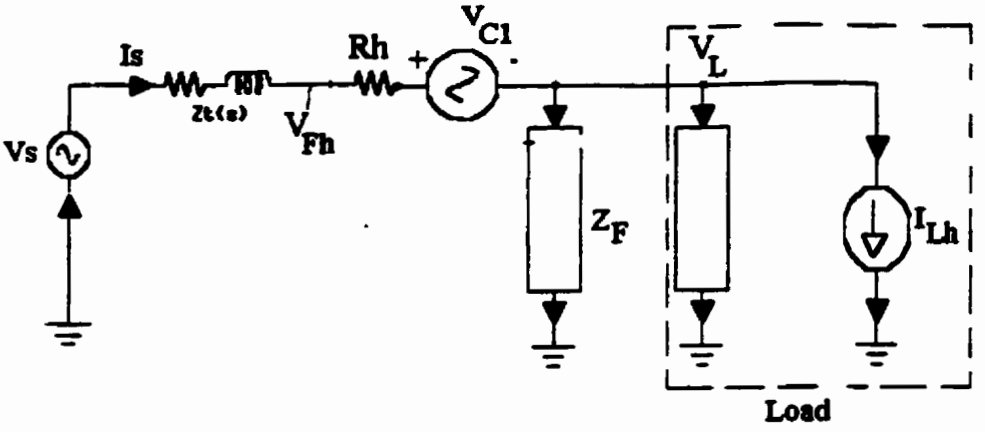

(a) Circuit with V_{Sh} and I_{Lh}

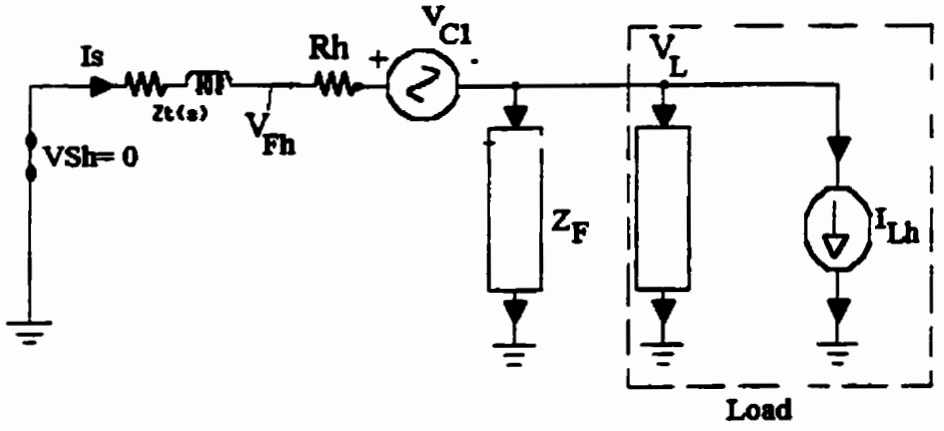

(b) Circuit with $V_{Sh} = 0$

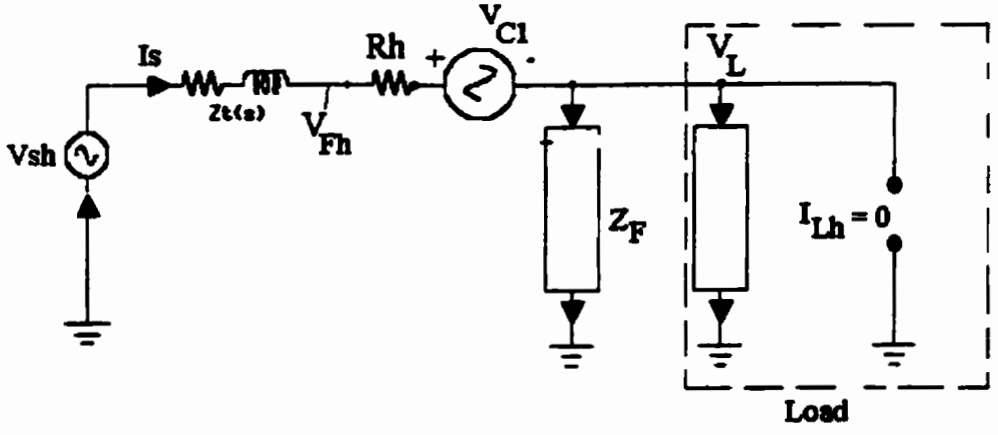

(c) Circuit with $I_{Lh} = 0$

Figure 4.3: Harmonic equivalent circuits of the hybrid series compensator

Using the superposition theorem the load voltage can be expressed in the Laplace domain as

$$V_{L_h}(s) = G_1(s) \cdot V_{S_h}(s) + G_2(s) \cdot I_{L_h}(s) \tag{4.3}$$

where,

$$G_1(s) = \frac{V_{L_h}(s)}{V_{S_h}(s)} \mid_{I_{L_h}=0} \tag{4.4}$$

$$G_2(s) = \frac{V_{L_h}(s)}{I_{L_h}(s)} \mid_{V_{S_h}=0} \tag{4.5}$$

The transfer function $\frac{V_{L_h}(s)}{V_{S_h}(s)}$ is derived as follows:

Note that all the variables are in Laplace domain, and for simplicity, the Laplace variables are represented as $X(s) = \mathbf{X}$.

$$\mathbf{I_{S_h}} = \frac{\mathbf{V_{L_h}}}{\mathbf{Z_F}||\mathbf{Z_L}} + \mathbf{I_{L_h}} \tag{4.6}$$

$$\mathbf{V_{F_h}} = \mathbf{V_{C_h}} + \mathbf{V_{L_h}} \tag{4.7}$$

From (4.2), (4.6) and (4.7), the voltage at the point of common coupling is obtained as

$$\mathbf{V_{F_h}} = \frac{R_h \cdot \mathbf{I_{S_h}} + \mathbf{V_{L_h}}}{(1 - K_v)} \tag{4.8}$$

Applying KVL to the loop containing the supply and the shunt filter,

$$\mathbf{V_{S_h}} - \mathbf{I_{S_h}} \cdot \mathbf{Z_t} - \mathbf{V_{F_h}} = \mathbf{0} \tag{4.9}$$

From (4.6), (4.8) and (4.9)

$$\frac{V_{L_h}(s)}{V_{S_h}(s)} = G_1(s) = \frac{(\mathbf{Z_F}||\mathbf{Z_L}) \cdot (1 - K_v)}{[(1 - K_v) \cdot \mathbf{Z_t} + R_h + \mathbf{Z_F}||\mathbf{Z_L}]} \tag{4.10}$$

It is observed from (4.10) that the terminal voltage distortion $|\mathbf{V}_{L_h}|$ approaches zero as K_v approaches unity. Replacing $Z_t(s)$ and $Z_F(s)$ with their equivalent transfer functions give

$$\mathbf{Z_t} = s \cdot L_t \tag{4.11}$$

$$\mathbf{Z_F} = \mathbf{Z_5}||\mathbf{Z_7}||\mathbf{Z_H} \tag{4.12}$$

$\mathbf{Z_5}$ and $\mathbf{Z_7}$ are the impedances of the fifth and seventh harmonic filters while $\mathbf{Z_H}$ is the impedance of the high pass filter for shunting harmonics higher than the 7th. Similarly, the transfer function $\frac{V_{L_h}(s)}{I_{L_h}(s)}$ is obtained as

$$\frac{V_{L_h}(s)}{I_{L_h}(s)} = G_2(s) = -\frac{(\mathbf{Z_F}||\mathbf{Z_L})[(1-K_v)\mathbf{Z_t} + R_h]}{[(1-K_v)\cdot\mathbf{Z_t} + R_h + \mathbf{Z_F}||\mathbf{Z_L}]} \tag{4.13}$$

Since the denominators of $G_1(s)$ and $G_2(s)$ are the same, only one of the two transfer functions, i.e. $G_1(s)$, is analyzed for stability.

4.3 Effects of Gain Parameters K_V and R_h on System Stability

As a feedforward compensation, the overall compensation loop gain is sensitive to fluctuations in the individual block gains. The blocks involved are sensors, filters, the pulse width modulator (PWM) and the inverter dc-link voltage. In the single-phase model, variations in K_V and R_h are representative of the loop gain changes. Their individual effects are verified by keeping one of the parameters constant while

varying the other. The MATLAB programs for carrying out the investigation are presented in Appendix B.

4.3.1 System and shunt filter parameters

Since all the load current harmonics are constrained to flow into the passive filter, the passive filter terminal voltage will have a distortion depending on the harmonic frequency versus impedance characteristics of the passive filter. Hence, the design of the passive filter is critical for the reduction of voltage distortion at the passive filter terminal and the rating of the series compensator. The system parameters used in this study are shown in Table 4.1. The impedance characteristics for Q=6 and 14 are shown in Fig. 4.4. The impedances offered by the shunt filter at the dominant harmonic frequencies 5^{th} and 7^{th} for Q=6 are approximately 25% higher than those at 'Q=14'. Hence a higher Q results in a lower harmonic distortion.

4.3.2 Influence of K_V on stability

For the system parameters given in Table 4.1, the root loci are obtained for two loading conditions: a light load with $|Z_L| = 4p.u$; a heavy load with $|Z_L| = 0.5p.u$ as shown in Figs 4.5 and 4.6 respectively. A choice of $R_h = 5\Omega$ is practical since it should be much larger than Z_F and the line impedance. For the two plots, K_V was varied between zero and 2.5 in steps of 0.05.

The loading conditions for the root-locus plots are at the two extremes, and in spite of this there is no significant change in the root-locus plots. The reason is that,

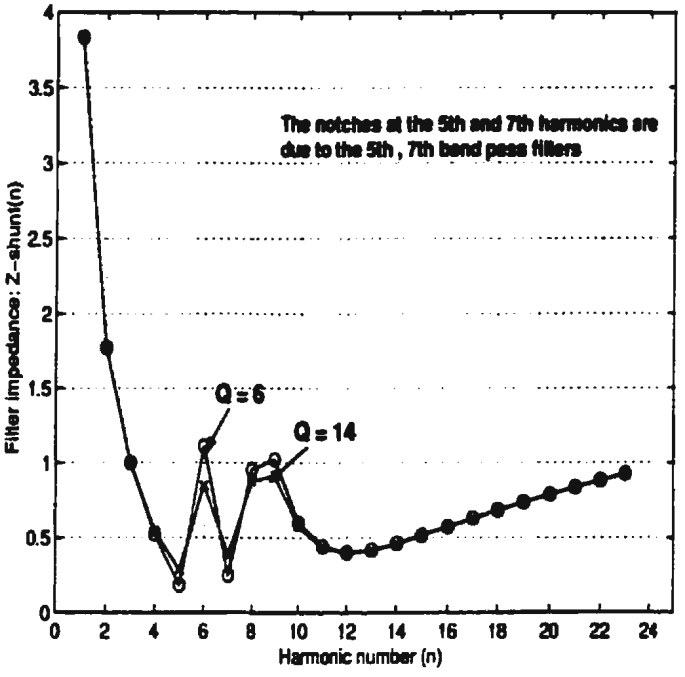

Figure 4.4: Impedance characteristics of the shunt passive filter

Table 4.1: System parameters for single-phase analysis

AC voltage source	100V (phase voltage), 60 Hz, THD = 15%
Line impedance	Lt = 0.1mH, Rt = 0Ω
Nonlinear load	5kVA, THD = 30%
Shunt filter	Q = 6, L5 = 0.82mH, C5 = 340mF L7 = 0.82mH, C7 = 170mF LH = 0.26mH, CH = 300mF, RH = 3Ω

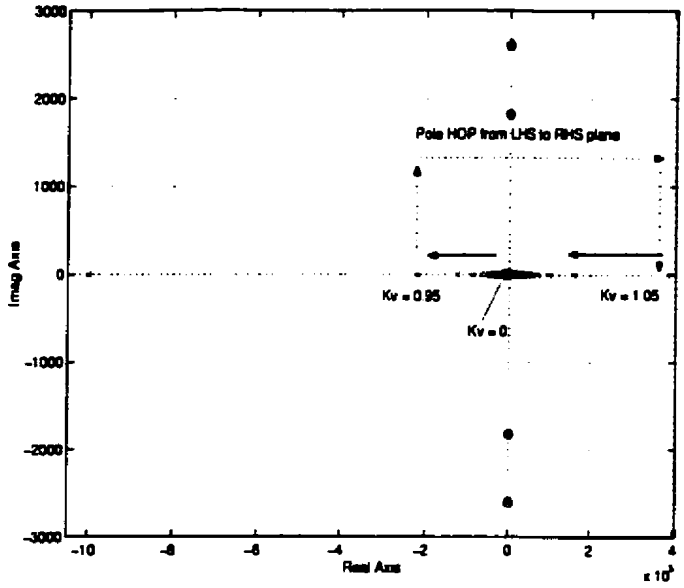

Figure 4.5: Root-locus plot with $R_h = 5$, $Z_L = 4$ p.u.

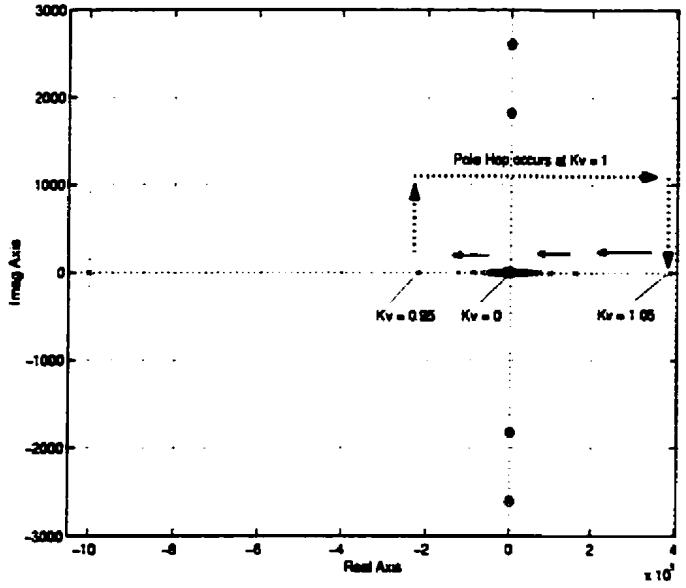

Figure 4.6: Root-locus plot with $R_h = 5$, $Z_L = 0.5$ p.u.

in most practical circumstances, $Z_F \ll Z_L$. Equation 4.10 therefore reduces to

$$G_1(s) = \frac{\mathbf{Z_F} \cdot (1 - K_v)}{[(1 - K_v) \cdot \mathbf{Z_t} + R_h + \mathbf{Z_F}]} \tag{4.14}$$

The Z_L term is absent in the transfer function. Hence the gain margin of the compensator is independent of load variations. As indicated in the figure, the system becomes unstable for $K_V > 1$. The desired value of K_V is unity. But due to stability problems K_V has to be a little below the critical loop gain of unity. A higher gain margin for K_V, can improve the range of voltage compensation.

To illustrate the unstable condition through an example, the filter transfer function, Z_F is expressed in terms of the equivalent shunt filter parameters as shown in (4.15), where C_F and L_F are the shunt filter parameters.

$$\mathbf{Z_F} = \frac{s^2 \cdot L_F \cdot C_F + 1}{C_F \cdot s} \tag{4.15}$$

Substituting (4.11), (4.12) and (4.15) into equation (4.14), the load voltage transfer function is obtained as

$$\frac{V_{L_h}(s)}{V_{S_h}(s)} = \frac{(1 - K_v) \cdot (1 + s^2 \cdot L_F \cdot C_F)}{[(L_F + L_t) \cdot C_F \cdot s^2 \cdot (1 - K_v) + R_h \cdot C_F \cdot s + 1]} \tag{4.16}$$

Routh-Hurwitz criterion for stability states that the system becomes unstable when all the coefficients of the characteristic equation do not have the same sign. Applying this condition to the transfer function given by (4.16), the coefficient of s^2 becomes negative for $K_v > 1$. Hence a necessary condition for the system to be stable is $0 < K_v < 1$.

4.3.3 Influence of R_h on stability

Since R_h serves as a series resistance, it is unlikely to cause instability (instead it may serve as a measure to counter it). From (4.14), it is observed that the powers of 's' will be positive for all $R_h > 0$. Hence the system will be stable for all positive values of R_h.

4.4 Harmonic Isolation

Qualitatively, harmonic isolation is a measure of the load current harmonics that appear in the source current. It is expressed as $\left[\frac{I_{S_h}}{I_{L_h}} \right]_{V_{S_h}=0}$. This quantity can be referred to as the harmonic distribution factor(HDF). A very small value of HDF indicates good harmonic isolation. This means that the series compensator stems the flow of harmonics from nonlinear loads into the supply line. From the single-phase model, setting $V_{S_h} = 0$, the transfer function for the distribution factor can be derived as

$$\frac{I_{S_h}(s)}{I_{L_h}(s)} = \frac{(\mathbf{Z_F}||\mathbf{Z_L})}{[(1 - K_v) \cdot \mathbf{Z_t} + R_h + \mathbf{Z_F}||\mathbf{Z_L}]} \tag{4.17}$$

Figure 4.7, shows the effect of R_h on the distribution factor for $L_t = 0.5$mH and $K_v = 0$. Plots for values of $R_h = 0$, 2 and 5 are shown. The series compensator reduces the distribution factor considerably (well below zero dB) at all frequencies for $R_h \geq 2$. Fig. 4.2, shows that if the fictitious series resistance, R_h is made much higher than the line and shunt filter impedances i.e. $R_h \gg |Z_F|, |Z_t|$, the line current

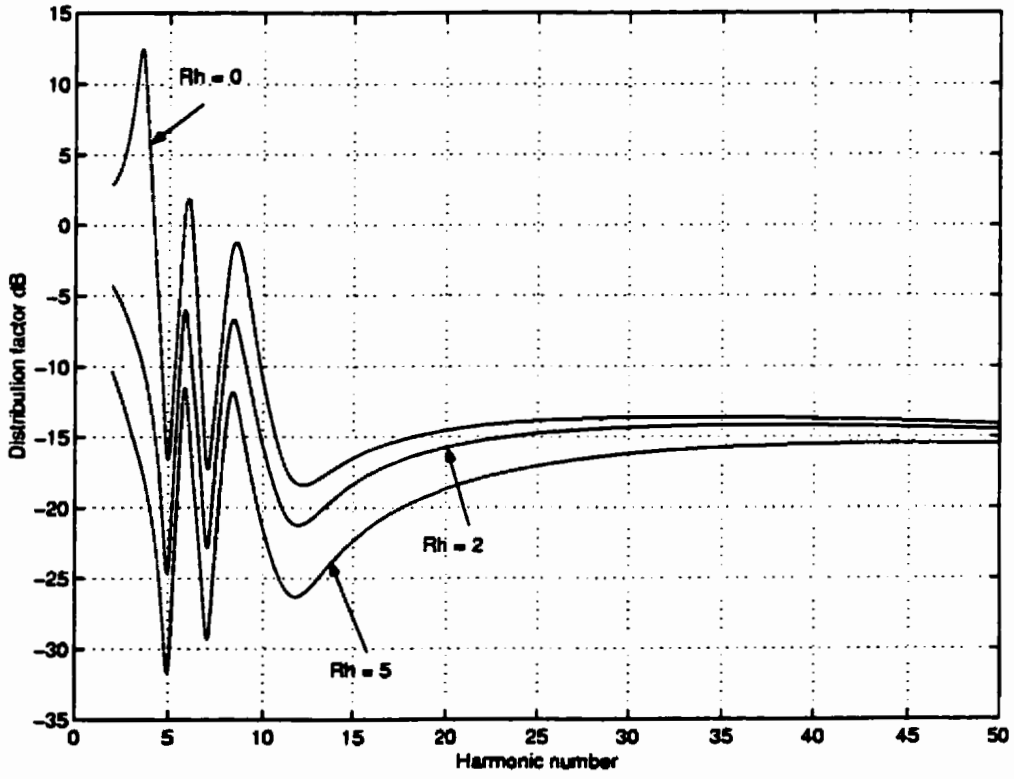

Figure 4.7: Harmonic distribution factor against frequency

distortion is greatly reduced. Moreover the load current is contained within the loop formed by the shunt passive filter and the distortion at the load due to the supply voltage harmonics is greatly reduced. This concept is illustrated in Fig. 4.8.

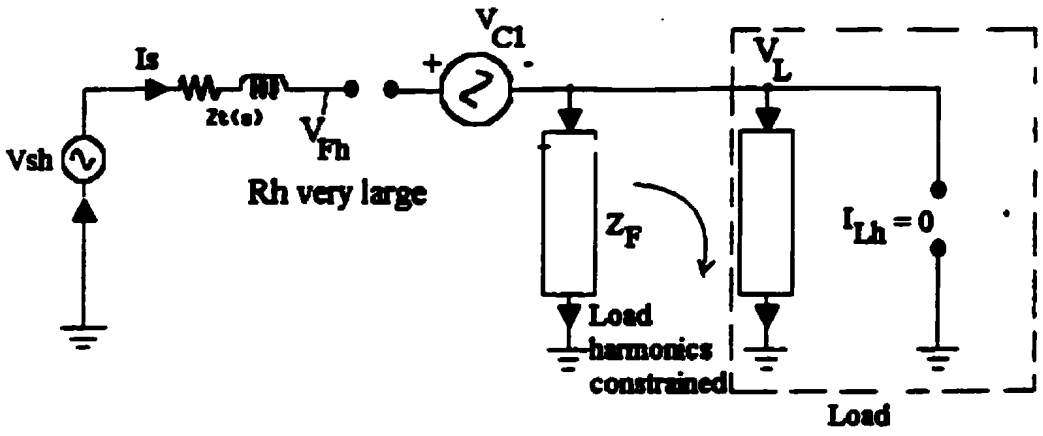

Figure 4.8: Circuit diagram illustrating harmonic isolation; $L_t = 0.5mH$, $K_V = 0, R_h = \infty$

4.5 Suppression of Terminal Voltage Distortion

As R_h approaches infinity, the terminal voltage distortion decreases according to equation (4.10). When the critical load is linear, the THD of the load voltage approaches zero. In other words, the compensator behaves like a sinusoidal current source. Large values of R_h can be obtained by using feedback control with a PI controller to make the line current sinusoidal [16].

Due to the finite quality factor Q, of the shunt filter for large nonlinear loads, the load voltage THD will increase because of the harmonic drop across the shunt

passive filter. The finite Q of the shunt passive filter thus places a lower limit on the compensation capability of the compensator.

Since K_V also plays a role in curtailing load and source distortion, a three-dimensional plot, shown in Figs 4.9 and 4.10, is employed to describe the effect of K_V and R_h on the THD of the load voltage. The surfaces of the plots in Figs 4.9 and 4.10, show the effect of the gain parameters on the terminal voltage distortion and current suppression respectively. The height of the surface at the origin corresponds to the THD in the absence of the compensator. For high values of R_h (greater than 5), the voltage component $R_h \cdot i_{S_h}$ dominates, forcing the compensator to behave more like a series resistance than a controlled harmonic voltage source. The THD of the load voltage beyond this value of R_h is independent of the two parameters (i.e. the THD stays almost constant at 7.5%). The harmonic voltage drop due to the harmonic current flowing in the loop of the shunt filter is responsible for this distortion. The supply current distortion decreases with increasing R_h as shown in Fig. 4.10. The distortion level reduces to zero for large values of R_h.

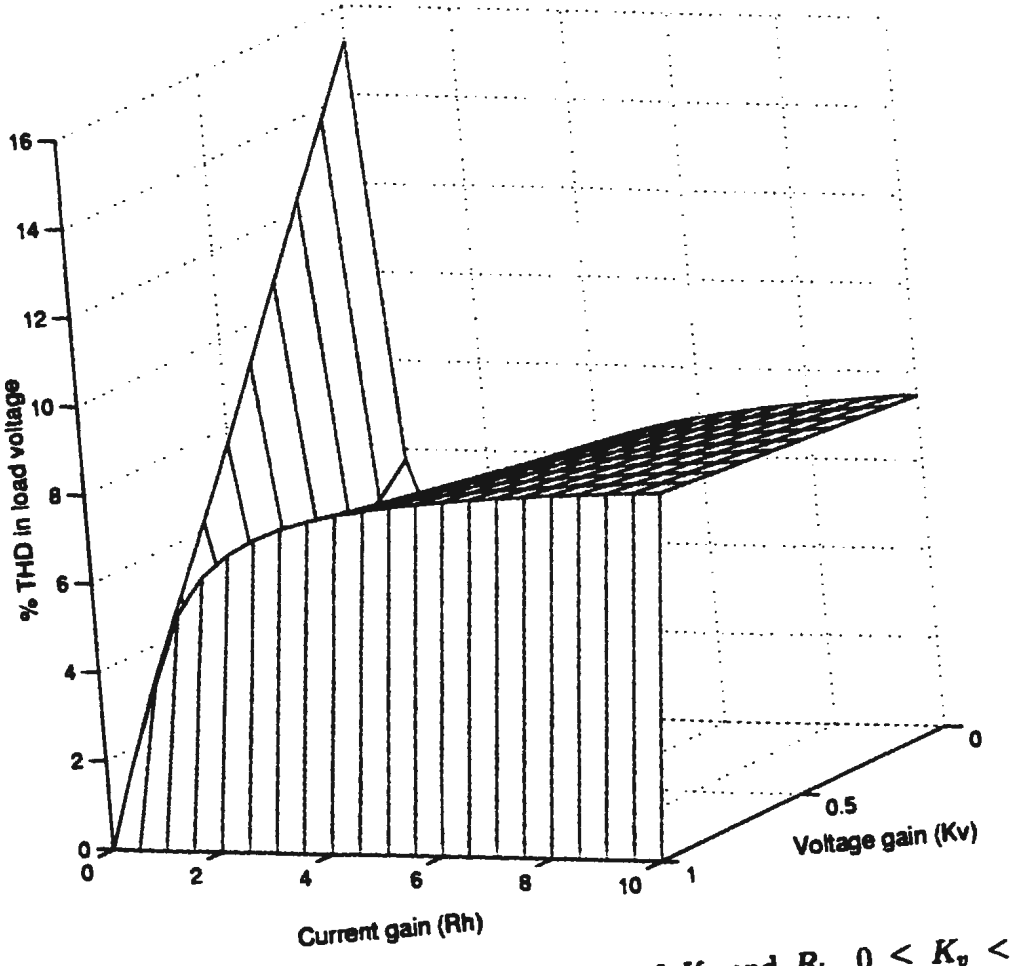

Figure 4.9: THD of load voltage as a function of K_v and R_h, $0 \leq K_v < 1$ and $0 \leq R_h < 10$

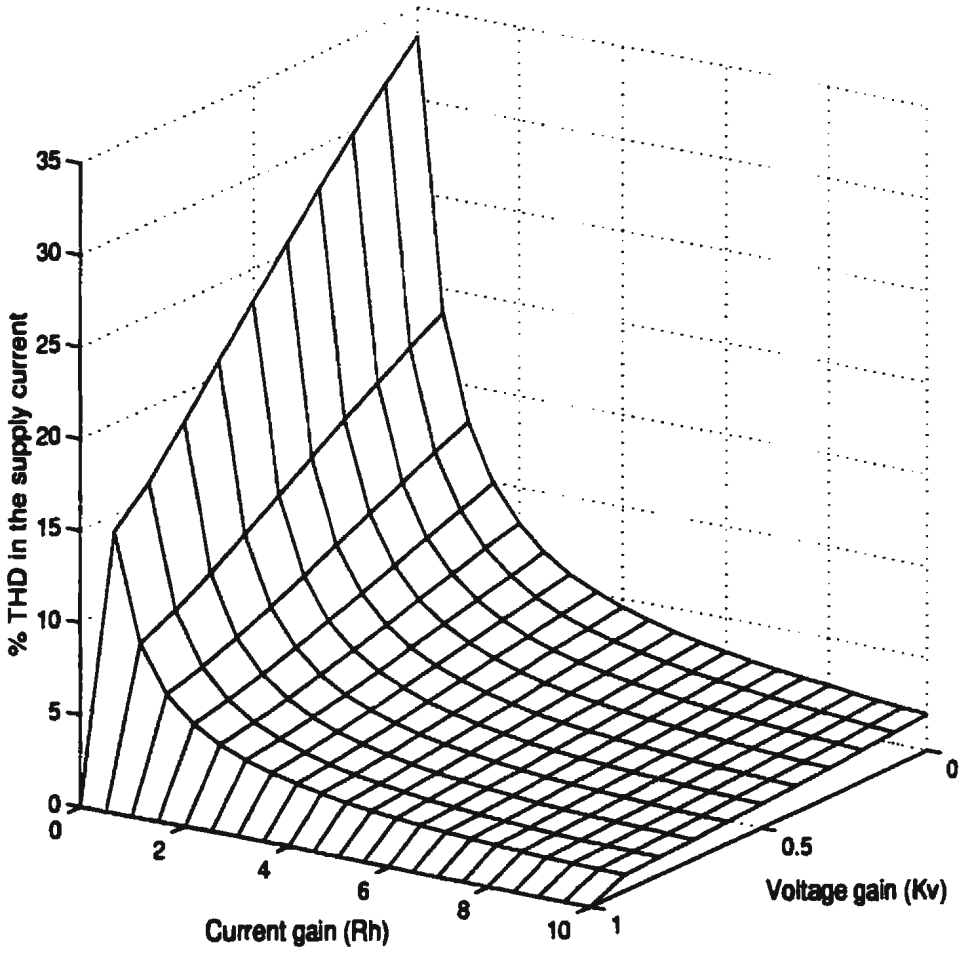

Figure 4.10: THD of supply current as a function of K_v and R_h, $0 \leq K_v < 1$ and $0 \leq R_h < 10$

4.6 Performance of the compensator under sag and swell conditions

As indicated in the earlier discussion on stability, a necessary condition for stability is that the voltage compensator gain K_V must be less than unity. A tolerance of 5% is necessary to allow for filter parameter variations and fluctuations in the dc-link voltage. Thus K_V should have an upper bound of 0.95. The impact of this upon sag/swell restoration is studied through the following fundamental frequency analysis:

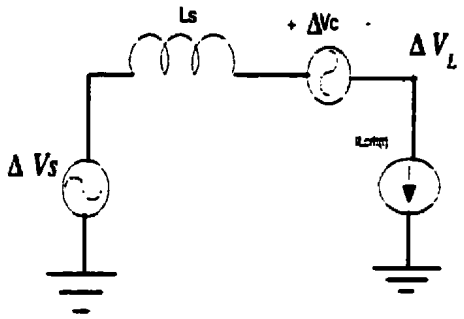

Figure 4.11: Fundamental equivalent circuit

As can be seen from Fig. 4.11, the change in load voltage ΔV_L, can be written as

$$\Delta V_L = (1 - K_v) \cdot \Delta V_F \tag{4.18}$$

A percentage compensation error($\%E_r$) for a nominal load voltage($V_{L_{nom}}$) and voltage

gain(K_v), can be derived as shown below:

$$\begin{aligned} E_r[\%] &= \frac{\Delta V_L}{V_{L_{nom}}} \cdot 100 \\ &= \frac{(1-K_v)\cdot\Delta V_F}{V_{L_{nom}}} \cdot 100 \\ &= \frac{Sag[\%]\cdot(1-K_v)\cdot V_{L_{nom}}}{V_{L_{nom}}} \\ &= Sag[\%] \cdot (1 - K_v) \end{aligned} \tag{4.19}$$

For an anticipated sag of 40% and $K_v = 0.95$, $\%E_r = 2\%$. This tolerance is acceptable for most computer and voltage sensitive loads as per the CBEMA curve [19].

Figure 4.12 shows the plot of compensation error versus K_V for two value of percentage sag. The compensation error is a linear function of the voltage gain K_V. Since the error must be compliant with the CBEMA curve, it can be observed from Fig. 4.12 that the acceptable range for K_V decreases from $0.67 < K_V < 1$ for a sag of 30% to $0.8 < K_V < 1$ for a 50% sag.

4.7 Compensator Ratings

The voltage injected by the compensator has two components; the fundamental component compensates for sags and swells, and the harmonic component suppresses the current distortion. The kVA rating of the series compensator is derived by superimposing the effects of these two components.

4.7.1 Steps to determine the compensator ratings

The rating of the compensator is determined in three steps:

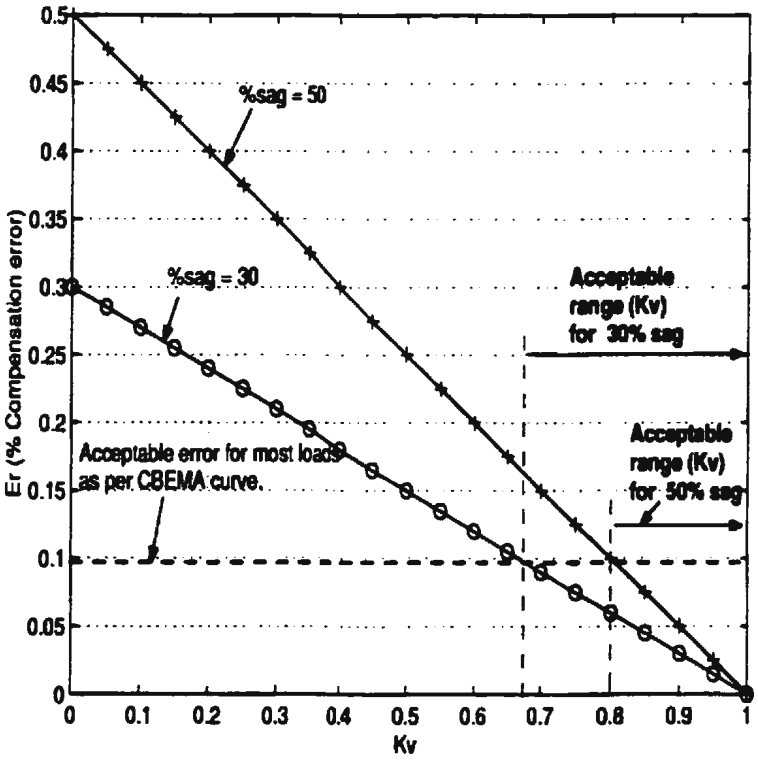

Figure 4.12: Compensation error as a function of voltage gain K_V.

- by calculating the harmonic component of the compensator voltage $\mathbf{V_{C_h}}$ and compensator current $\mathbf{I_{C_h}}$ based on harmonic equivalent circuit analysis.
- by determining the fundamental component of the compensator voltage $\mathbf{V_{C_1}}$ and current $\mathbf{I_{C_1}}$ using the load ratings and the supply voltage.
- by calculating the effective compensator voltage $\mathbf{V_C}$ and current $\mathbf{I_C}$ as

$$|\mathbf{V_C}| = \sqrt{|\mathbf{V_{C_1}}|^2 + |\mathbf{V_{C_h}}|^2} \tag{4.20}$$

$$|\mathbf{I_C}| = \sqrt{|\mathbf{I_{C_1}}|^2 + |\mathbf{I_{C_h}}|^2} \tag{4.21}$$

The KVA rating of the single compensator topology is then obtained as

$$KVA_C = |\mathbf{V_C}| \cdot |\mathbf{I_C}| \tag{4.22}$$

Using (4.7) and (4.9), the harmonic component of the compensator voltage is expressed as

$$\mathbf{V_{C_h}} = \mathbf{V_{S_h}} - \mathbf{I_{S_h}} \cdot \mathbf{Z_t} - \mathbf{V_{L_h}} \tag{4.23}$$

The harmonic component of the supply current I_{S_h} can be expressed as

$$\mathbf{I_{S_h}} = \frac{\mathbf{V_{L_h}}}{\mathbf{Z_F}||\mathbf{Z_L}} + \mathbf{I_{L_h}} \tag{4.24}$$

From (4.3), (4.10) and (4.13) the load voltage distortion component V_{L_h} is calculated as

$$\mathbf{V_{L_h}} = \mathbf{G_1} \cdot \mathbf{V_{S_h}} + \mathbf{G_2} \cdot \mathbf{I_{L_h}} \tag{4.25}$$

where

$$\mathbf{G_1} = \frac{\mathbf{Z_F Z_L} \cdot (1 - K_v)}{[(1 - K_v) \cdot \mathbf{Z_t}(\mathbf{Z_F} + \mathbf{Z_L}) + R_h(\mathbf{Z_F} + \mathbf{Z_L}) + \mathbf{Z_F Z_L}]} \tag{4.26}$$

$$\mathbf{G_2} = -\frac{\mathbf{Z_F Z_L}[(1 - K_v)\mathbf{Z_t} + R_h]}{[(1 - K_v) \cdot \mathbf{Z_t}(\mathbf{Z_F} + \mathbf{Z_L}) + R_h(\mathbf{Z_F} + \mathbf{Z_L}) + \mathbf{Z_F Z_L}]} \tag{4.27}$$

Since the compensator is connected in series with the supply, the compensator current is given by

$$\mathbf{I_C} = \mathbf{I_S} \tag{4.28}$$

which consequently implies,

$$\left.\begin{aligned} \mathbf{I_{C_h}} &= I_{S_h} \\ \mathbf{I_{C_1}} &= I_{S_1} \end{aligned}\right\} \tag{4.29}$$

From the fundamental frequency analysis, the fundamental components of the compensator voltage and current for a maximum sag of 30% are calculated using

$$|\mathbf{V_{C_1}}| = 0.3 \cdot K_V \cdot V_s \tag{4.30}$$

$$|\mathbf{I_{C_1}}| = \frac{Rating(linearload) + Rating(NLload)}{V_s} \tag{4.31}$$

Finally, the KVA rating of the single compensator can be calculated using (4.20), (4.21) and (4.22).

4.7.2 Effect of controller gain on compensator ratings

The effects of an increase in the current gain R_h on supply current distortion was discussed in the distortion analysis presented in Section 4.4. A high current gain R_h is desired for two main reasons: to provide better isolation and to prevent

nonlinear loads at the supply side from pumping harmonics into the shunt passive filter consequently increasing the passive filter ratings. However, the impact of R_h on the compensator ratings was not examined. The following analysis examines the effect of increasing current gain on the compensator kVA rating and also the degree of harmonic isolation for different values of R_h.

With $V_{S_h} = 0$ the harmonic distribution factor can be obtained from (4.24), (4.25) and (4.27) as

$$\frac{\mathbf{I_{S_h}}}{\mathbf{I_{L_h}}} = 1 - \frac{(\mathbf{Z_F} + \mathbf{Z_L})[(1 - K_v)\mathbf{Z_t} + R_h]}{[(1 - K_v) \cdot \mathbf{Z_t}(\mathbf{Z_F} + \mathbf{Z_L}) + R_h(\mathbf{Z_F} + \mathbf{Z_L}) + \mathbf{Z_F}\mathbf{Z_L}]} \tag{4.32}$$

Since the fundamental component of the voltage injected by the compensator is much higher than the harmonic component, the compensator rating can be approximated to be a function of the supply current distortion alone. The harmonic component of the supply current is in effect a function of three main parameters: the current gain R_h which isolates the load from the supply; the voltage gain K_V, which partially cancels the supply distortion and thus helps in improving the supply current profile; the quality factor of the shunt passive filter Q, which aids in harmonic isolation.

In Fig. 4.13(a), the compensator rating is calculated for a set of values of the current gain R_h while the voltage gain K_V is set to 0.8 (the same value chosen by Peng, et al. [10]). It is to be noted that in the implementation of a single compensator topology, the value of K_V must be a little less than unity to ensure system stability.

The calculations are done for different values of the passive filter Q-factor. The MATLAB routine for generating the plots is given in Appendix B. The corresponding system parameters are as follows:

- Supply voltage $V_S = \frac{200}{\sqrt{3}} = 115.47$V, 60 Hz
- Line impedance: R_t 1mΩ, L_t = 1mH
- Linear load: 2.67kVA (8kVA three-phase), $|Z_L| = 5\Omega$
- Nonlinear load : 7kVA (21kVA three-phase), $THD_i = 30\%$
- Two band pass filters for the fifth and seventh dominant harmonics were connected in parallel to form the passive shunt filter with Q = 10.

It can be observed from Fig. 4.13(a) that the rating of the single compensator decreases with an increase in current gain primarily because of a consequent reduction in the supply current THD. The reason for the high compensator ratings for small values of R_h can be reasoned is as follows: Equation (4.9) can be rearranged and written as

$$\mathbf{V_{F_h}} = \mathbf{V_{S_h}} - \mathbf{I_{S_h}} \cdot \mathbf{Z_t} \tag{4.33}$$

Equating (4.8) and (4.33) we get

$$\mathbf{V_{S_h}} - \mathbf{I_{S_h}} \cdot \mathbf{Z_t} = \frac{R_h \cdot \mathbf{I_{S_h}} + \mathbf{V_{L_h}}}{(1 - K_v)} \tag{4.34}$$

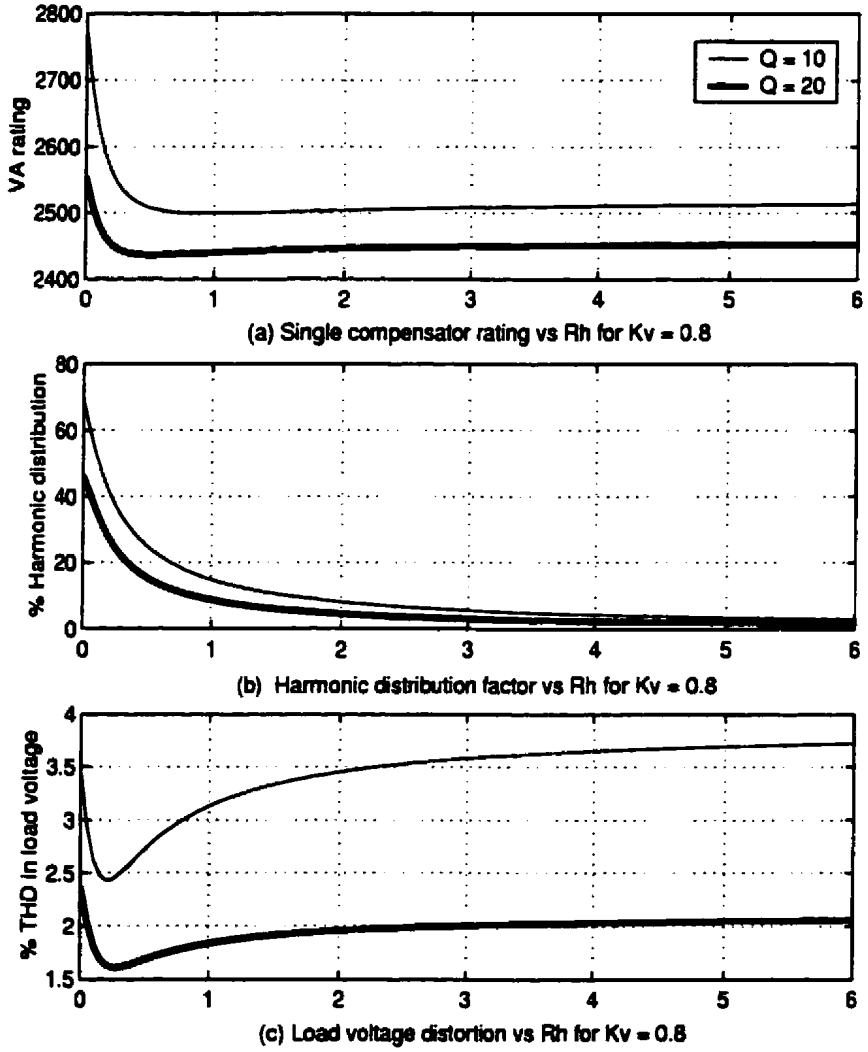

Figure 4.13: Single compensator rating and supply current distortion as a function of R_h

which can be rewritten as

$$(1 - K_v)\mathbf{V_{S_h}} - [\mathbf{Z_t}(1 - K_v) + R_h] \cdot \mathbf{I_{S_h}} - \mathbf{V_{L_h}} = \mathbf{0} \tag{4.35}$$

Equation (4.35) shows that due to the presence of the harmonic voltage cancellation component, the effective supply end distortion is reduced to $(1 - K_V)V_{S_h}$, while the effective line impedance is $(1 - K_V)Z_t + R_h$. The effective line impedance becomes very small for a relatively small current gain R_h at $K_V = 0.8$. The effect of the small value of the line impedance is to increase the supply current distortion.

Fig. 4.13(b) shows that for R_h below 0.5, between 30 and 70 percent of the load current harmonics enter the supply. An increase in the Q-factor from 10 to 20 improves isolation since the fraction of load current in the supply is reduced to 15 to 40 percent. A high Q also minimizes load voltage distortion because of a much smaller passive filter voltage drop. The marginal reduction in supply current distortion for a Q-factor of 20 reflects in a reduction of 50VA in the compensator rating. For a relatively low quality factor, the distortion level is high. Thus a tradeoff between the filter cost and the level of terminal voltage distortion would be necessary. The rating of the compensator remains almost constant for $R_h > 1$, because the supply current distortion becomes relatively insignificant for high values of R_h. It can therefore be concluded that an increase in the current gain for $R_h > 1$ does not increase the compensator ratings.

4.8 Summary

In this chapter, a single-phase harmonic equivalent model was developed for the single compensator topology, mainly from the point of view of obtaining a qualitative idea about the effect of load changes and other parameter variations on the system stability and compensation. The root-locus plots were obtained for variations in the voltage gain K_V for various loading conditions.

From the root-locus plots, it was observed that the system was stable for the range $0 < K_V < 1$ for a wide load variation. This implies that the operating gain will have to be lowered a little below unity to provide some additional tolerance for loop gain variations (or else incorporate feedback control). The closed loop system was observed to be unstable for K_V greater than unity, while the current gain, R_h had no impact on stability. The compensation error was found to be maximum for $K_V = 0$ and it decreased linearly with increasing K_V. To ensure a stable system operation, K_V was maintained at a value typically between 0.8 and 0.9, to account for filter parameter variations, quantization errors. This setting resulted in non-zero compensation error. In order to minimize the compensation error while maintaining a stable system operation, it is necessary to set K_V in the neighborhood of 0.8.

A large value of R_h is instrumental in providing good harmonic isolation and suppressing voltage distortion. For a relatively large value of R_h (R_h ¿ 5), the load current harmonics were constrained to flow within the passive shunt filter. The passive

filter terminal voltage distortion was found to depend on the harmonic frequency characteristic of the passive filter. For a relatively low quality factor (Q = 6), the distortion level was high. Thus a tradeoff between the filter cost and the level of terminal voltage distortion would be necessary.

The compensator ratings were calculated as a function of the controller parameters. An increase in current gain does not influence the compensator rating. However an increase in the quality factor of the shunt passive filter reduces the supply current harmonics and hence the effective compensator rating.

Chapter 5

Proposed Hybrid Topology - Two Series Compensators

Introduction

Some of the major drawbacks in the basic hybrid compensator for voltage compensation and harmonic suppression are the limited range for the gain of the voltage compensator and high terminal voltage distortion due to the drop across the shunt passive filter. In this chapter, a solution is proposed in the form of a two-compensator topology. The corresponding single-phase model for the proposed topology, along with the frequency domain analysis and stability evaluation, are discussed. Furthermore, the rating of the proposed two-compensator topology is determined and compared with the basic hybrid compensator. It is shown that though the rating of the proposed compensator is approximately 10% higher than the basic topology, the proposed compensator provides better terminal voltage regulation and increased gain margin for voltage control.

5.1 Development of the Proposed Two-compensator Topology

The basic series hybrid compensator employs a single injected voltage to provide harmonic isolation and load voltage compensation. The voltage injected by the compensator is equal to the weighted sum of the compensator current I_{S_h} and the voltage at the supply end of the compensator V_F.

Limited margin for gain variation was one of the primary drawbacks in the basic componsator. One of the possible reasons for this limitation is the use of one compensator to provide the two voltage components V_{c1} and V_{c2}, which places stability constraints on the gain margin. Another drawback is that for load currents with high distortion levels, the drop across the shunt passive filter contributes significantly to the terminal load voltage distortion.

A two-compensator topology can be used to reduce the interaction between the voltage and current signals and allow independent control of the two voltage components thereby increasing the stability limit. The basic compensation principle given in (4.2) remains the same, except that the two voltage components are provided by two separate inverters. The node common to the two series compensators is connected to the shunt passive filter. Thus, the two series compensators form a T with the shunt filter. The functions of the individual components of the power block can be described as follows:

- The series compensator towards the supply end of the filter serves as a harmonic isolator. It functions to constrain the load current harmonics within the load-filter loop thereby preventing the contamination of the supply current. The voltage injected by this inverter is given by $V_{C1} = R_h \cdot i_{S_h}$.

- The second series component towards the load end of the filter helps to regulate the load end voltage and to compensate for the drop across the filter. The second component is provided by $V_{C2} = K_V(V_F - V_{F_{ref}})$.

Figure 5.1 shows the single-phase equivalent circuit of the two series compensator topology.

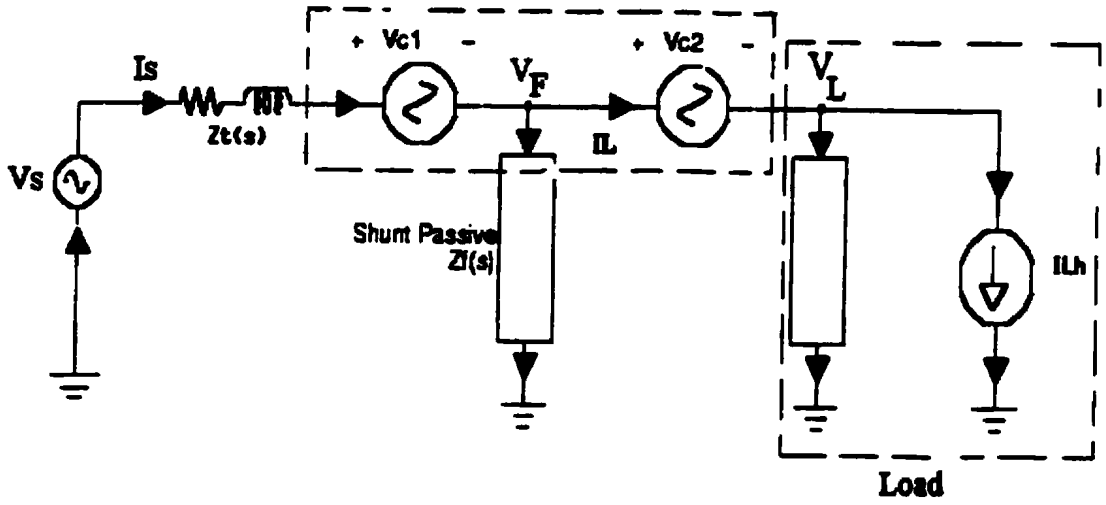

Figure 5.1: Proposed series hybrid compensator

In the figure, compensator C1 acts as a harmonic isolator and C2 serves as a

voltage compensator. The harmonic components of the voltages injected by the compensators are given by

$$V_{C_{h_1}} = R_h \cdot i_{S_h} \tag{5.1}$$

$$V_{C_{h_2}} = K_V \cdot V_{F_h} \tag{5.2}$$

where i_{S_h} and V_{F_h} are the harmonic components of the supply current and the voltage drop across the passive filter, respectively.

5.2 Single-phase Analysis of the Two-compensator Topology

In the single-phase model , the nonlinear critical load is represented as a current source shunted by a linear R-L load. The analysis is carried out in the harmonic domain without any loss of generality. The determination of the effect of the gain parameters K_V and R_h on stability and suppression of voltage and current distortion are the final objectives of this analysis. The two-compensators are modeled as two controlled voltage sources, whose reference voltages are calculated using (5.1) and (5.2). Since C1 serves as a harmonic isolator, it may be replaced by a resistance R_h. Figure 5.2 shows the equivalent circuit with C1 replaced by R_h. To be consistent with the analysis and notations used in Chapter 4, the Laplace variable x(s) is written as x. Applying KCL to the node to which the shunt filter is connected gives

$$\mathbf{I_{S_h}} = \frac{(\mathbf{V_{S_h}} - \mathbf{V_{F_h}})}{(\mathbf{Z_t} + R_h)} = \frac{\mathbf{V_{F_h}}}{\mathbf{Z_F}} + \frac{\mathbf{V_{L_h}}}{\mathbf{Z_L}} + \mathbf{I_{L_h}} \tag{5.3}$$

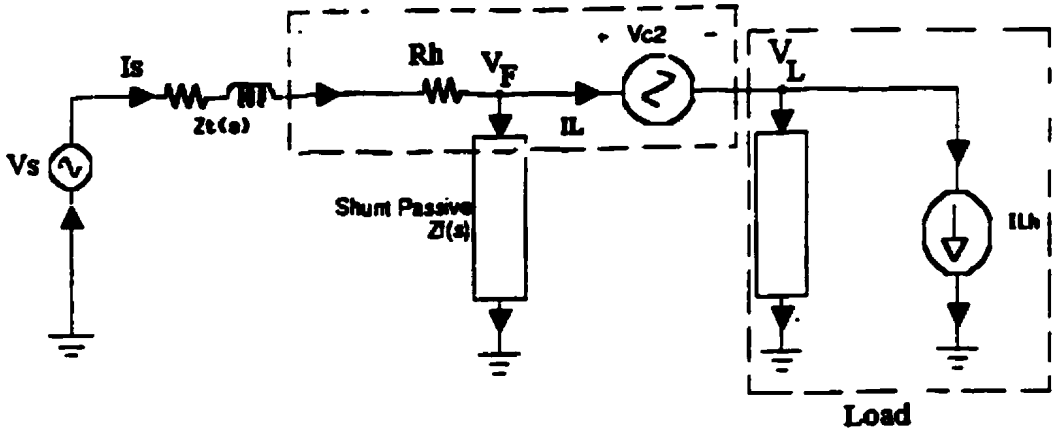

Figure 5.2: Harmonic equivalent circuit derived from Fig. 5.1

Since $\mathbf{V_{L_h}} = \mathbf{V_{F_h}} - \mathbf{V_{C_{h_2}}}$, using (5.2), the terminal load voltage can be written as

$$\mathbf{V_{L_h}} = (1 - K_V) \cdot \mathbf{V_{F_h}} \tag{5.4}$$

The load voltage is a superposition of the response due to the supply end distortion and load current harmonics and is given by

$$V_{L_h}(s) = \left[\frac{V_{L_h}(s)}{V_{S_h}(s)}\right]_{I_{L_h}=0} \cdot V_{S_h}(s) + \left[\frac{V_{L_h}(s)}{I_{L_h}(s)}\right]_{V_{S_h}=0} \cdot I_{L_h}(s) \tag{5.5}$$

By setting the harmonic current source I_{L_h} to zero and using (5.1)-(5.4), the load transfer function can be written as

$$\left[\frac{V_{L_h}}{V_{S_h}}\right]_{I_{L_h}=0} = \frac{\mathbf{Z_F Z_L}(1 - K_V)}{[(\mathbf{Z_t} + R_h)(1 - K_V) + (\mathbf{Z_t} + \mathbf{Z_F} + R_h)\mathbf{Z_L}]} \tag{5.6}$$

By examining the root-locus of this transfer function for various gain values, the system stability can be evaluated.

5.2.1 Effects of gain parameters K_V and R_h on system stability

The stability analysis is carried out by varying the voltage gain K_V over the range, $0 < K_V < 3$ for different values of R_h. For the single compensator hybrid topology (discussed in Chapter 4), the current gain R_h does not have any effect on stability limits. The voltage gain however, strongly influences the stability margin. In the case of the two-series compensator, it is found that both R_h and the load impedance affect the gain margin. This is because the compensator towards the load side, which corrects the voltage distortion in the passive filter does not allow the shunt passive filter to completely mask the load variations. The system and filter parameters used in this investigation are shown in Table 5.1.

The root-locus plots, shown in Figs 5.3 to 5.5) are obtained for three different loading conditions; $|Z_L| = 0.5p.u$(Heavy load), $|Z_L| = 2p.u$ and $|Z_L| = 4p.u$(Light load). The maximum value of K_V that leads to instability for a given value of Z_L and R_h is termed as the critical gain $K_{V_{crit}}$. The MATLAB codes for the root-locus plots are given in Appendix B.

Table 5.1: System parameters for single-phase analysis

AC voltage source	200V (phase voltage), 60 Hz, THD = 15%
Line impedance	Lt = 0.1mH, Rt = 0Ω
Nonlinear load	20kVA, THD = 30%
Shunt filter	Q = 6, L5 = 0.82mH, C5 = 340μF L7 = 0.82mH, C7 = 170μF LH = 0.26mH, CH = 300μF, RH = 3Ω

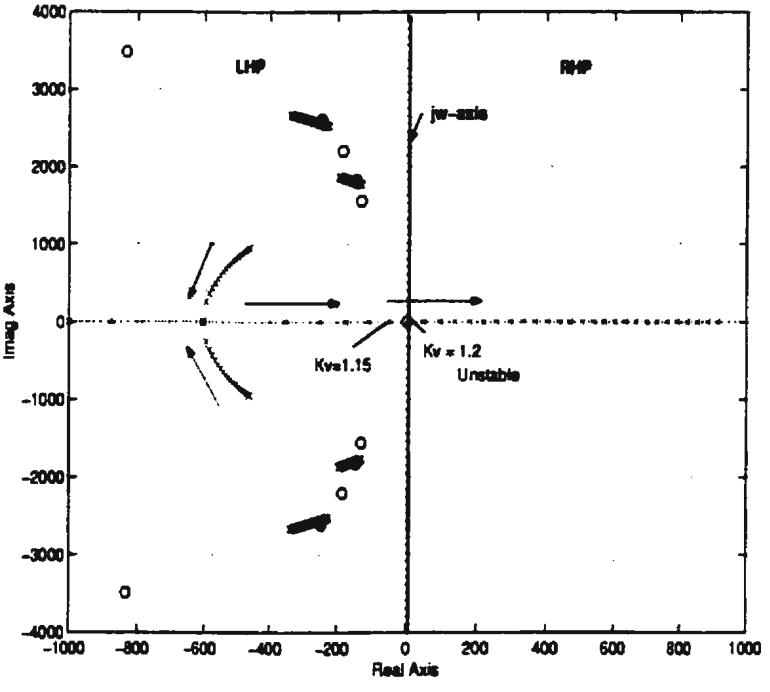

Figure 5.3: Root-locus plot with $R_h = 5$, $Z_L = 0.5$ p.u.

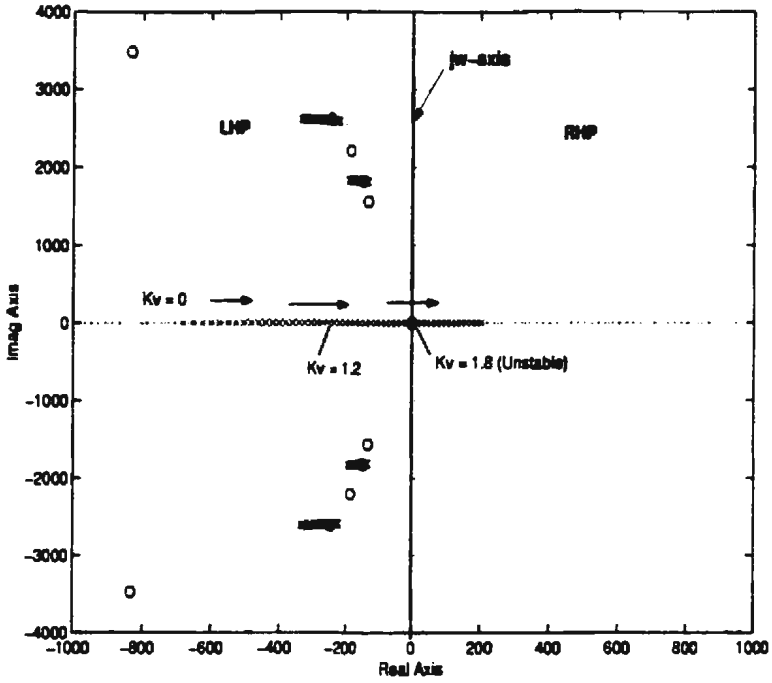

Figure 5.4: Root-locus plot with $R_h = 5$, $Z_L = 2.0$ p.u.

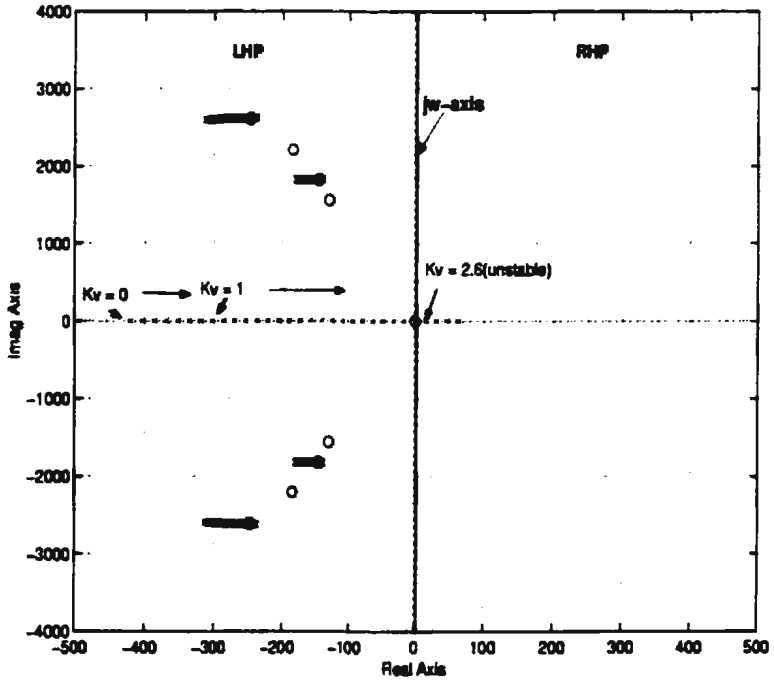

Figure 5.5: Root-locus plot with $R_h = 5$, $Z_L = 4.0$ p.u.

Table 5.2: Effect of load changes on the stability margin

Load Z_L(p.u)	Critical gain ($K_{V_{crit}}$)
0.5	1.2
2	1.8
4	2.6

The critical gain is read off the root-locus plot and shown in Table 5.2. From the results shown in Table 5.2, it is observed that for a fixed value of R_h, the critical gain $K_{V_{crit}}$ increases with increasing load impedance. What this means, is that for a load variation between 0.5p.u and 4p.u, it is possible to keep the voltage gain K_V around the desired 'unity' value without violating the stability limit.

A plot of $K_{V_{crit}}$ against load impedance Z_L in Fig. 5.6 indicates the shift in the stability boundary for three different values of R_h. It is observed that as R_h increases the stability boundary for the proposed topology drops and for very high values the boundaries for the basic series compensator and the proposed two-compensator topology coincide.

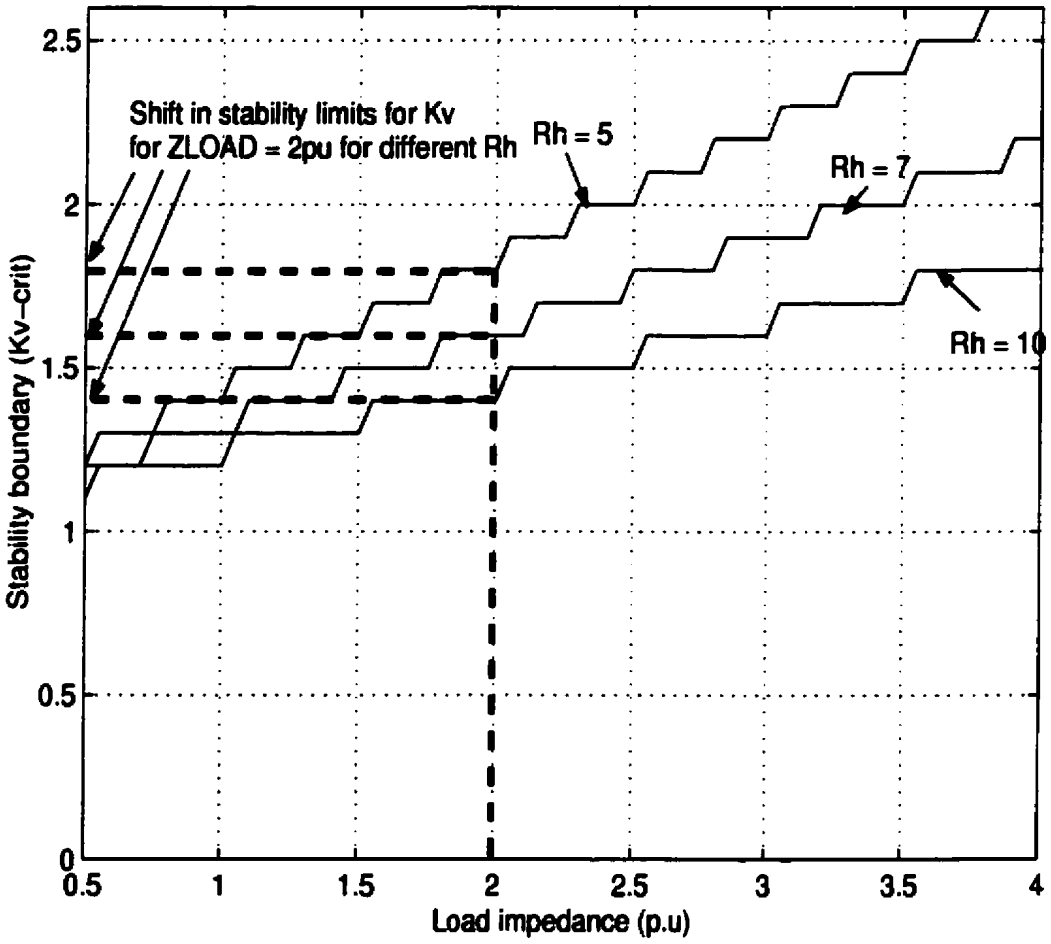

Figure 5.6: Change in critical gain $K_{V_{crit}}$ with load for $R_h = 5, 7, 10$.

5.3 Harmonic Isolation and Suppression of Voltage Distortion

The curves for harmonic isolation are the same as shown in Fig. 4.7 since the transfer function $\frac{I_{S_h}(s)}{I_{L_h}(s)}$ takes the same form as in (4.32) for $K_V = 0$. The properties of the two-compensator topology can be described by plotting the distortion in the load voltage and distortion in supply current (measure of harmonic isolation) against K_V and R_h. A SIMULINK model was constructed for the single-phase harmonic equivalent model of Fig. 5.2. The details of the SIMULINK models are given in Appendix A. The resulting plots of the distortion in the load voltage and supply current are shown in Figs 5.7 and 5.9. Corresponding plots for the single compensator topology are shown in Figs 5.8 and 5.10. The results are compared to highlight the improvements in compensation for the proposed two-compensator topology. From Figs 5.7 and 5.8 it is seen that for the two-compensator topology, the load voltage THD is approximately 0% for $K_V = 0.95$ and $R_h = 10$. The corresponding voltage distortion level with the single compensator topology is 7.5%. Figs 5.9 and 5.10 show that for $R_h = 10$ and any value of K_V, both topologies provide almost perfect isolation, since the THD in the supply current is almost zero. The above two observations confirm the fact that the residual distortion seen in the voltage plot for the single compensator is due to the passive filter drop caused by the circulation of the load current harmonics within the filter-load loop. The second compensator helps in cancelling the residual

distortion.

Since the second compensator is installed at the load side of the shunt passive filter any changes in K_V will have little impact on the distortion levels of the load current. Consequently, for a fixed value of R_h, there is hardly any variation in the load current distortion. However, this is not the case for the single compensator topology.

One important fact to be noted from Fig. 5.7 is that although the load voltage distortion reaches a local minimum for $0 < K_V < 1$, and $R_h < 2$, it does not coincide with the minimum for the supply current distortion plot. A choice of optimum parameters is made by observing both the current and voltage distortion plots and choosing that set of values that minimizes THD in the load voltage and supply current. From the plots shown, $K_V = 1.0$ and $R_h = 10$ meet the requirement for the proposed topology. Stability considerations serve as additional constraints in the selection of the parameters. For a given load impedance, an increase in R_h reduces the stability limit (Fig. 5.6).

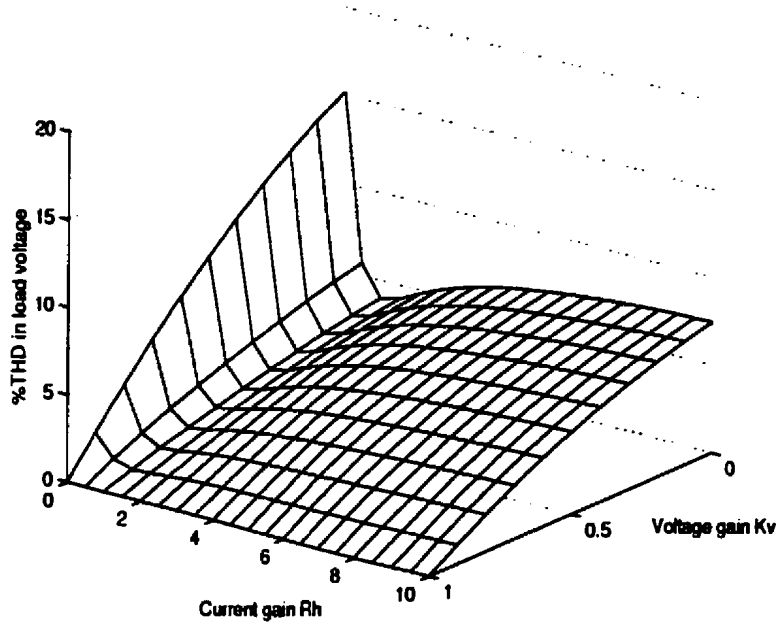

Figure 5.7: Terminal voltage distortion as a function of the gain parameters for the proposed two-compensator topology

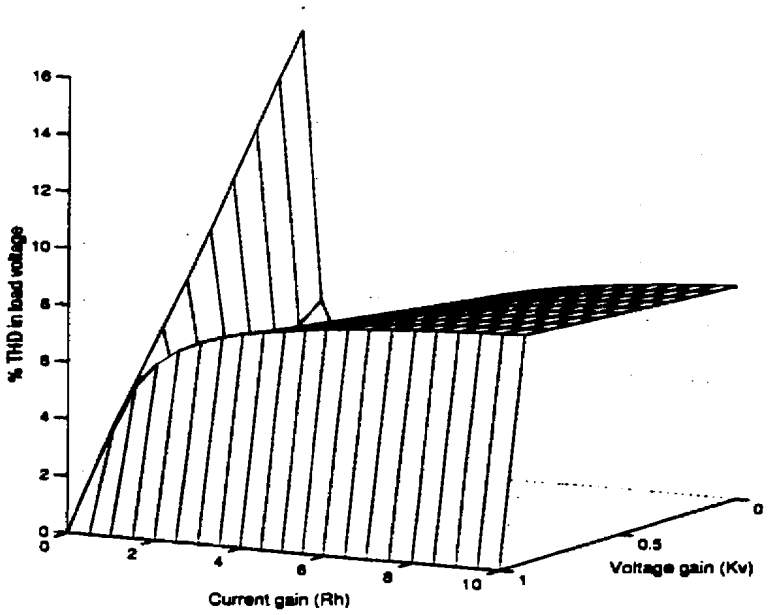

Figure 5.8: Terminal voltage distortion as a function of the gain parameters for the single compensator topology

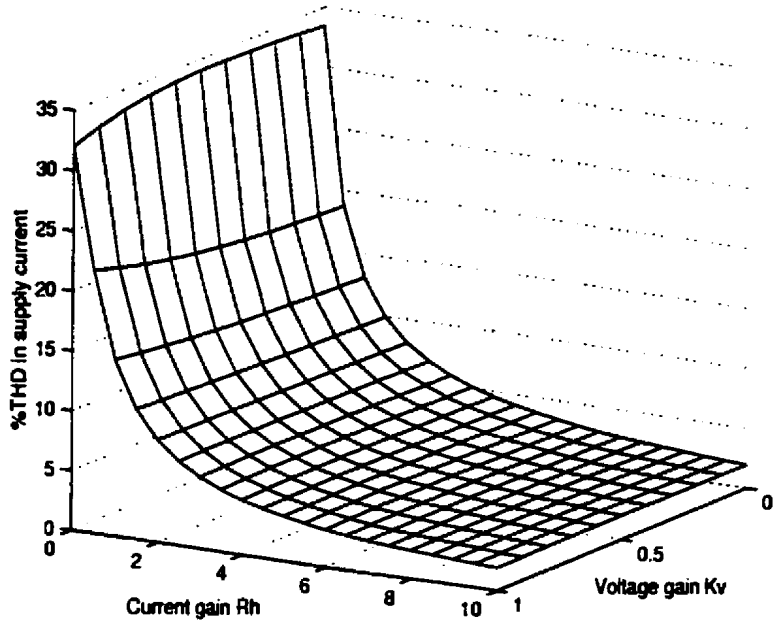

Figure 5.9: Supply current distortion as a function of the gain parameters for the proposed two-compensator topology

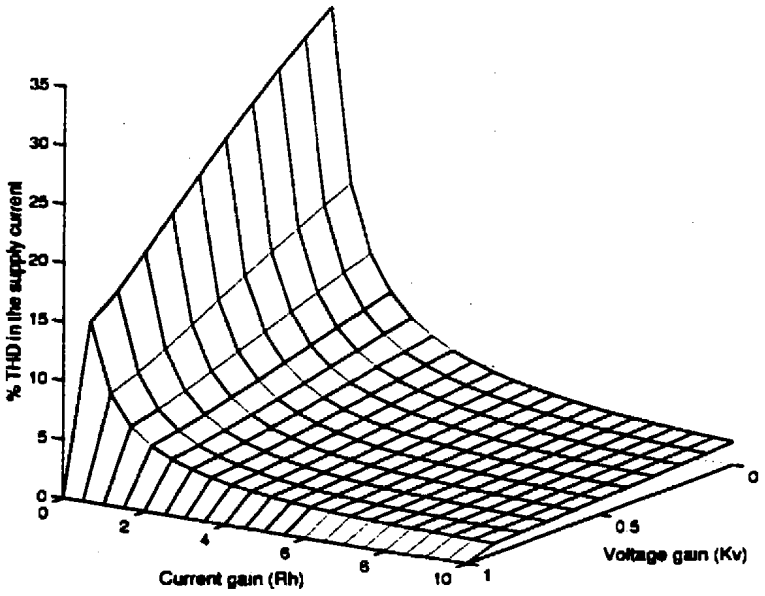

Figure 5.10: Supply current distortion as a function of the gain parameters for the single compensator topology

5.4 Compensator Ratings

In the two-compensator topology, the kVA rating of the harmonic isolator C1 (located at the supply side of the shunt passive filter) is expected to be lower than the rating of the voltage compensator C2 (located at the load side of the shunt filter). The ratings of the respective compensators are calculated below.

The same steps outlined in Chapter 4 for determining the ratings are followed here. The only difference here is that to compute the ratings of the individual compensators two sets of parameters need to be determined: V_{C1}, V_{C1_1} and V_{C1_h} for compensator C1; V_{C2}, V_{C2_1} and V_{C2_h} for compensator C2. The ratings of the harmonic isolator C1 and the voltage compensator C2 are given by

$$KVA_{C1} = |\mathbf{V_{C1}}| \cdot |\mathbf{I_{C1}}| \tag{5.7}$$

$$KVA_{C2} = |\mathbf{V_{C2}}| \cdot |\mathbf{I_{C2}}| \tag{5.8}$$

where

$$\left.\begin{aligned} \mathbf{V_{C1}} &= \sqrt{\mathbf{V_{C1_1}^2} + \mathbf{V_{C1_h}^2}} \\ \mathbf{I_{C1}} &= \sqrt{\mathbf{I_{C1_1}^2} + \mathbf{I_{C1_h}^2}} \end{aligned}\right\} \tag{5.9}$$

$$\left.\begin{aligned} \mathbf{V_{C2}} &= \sqrt{\mathbf{V_{C2_1}^2} + \mathbf{V_{C2_h}^2}} \\ \mathbf{I_{C2}} &= \sqrt{\mathbf{I_{C2_1}^2} + \mathbf{I_{C2_h}^2}} \end{aligned}\right\} \tag{5.10}$$

Using (5.15) and (5.18), the harmonic components of the two-compensator voltages are calculated as

$$\mathbf{V_{C1_h}} = R_h \cdot \mathbf{I_{S_h}} \tag{5.11}$$

$$\mathbf{V_{C2_h}} = (\mathbf{I_{S_h}} - \mathbf{I_{L_h}}) \cdot \mathbf{Z_F} \tag{5.12}$$

The harmonic components of the currents flowing through the compensators are given by

$$\mathbf{I_{C1_h}} = \mathbf{I_{S_h}} \tag{5.13}$$

$$\mathbf{I_{C2_h}} = \mathbf{I_{L_h}} + \frac{\mathbf{V_{L_h}}}{\mathbf{Z_L}} \tag{5.14}$$

The load voltage distortion can be expressed as

$$\mathbf{V_{L_h}} = \mathbf{G_1} \cdot \mathbf{V_{S_h}} + \mathbf{G_2} \cdot \mathbf{I_{L_h}} \tag{5.15}$$

where

$$\mathbf{G_1} = \frac{\mathbf{Z_F Z_L}(1 - K_V)}{[(\mathbf{Z_t} + R_h)(1 - K_V) + (\mathbf{Z_t} + \mathbf{Z_F} + R_h)Z_L]} \tag{5.16}$$

$$\mathbf{G_2} = \frac{-\mathbf{Z_L Z_F}(\mathbf{Z_t} + R_h)(1 - K_V)}{[\mathbf{Z_L}(\mathbf{Z_F} + \mathbf{Z_t} + R_h) + (1 - K_V)\mathbf{Z_F}(\mathbf{Z_t} + R_h)]} \tag{5.17}$$

The supply current distortion is determined using

$$\mathbf{I_{S_h}} = \mathbf{I_{L_h}} + \frac{\mathbf{V_{L_h}}}{\mathbf{Z_L}} + \frac{\mathbf{V_{L_h}}}{(1 - K_V)\mathbf{Z_F}} \tag{5.18}$$

Since the compensator C1 injects a voltage in phase with the harmonic component of the supply current, the fundamental component of the injected compensator C1 voltage V_{C1_1} is zero. Assuming a 30% sag, the fundamental component of the compensator voltage is obtained as

$$|\mathbf{V_{C2_1}}| = 0.3 \cdot V_S \tag{5.19}$$

$$|\mathbf{I_{C1_1}}| = |\mathbf{I_{C2_1}}| = \frac{Rating(linearload) + Rating(NLload)}{V_S} \tag{5.20}$$

The effective magnitudes of the compensator voltages and currents are calculated using the same procedure discussed in Chapter 4. Finally, the ratings of the two-compensators are determined using (5.7) and (5.8). The effective two-compensator rating, which is a measure of its cost is given by

$$KVA_{eff} = KVA_{C1} + KVA_{C2} \tag{5.21}$$

5.4.1 Effect of controller gain on compensator ratings

The compensator ratings were calculated using the MATLAB routine given in Appendix B for Q = 10 and 20 for the same system parameters used in Section 4.7.2. It must be noted that the two-compensator topology can operate at a voltage gain K_V of unity. This helps in eliminating the compensation error E_r in the fundamental component of the load voltage.

Fig. 5.11(a) shows that the effective rating KVA_{eff}, of the two-compensator configuration increases with an increase in current gain R_h. The rating of the harmonic isolator increases with R_h because of the increasing power dissipation due to the harmonics. A high Q reduces the VA rating of the harmonic isolator by shunting a higher percentage of the load current harmonics through the passive filter. An increase in Q reduces the voltage distortion seen by the voltage compensator C2 but has a marginal effect on its rating since the distortion component is relatively small as compared to the fundamental. As in the previous chapter, by setting $V_{S_h} = 0$ in (5.15) and (5.18)

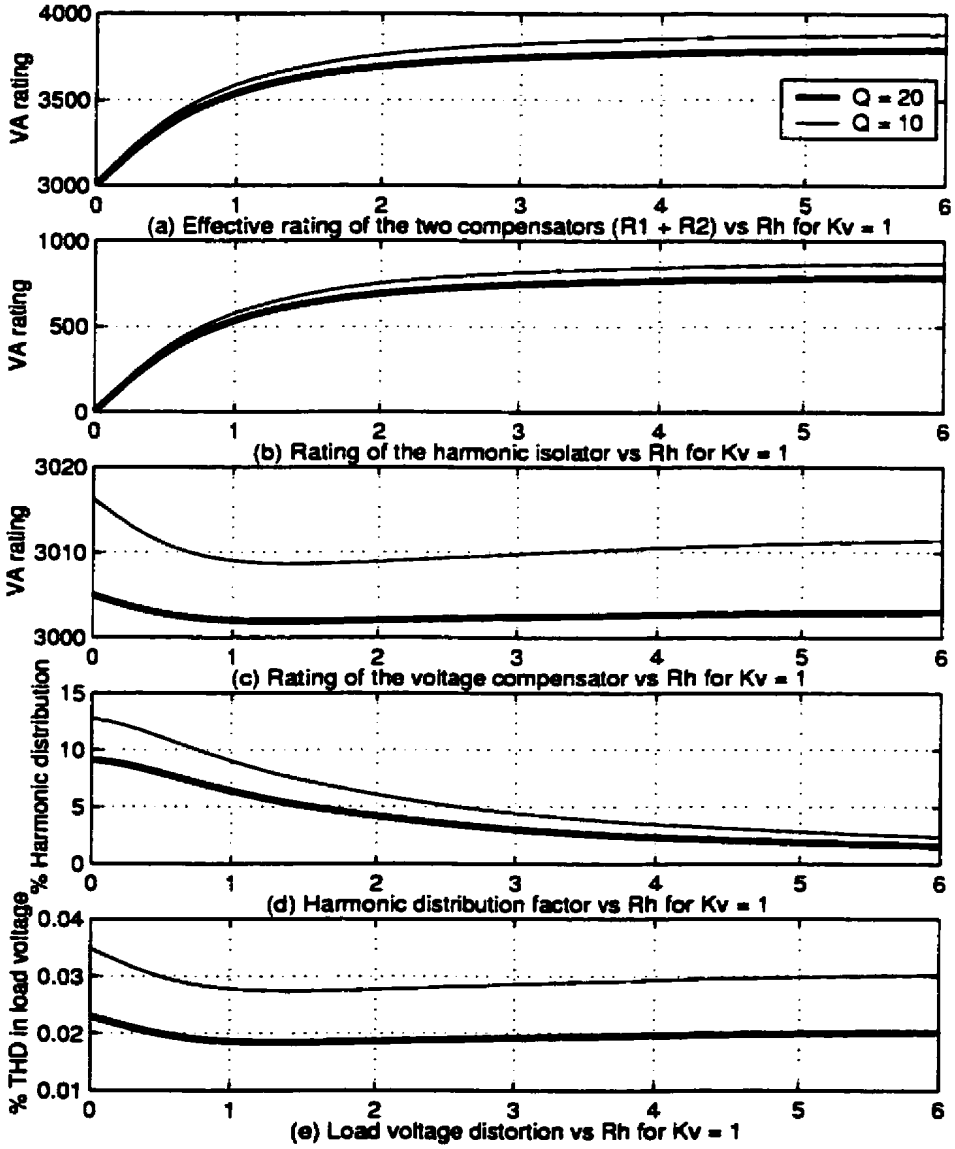

Figure 5.11: Two compensator ratings and supply current distortion as a function of R_h

the harmonic distribution factor can be written as

$$\frac{\mathbf{I_{S_h}}}{\mathbf{I_{L_h}}} = 1 - \frac{(\mathbf{Z_L} + (1 - K_V)\mathbf{Z_F})(\mathbf{Z_t} + R_h)}{[\mathbf{Z_L}(\mathbf{Z_F} + \mathbf{Z_t} + R_h) + (1 - K_V)\mathbf{Z_F}(\mathbf{Z_t} + R_h)]} \tag{5.22}$$

By increasing R_h the harmonic distribution factor reduces considerably. The other advantage of having a high R_h is to prevent other nonlinear loads at the supply end from pumping harmonics into the shunt passive filter. The consequence is that for a high value of R_h the rating of the shunt filter reduces, since it has to bypass harmonics drawn only from the critical load.

5.5 Quantitative comparison of the two topologies

The KVA ratings of the single compensator and two-compensator topologies are compared by assuming a harmonic distribution factor of 5%, i.e. 5% of the load induced harmonics is allowed to flow into the supply side. The corresponding current gains at Q = 10 for the single and two-compensator topologies are R_h = 3.5 and R_h = 2.5, respectively. The VA ratings of the single and two-compensator compensator topologies are 2500 VA and 3700 VA respectively. For the same degree of isolation (5%), the corresponding current gain required is much higher. One of the reasons for a higher R_h is because of the apparent reduction in line impedance due to the voltage cancellation term $K_V \cdot V_{F_h}$ in the injected voltage. Thus, there is a higher power dissipation in the transformer windings of the single compensator.

Table 5.3 provides a quantitative comparison of the key performance measures of

the two topologies. The proposed two-compensator topology provides a distinct improvement over the single compensator topology in terms of the percentage reduction in the compensation error and reduction in load voltage distortion. To achieve the same level of harmonic isolation, the two-compensator topology requires a relatively smaller current gain R_h which reduces the power dissipation in the harmonic isolator. The proposed topology permits a wider voltage gain margin (Fig.5.6) which allows the compensator to be operated at the desired gain value of unity without compromising the stability margin.

Table 5.3: Quantitative comparison of the two topologies

Aspects	Single compensator	Two-compensator
Compensation error (%)	10	0
Harmonic distribution factor (%)	5	5
Current gain (R_h)	3.5	2.5
Load voltage distortion (%)	3.7	0.03
Stability margin (%)	< 1	< 1.5
Compensator rating (kVA) (%)	2.5	3.7

5.6 Summary

In this chapter, a topology comprising two series compensators was proposed. The functions of harmonic isolation and voltage compensation were split into two series compensators. The compensator at the load side improves the load voltage profile by cancelling out the harmonic distortion induced by the current flowing through the shunt passive filter, while the one at the source end serves as a harmonic isolator. The

analysis shows that for lighter loads (large load impedances), the voltage compensator can operate at the desired value of K_V, which is unity. This is possible because the critical voltage gain $K_{V_{critical}}$ is much larger than unity for large load impedances. However, $K_{V_{critical}}$ decreases and approaches unity as the load impedance decreases. Hence for very small load impedances, the operating gain must be at least 10-20% below unity, which means there will be an error in the voltage compensation.

From the stability-boundary plot, it was inferred that an increase in R_h reduces the stability limit and thus decreases the critical voltage gain of the compensator. A high R_h reduces the THD of the supply current and load voltage, but on the other hand it reduces the value of the critical gain. Hence the value of R_h must be chosen on the basis of a tradeoff between the stability limit and the degree of harmonic suppression.

To determine the additional tradeoffs required in selecting the current gain R_h, the compensator ratings and the corresponding harmonic distribution and load voltage distortion levels were calculated for different values of R_h . The proposed two-compensator topology was shown to provide a distinct improvement over the single compensator topology in terms of the percentage reduction in the compensation error and reduction in load voltage distortion. The price that will be paid for these improvements is two series compensators.

Chapter 6

Simulation of the Overall System

Introduction

In the previous chapter a new topology based on two series compensators was proposed and an analysis of its single-phase equivalent circuit was carried out. In this chapter, simulation results of the two-compensator topology are presented. The results are shown for different cases to illustrate the roles played by the two compensators in suppressing the supply current harmonics, and cancelling the harmonics and negative sequence components in the load voltage.

6.1 System Configuration and Parameters

The complete system of the two series compensators simulated in this chapter is shown in Fig. 6.1. The system comprises two series compensators (C1 and C2), matching transformers and a passive shunt filter. The compensator C1 is connected in series with the supply through a matching transformer, while the second compensator C2 is connected in series with the load. The control unit, which is common to both the

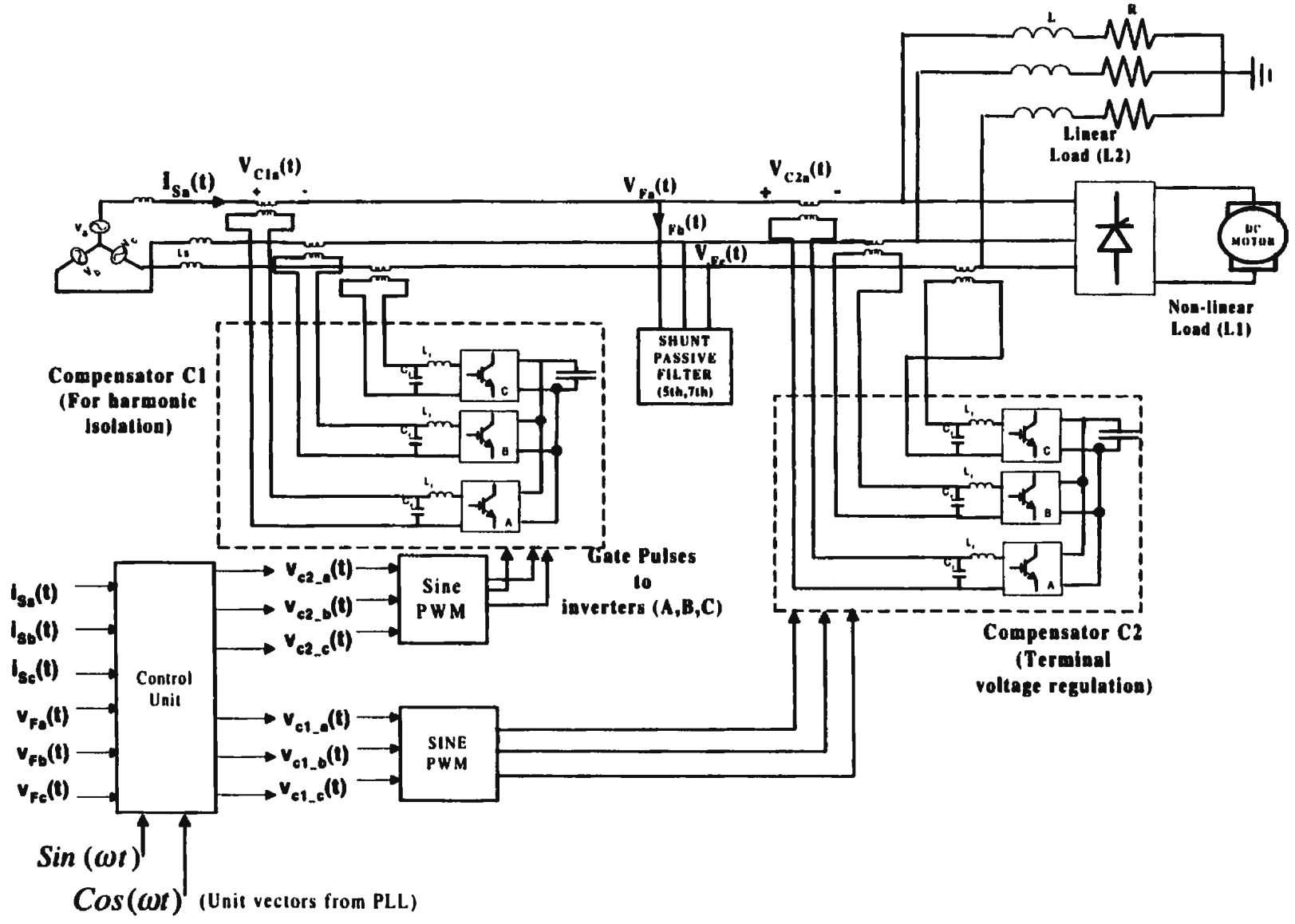

Figure 6.1: Complete system with two series compensators

compensators, controls C1 as a harmonic isolator and C2 as a voltage compensator. The internal details of the respective voltage and current compensation units, VCU and HCEU, are as described in Chapter 3 (Figs 3.2 and 3.12). Two different loads are connected in shunt with the passive filter (PF); a harmonic producing load (L1), which is modeled as a constant current source, and a linear R-L load (L2). The exact harmonic constitution of the nonlinear load is shown in Table 6.1.

To compare the results, the supply and load parameter values are chosen exactly the same as in [10]. The passive filter consists of 5^{th}, 7^{th} tuned filter banks and a high pass filter. The passive filter parameters are shown in Table 6.2 and the system parameters are as follows:

- Source: 200V, 60Hz, THD = 12%; Source inductance, $L_t = 0.5$mH.
- Nonlinear load (L1): 20kVA, $THD_{L_1} = 27.3\%$
- Linear load (L2): 10kVA, R = 4Ω, L = 2mH
- Controller Parameters: $K_V = 1.0$, $R_h = 2.5$

Table 6.1: Harmonic components of load current(L1)(THD = 27.3%)

Harmonic Order(n)	$I_{L_n}\%$
5^{th}	20
7^{th}	14.3
11^{th}	9.1
13^{th}	7.3

Table 6.2: Passive filter parameters

Type	L(mH)	C(uF)	Q
5^{th}	0.82	340	6
7^{th}	0.82	170	6
HPF	0.26	300	6

6.2 Simulink Model of the Overall System

A prototype model of the system was constructed in SIMULINK to verify the functionality and performance of the two series compensator topology. The details of the SIMULINK model are given in Appendix A.

The ideal control gain of the harmonic isolator is $R_h = \infty$ and that of the voltage compensator is $K_V = 1$. In the simulation however the gain of the current compensator was restricted to $R_h = 2.5$. It was observed that for much larger values of R_h, K_V had to be lowered to a value less than unity to ensure convergence. This observation was consistent with the analysis of the effects of gain parameter changes on stability and terminal voltage distortion in Chapter 5. The optimum set of values of the compensator gains was obtained on the basis of a tradeoff between stability and voltage compensation during sags and swells.

In the VCU, the reference d-q-0 coordinates were set to compensate for any phase difference between the PLL sine reference signal and the fundamental component of the reference voltage. The input signal to the PLL was filtered to eliminate the possibility of getting multiple zero crossings. The corresponding changes to the reference d,

q coefficients in the VCU was made to account for this filter delay. The consequences of this phase difference are discussed in Appendix C.

The simulation model for the overall system was constructed using the SIMULINK toolboxes (Control System and Power System toolboxes) in MATLAB. The linear control system model was developed based on signal flow graphs, as an approximation to the practical system. In this SIMULINK model, the transformers were assumed to be ideal and the inverter was represented by a gain block. Thus on the whole, the compensator was represented as an ideal controllable voltage source, which simplified the SIMULINK model, reduced the total simulation time and also minimized convergence errors introduced by the differential equation solvers. The MATLAB routine for initializing the parameters is given in Appendix B. The THD and FFT computations were carried out using the MATLAB routine described in Appendix B.

6.3 Simulation Results

In order to investigate the compensation capability of the overall system, three different cases were considered:

- Case 1 (PF): Compensation with the passive shunt filter alone (with both linear and nonlinear loads).

- Case 2 (PF + C1): Compensation with passive shunt filter and harmonic isolator for $R_h = 2.5$.

- Case 3 (PF + C1 + C2): Compensation with the passive shunt filter and two compensators for $R_h = 2.5$ and $K_V = 1$.

In all the cases, a 30% single-phase sag was introduced in phase-a to simulate an imbalance in the supply voltage. Generally, the third harmonics are prevented from circulating in the power system by wye-delta connections. The third harmonic, if present, can be extremely deleterious mainly because it is not bypassed by the passive shunt filter. The presence of the harmonic isolator (C1) in such a case, is very beneficial. Further analysis of the graphical data for the three cases to determine the THD of the supply and load voltage and currents are carried out. The results are presented in Table 6.3. The progressive improvement in the current and voltage profiles of the load voltage and supply current waveforms are demonstrated in the following sections. The effects of increasing the current gain R_h and voltage gain K_V on the supply current distortion and compensation error are discussed in Appendix C.

6.3.1 Compensation with passive filter (PF)

In this case, only the passive filter is connected to the system. The other two compensators are disconnected. Since the passive filter comprises tuned L-C filters for 5^{th} and 7^{th}, and a high pass filter for the higher-order harmonics, the third harmonic, if present, will flow into the load. The simulation waveforms for this case are presented in Fig. 6.2. The percentage third harmonic distortion in the load voltage (V_{L_3} =

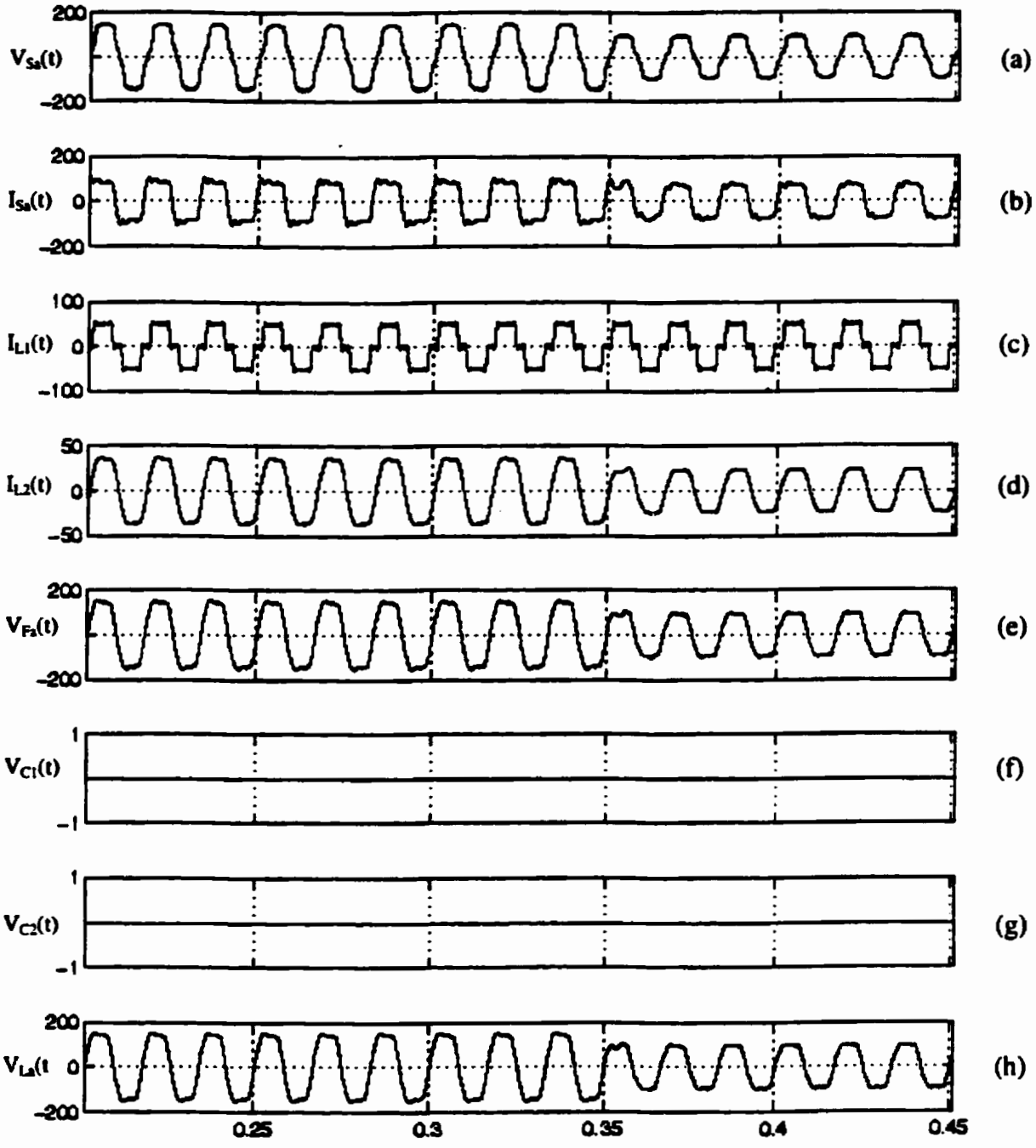

Figure 6.2: Simulation waveforms when both series-compensators are not connected ($\mathbf{K_V = 0, R_h = 0}$).
(a) Supply voltage (phase-a); (b) Supply current, $I_{Sa}(t)$; (c) Non-linear load (L1) current, $I_{L1}(t)$; (d) Linear load (L2) current; (e) Voltage across passive filter; (f) Voltage injected by harmonic isolator (COM1); (g) Voltage injected by COM2; (h) Terminal load voltage, $V_{La}(t)$

Table 6.3: Distortion levels in the supply and load voltages and currents

OPERATION MODE	$V_{S_{a_h}}$[%]	$I_{S_{a_h}}$[%]	$I_{L_{1_h}}$[%]	$I_{L_{2_h}}$[%]	$V_{F_{a_h}}$[%]	$V_{L_{a_h}}$[%]
K_V=0,R_h=0.0	12.1	29.8	27.3	12.8	14.7	14.7
K_V=0,R_h=2.5	12.1	7.2	27.3	2.2	3.1	3.1
K_V=1,R_h=2.5	12.1	7.2	27.3	1.3	2.7	1.6

$V_{S_{a_h}}$ Harmonic component of the supply voltage
$I_{S_{a_h}}$ Harmonic component of the supply current
$I_{L_{1_h}}$ Harmonic component of the nonlinear load (L1) current
$I_{L_{2_h}}$ Harmonic component of the critical load (L2) current
$V_{F_{a_h}}$ Passive filter voltage drop
$V_{L_{a_h}}$ Load voltage distortion

14.7%) is almost twice that of the source (V_{S_3} = 7.3%). This reflects as a flat top in the load voltage waveform, v_{L_a}(t). The reason for this unexpected increase in third harmonic distortion is because the shunt passive filter behaves as a capacitor for frequencies below the 5^{rd} harmonic. However, due to the tuned L-C filters and high pass filter, the 5^{th}, 7^{th} and higher-order harmonics are suppressed.

In the absence of the harmonic isolator, much of the harmonic load current flows into the supply lines thereby increasing the source current THD (I_{S_h} = 29.8%). The third harmonic supply voltage component also contributes to the increased distortion in the supply current, i_{S_a}(t). Also, in the absence of the voltage compensator the sag in the supply voltage is not corrected at the load.

The current flowing through the critical load, i_{L_2}(t), has a high harmonic content ($I_{L_{2_h}}$ = 12.8%) mainly due to the terminal load voltage distortion.

6.3.2 Compensation with passive filter and harmonic isolator (PF+C1)

With the compensator C1 connected, the terminal load voltage distortion reduces from 14.7%(Case 1) to 3.1%. This THD is the residual total harmonic distortion primarily due to the harmonic drop across the shunt passive filter. The third harmonic in the load voltage is suppressed due to the fictitious series resistance $R_h = 2.5\Omega$.

As a result of this decrease in load voltage distortion, the harmonics in the linear load, i_{L_2} ($I_{L_{2_h}} = 2.2\%$) is reduced to about one-sixth its rms value from that of Case-1. There is, however, a reduction by a factor of four from that of Case 1 in the supply current distortion ($I_{S_h} = 7.2\%$).

The compensator C1 injects a harmonic voltage, $V_{C_1}(t)$, with an rms value of around 15V (Fig. 6.3(f)). At the time of the sudden single-phase voltage transition, the output voltage of C1 picks up a fundamental component but recovers in about $1\frac{1}{2}$ cycles. The load voltage waveform shows that the harmonic isolator does not correct for the voltage sag.

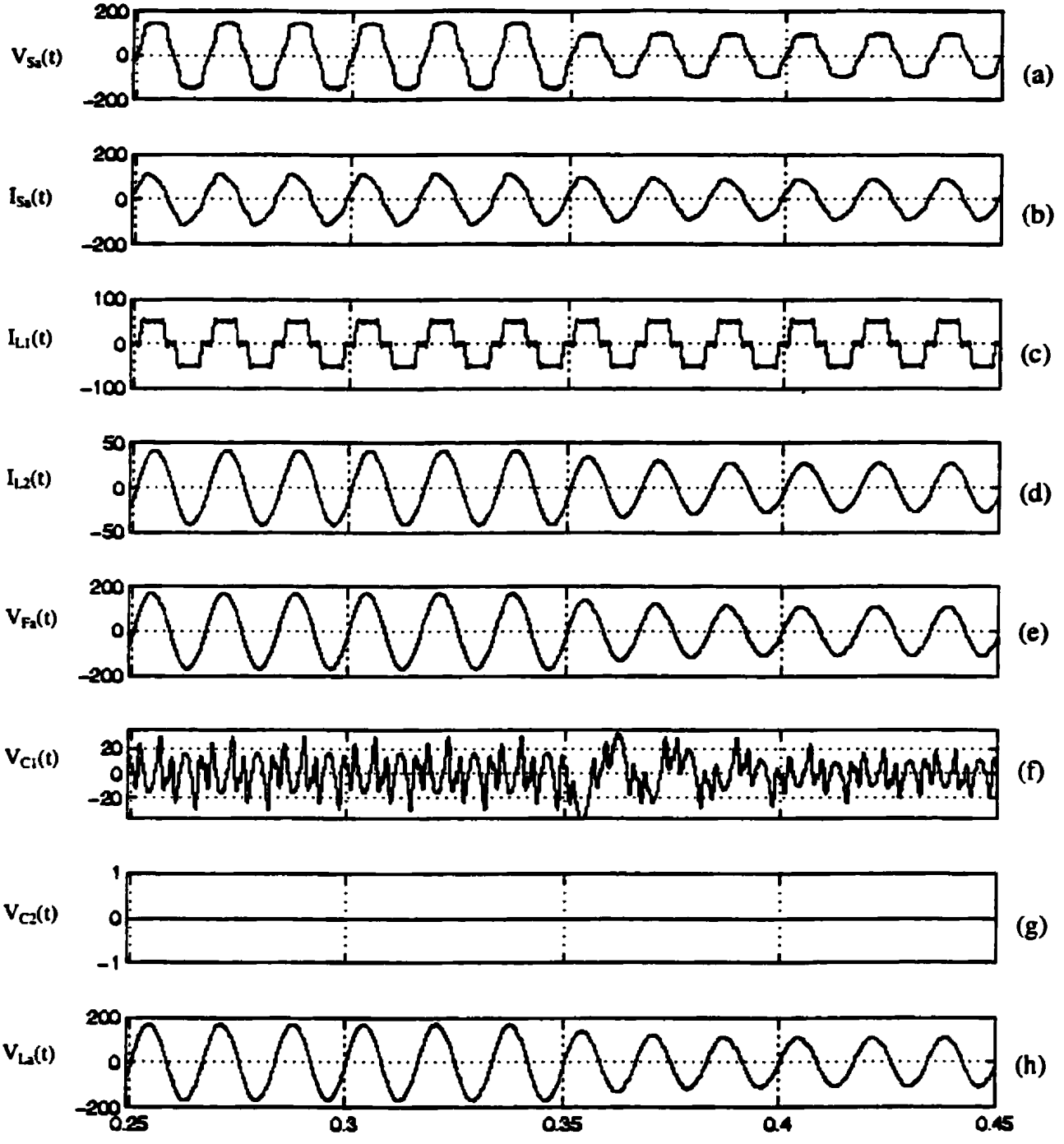

Figure 6.3: Simulation waveforms with harmonic isolator and passive filter ($K_V = 0$, $R_h = 2.5$).
(a) Supply voltage (phase-a); (b) Supply current, $I_{Sa}(t)$; (c) Non-linear load (L1) current, $I_{L1}(t)$; (d) Linear load (L2) current; (e) Voltage across passive filter; (f) Voltage injected by harmonic isolator (COM1); (g) Voltage injected by COM2; (h) Terminal load voltage, $V_{La}(t)$

6.3.3 Compensation with passive filter, harmonic isolator and voltage compensator (PF + C1 + C2)

In this case, the passive filter and the two compensators are connected. When a voltage sag is introduced in the supply voltage, the voltage compensator C2 not only restores the fundamental component but also cancels the shunt filter distortion as shown in Fig. 6.4. The compensator C2 also injects a voltage to overcome the voltage drop across the line impedance.

The voltage compensation appears to be almost instantaneous due to the ideal transformer and inverter characteristics Fig. 6.4(h). However, non-ideal characteristics of components will delay the response time and introduce a nonlinearity in the phase response. The consequences may reflect as short term glitches or oscillations in the load voltage.

The second compensator reduces the load voltage THD further to 1.6%. The harmonics in the critical load current (i_{L_2}) are almost completely nullified by the harmonic voltage cancellation of C2. The supply current distortion remains the same as in Case 2 (7.2%), indicating that C2 does not affect the harmonic isolation provided by C1.

Additional results for two sets of voltage and current gains are given in Appendix C. The results indicate that increasing the current gain decreases the supply current distortion. However, from stability considerations higher values of current gain require

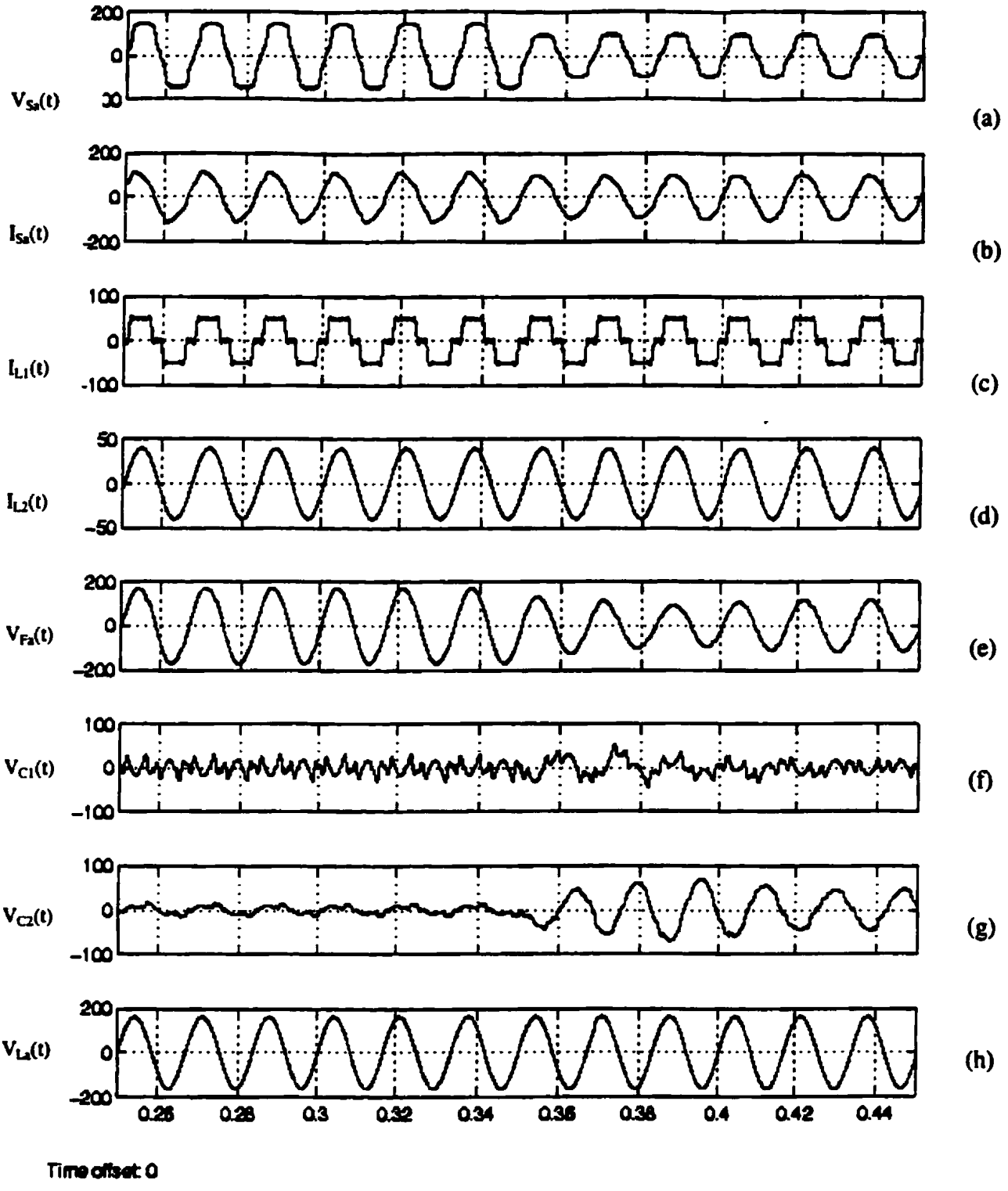

Figure 6.4: Simulation waveforms with harmonic isolator and passive filter ($K_V = 1$, $R_h = 2.5$).
(a) Supply voltage (phase-a); (b) Supply current, $I_{Sa}(t)$; (c) Non-linear load (L1) current, $I_{L1}(t)$; (d) Linear load (L2) current; (e) Voltage across passive filter; (f) Voltage injected by harmonic isolator (COM1); (g) Voltage injected by COM2; (h) Terminal load voltage, $V_{La}(t)$

that the voltage gain be reduced. On the other hand a reduction in the voltage gain increases the compensation error.

6.4 Summary

The functionality of the new topology based on two compensators was verified for a varied choice of controller parameters. Higher values of R_h had to be traded off against a reduced value of voltage gain, K_V due to stability problems.

The second compensator C2, almost completely eliminates the distortion in the load voltage. The two controller units, VCU and HCEU, performed effectively in the presence of imbalance, zero sequence components and considerable supply voltage and current distortion. The results not only demonstrate the improved performance of the proposed topology, but also illustrates the effectiveness of the d-q-0 based scheme.

Chapter 7

Conclusions and Scope for Future Research

7.1 Summary and Conclusions

The main objective of this research work was to develop a suitable topology and control scheme to improve the load voltage and supply current profiles for critical load supplies. The use of one series active compensator with a passive shunt filter, termed the hybrid series compensator topology, was identified as a cost effective solution to current harmonic suppression. As the first step in the present research, the fundamental compensation principle was extended by adding the function of load voltage compensation.

The existing p-q based control scheme, applied to harmonic extraction, did not perform effectively under load imbalance and zero sequence components. Since the scheme was based on instantaneous power calculations, there was a strong coupling between the supply voltage and current components. Any fault in the supply voltage affected the process of current harmonic extraction. The p-q computation seemed

a redundant step toward harmonic extraction. To address this issue, and moreover to perform the additional function of voltage compensation, a more robust control scheme based on synchronous d-q-0 transformation was proposed. The control unit was split into two mutually decoupled functional units: the harmonic current extraction unit (HCEU) and the voltage compensation unit (VCU).

In the HCEU, two methods were proposed to extract the harmonic components. The first method, applicable to balanced load currents without any zero sequence components, gave the same advantages as the IRP scheme, albeit it was simpler to implement. The second method was slightly more complex, but was more robust and immune to imbalance and zero sequence components. In the second method, a balanced set of currents for each phase were generated and subjected to d-q-0 transformation and high-pass filtering to accurately determine the harmonic components of the supply current.

Having developed the control scheme, the next step was to investigate the effects of the voltage and current gains K_V and R_h, respectively, on the performance of the system. A single-phase equivalent circuit model was developed and used to study the effect of gain variations on stability and harmonic suppression. It was observed that in the single compensator model, K_V had to be restricted to a value less than unity to ensure system stability. R_h, on the other hand, had no effect on system stability. For the single compensator topology, characteristics plots of the load and

supply distortions versus the two gain parameters showed that for high values of R_h (i.e. $R_h > 5$), the THD of the load voltage was independent of K_V. This is because of the residual distortion developed across the shunt passive filter.

A new two-series compensator topology was proposed to overcome the residual distortion and increase the stability limits. By having two separate compensators to perform the functions of voltage compensation and isolation, the stability limits were increased. However, the critical gain margin for K_V was found to be dependent on R_h and the load. For a single-phase model, it was observed that an increase in R_h resulted in a decrease in the gain margin. To determine the additional tradeoffs required in selecting the current gain R_h, the compensator ratings and the corresponding harmonic distribution and load voltage distortion levels were calculated for different values of R_h. The proposed two-compensator topology was shown to provide a distinct improvement over the single compensator topology in terms of the percentage reduction in the compensation error and reduction in load voltage distortion. The price that will be paid for these improvements is an additional series compensator and two separate dc-link capacitor banks for the two compensators.

For controller gain values of $R_h = 2.5$ and $K_V = 1$, it was found that the supply current distortion was reduced considerably and the load voltage was balanced, sinusoidal and unperturbed by a single-phase fault. With R_h increased to 3.5 and K_V reduced to 0.3, the simulation results showed that the load voltage was restored to

75% of the nominal value during a single-phase fault, and the supply current distortion was reduced to a greater extent than the previous case. The results demonstrate that while a high value of R_h significantly reduces the current harmonics, from stability considerations R_h must be chosen to achieve a reasonable level of harmonic suppression in order to allow for a wide range of voltage compensation.

7.2 Scope for Future Research

In this research, the effects of the controller gain parameters on stability, and voltage and current profiles for the single and proposed two-compensator topologies were examined. The controller gain parameters can be optimized under constraints posed by the performance criteria of the system, such as: THD levels of load voltage and supply current, power dissipation in the series transformer, stability, dynamic response and load variation. A preliminary investigation regarding the influence of the gains on the first two criteria was carried out in this thesis. The effects of the other criteria on the gains was beyond the scope of this research. The formulation and solution of the constraint equations can be carried out for a specific system configuration. The challenge here would be, the choice of system configuration (based on its simplicity and extensibility) and the nature of the compensation equation.

In the two-compensator topology one of the compensators was controlled as a harmonic isolator and the other as a voltage compensator. This arrangement imposes mutual constraints on the values of gain parameters. A desired high current gain is

achieved at a price of a reduced voltage gain and consequently reduced range of voltage compensation. One possible solution to this problem is to use one of the two series compensators as a combined voltage compensator and harmonic isolator and the other as a voltage compensator. Three gain variables come into play R_h, K_{V_1} for COM1 and K_{V_2} for COM2. The conflict may be resolved by selecting different values of gains for various operating modes. For instance high R_h and low K_V may be selected for unfaulted conditions, and a relatively low R_h and unity voltage gain for fault conditions. It is expected that this approach can improve the voltage and current profiles. Further study is required to confirm the feasibility of this approach.

The proposed DHCE based harmonic extraction scheme provides an accurate estimate of the harmonics in the presence of zero and negative sequence components. However its implementation is relatively complex. Simplification of the harmonic extraction scheme, without compromising its desired features will be a worthwhile challenge.

Since the compensation is dependent on the filter response in the control path and sensor gains, it is important to track and compensate any filter nonlinearities, L,C parameter variations or sensor gain variations. A combination of feedback and feed-forward approach with an adaptive compensation scheme based on fuzzy or linear adaptive filtering techniques can account for load fluctuations and time varying parameters.

References

[1] N. Abi-Samra, D. Carnovale, A. Sundaram, and W. Malcolm, "The role of distribution system dynamic voltage restorer in enhancing the power at sensitive facilities," in *Conference Proceedings of WESCON 96*, Anaheim, California, pp. 167–181, Oct 22-24, 1996.

[2] T. Jauch, A. Kara, R. Mohamed, and D. Westermann, "Power quality ensured by dynamic voltage restoration," *ABB Review 4*, pp. 25–36, May 1998.

[3] J. Alfonso, C. Couto, and J.Martins, "Active filters with control based on the p-q theory," *IEEE Industrial Electronics Society Newsletter*, vol. 47, pp. 5–10, Sept 2000.

[4] H. Akagi, A. Kanazawa, and A.Nabae, "Instantaneous reactive power compensators comprising switching devices without energy storage elements," *IEEE Transactions on Industry Applications*, vol. IA-20, pp. 625–630, May/June 1984.

[5] B. Singh and A. Chandra, "A review of active filters for power quality improvement," *IEEE Transactions on Industrial Electronics*, vol. 46, pp. 960–971, Oct

1999.

[6] V. B. Bhavaraju and P. N. Enjeti, "Analysis, design of an active power filter for balancing unbalanced loads," *IEEE Transactions on Power Electronics*, vol. 8, pp. 640–647, Oct 1993.

[7] A. Campos, G. Joos, P. D. Ziogas, and J. F. Lindsay, "Analysis, design of a series voltage unbalanced compensator based on a three-phase VSI operating with unbalanced switching functions," *IEEE Transactions on Power Electronics*, vol. 9, pp. 269–274, May 1994.

[8] C. Hochgraf and R. H. Lasseter, "Statcom controls for operation with unbalanced voltages," *IEEE Transactions on Power Delivery*, vol. 13, pp. 538–544, April 1998.

[9] N. G. Hingorani and L. Gyugi, "Understanding facts - concepts and technology of flexible ac transmission systems," IEEE Press, 1999.

[10] F. Z. Peng, H. Akagi, and A. Nabae, "A new approach to harmonic compensation in power systems - A combined system of shunt passive and series active filters," *IEEE Transactions on Industry Applications*, vol. 26, pp. 983–990, Nov 1990.

[11] S. Bhattacharya and D. Divan, "Synchronous frame based controller implementation for a hybrid series active filter system," in *IEEE Industry Applications Conference (IAS)*, Orlando, Florida, vol. 3, pp. 2531–2540, Oct 8-12, 1995.

[12] C. Hochgraf and R. H. Lasseter, "Statcom controls for operation with unbalanced voltages," *IEEE Transactions on Power Delivery*, vol. 13, pp. 538–544, April 1998.

[13] T. Wunderlin, O. Amhof, P. Dahler, and H. Guning, "Power supply quality improvement with a dynamic voltage restorer (DVR)," in *IEEE International Conference on Energy Management and Power Delivery*, Singapore, pp. 518–525, March 1998.

[14] M. Aredes, K. Heumann, and E. H. Watanabe, "An universal active power line conditioner," *IEEE Transactions on Power Delivery*, vol. 13, pp. 545–551, April 1998.

[15] H. Fujita, Y. Watanabe, and H. Akagi, "Control and analysis of unified power flow controller," in *IEEE Power Electronics Specialists Conference (PESC)*, Fukuoka, Japan, vol. 1, pp. 805–811, May 17-22, 1998.

[16] J. W. Dixon, G. Venegas, and L. A. Moran, "A series active power filter based on sinusoidal current-controlled voltage-source inverter," *IEEE Transactions on Industrial Electronics*, vol. 44, pp. 612–619, Oct 1997.

[17] M. Rastogi, N. Mohan, and A. Edris, "Hybrid active filtering of harmonic currents in power systems," *IEEE Transactions on Power Delivery*, vol. 10, pp. 1994–2000, Oct 1995.

[18] T. M. W. Inc., "Matlab, version 4.2a.," Natick, Massachusetts, 1994.

[19] E. Wirth, T. Jauch, A. Kara, K. Chan, and A. Arora, "Innovative system solutions for power quality enhancement," *ABB Review 3*, pp. 4–12, April 1998.

Appendix A

Simulink Blocks

The overall three-phase system with the two compensator topology was constructed using the Control, Power and General toolboxes in SIMULINK. Because of the diversity of the dynamic system behaviour, using one type of an integro-differential solver does not necessarily guarantee identical results with another solver. Each solver is tailored to suit a particular dynamic model. A *stiff system*, such as the power system model, is characterized by fast and slow dynamics. Hence a stiff method (ODE45) was used to reduce simulation time.

For the simulation procedures, a linear transfer function(TF) based circuit model was used to verify the control operation. Although the linear TF-based model is not a very good approximation of a power system it has been used for quick verification of the control algorithm and to investigate the effects of parameter variations for off-line tuning of the controller. However it is understood that, in most simulation programs, any power-electronic circuit is approximated as a switched linear model in which the states in the system change dynamically. This dynamic alteration of the state-space

matrices makes the recursive solution method far more complex and time consuming.

The hierarchy of the SIMULINK blocks is illustrated by the chart shown in Figure A.1.

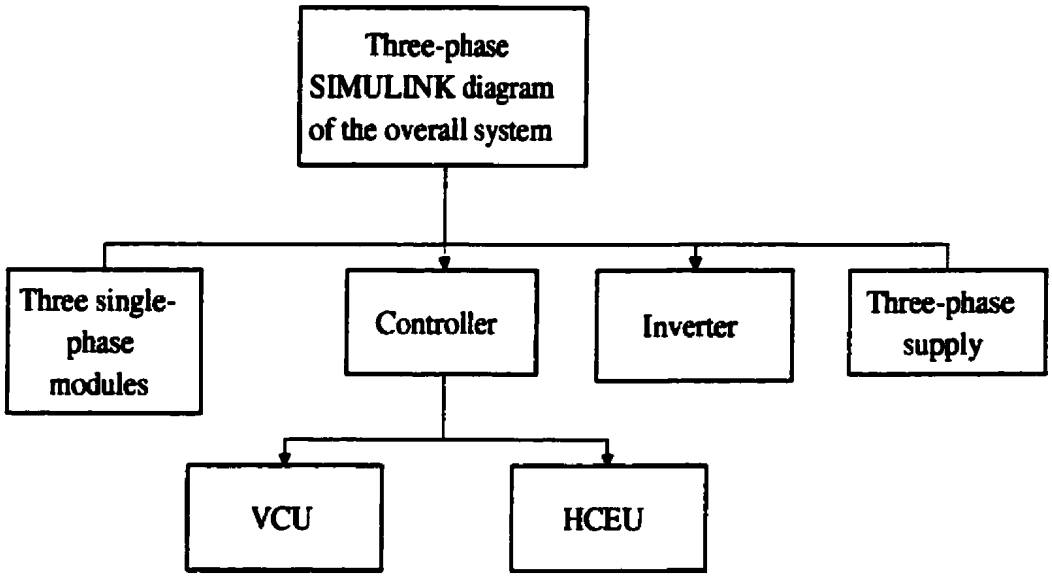

Figure A.1: Chart showing the top-down modularity of the SIMULINK blocks

A.1 Simulink Model of the Overall System

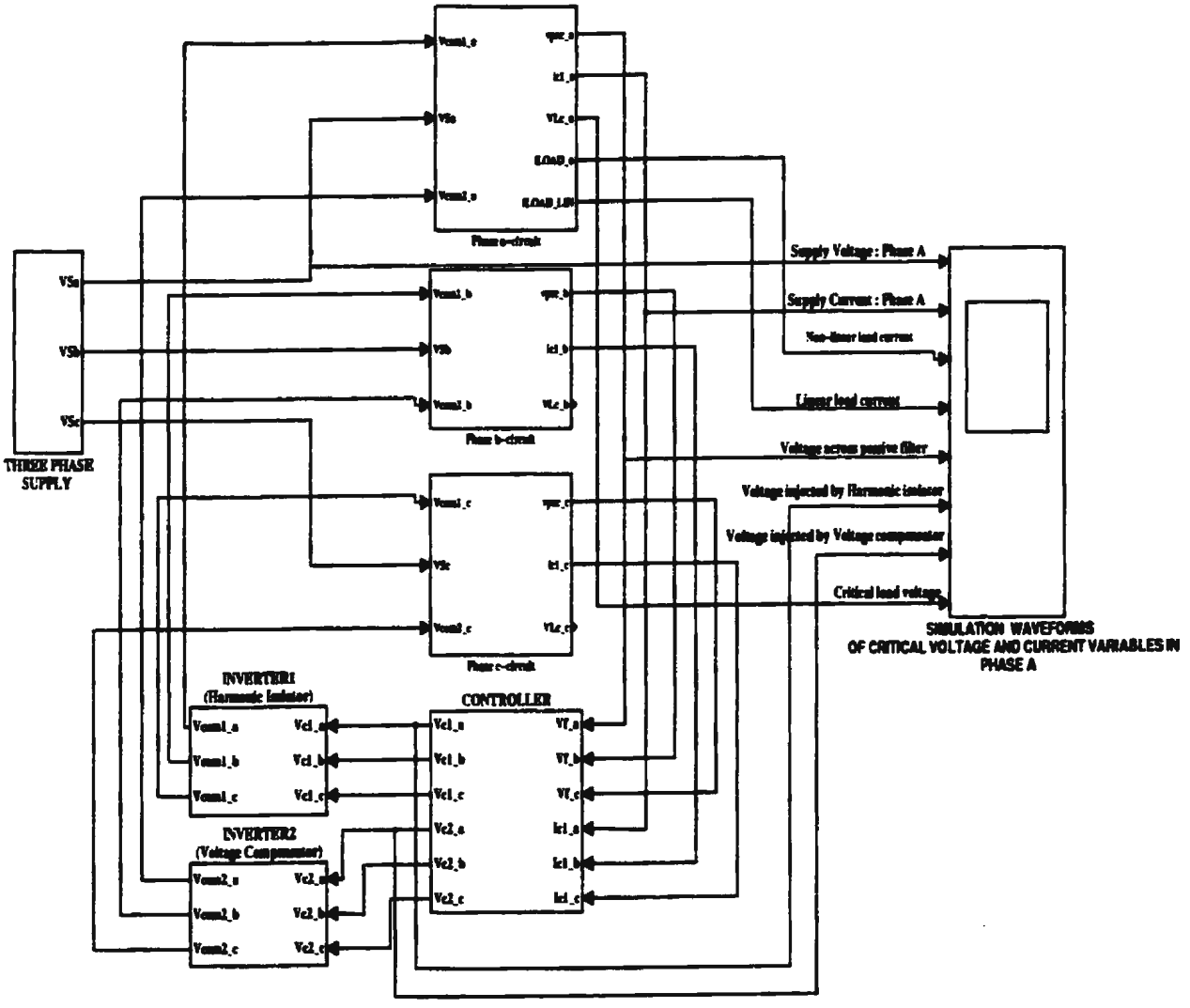

Figure A.2: Simulink model of the overall system

A.1.1 Controller

The Simulink block diagrams of the two control units and their internal compositions are shown in the following figures:

1. Voltage Compensation Unit(VCU)

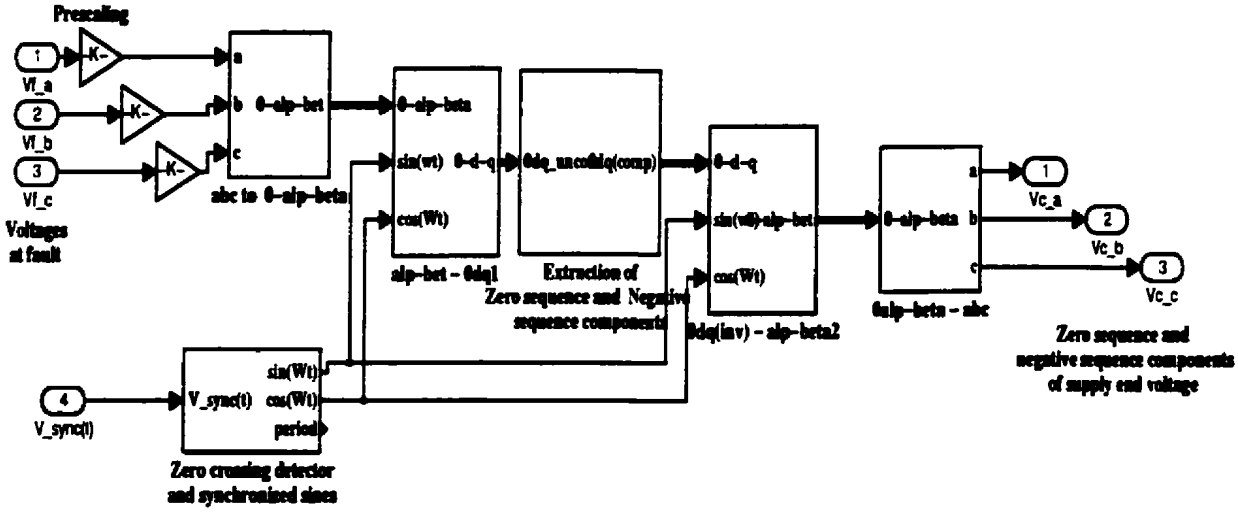

Figure A.3: Simulink diagram of VCU

2. Harmonic Current Extraction Unit(HCEU)

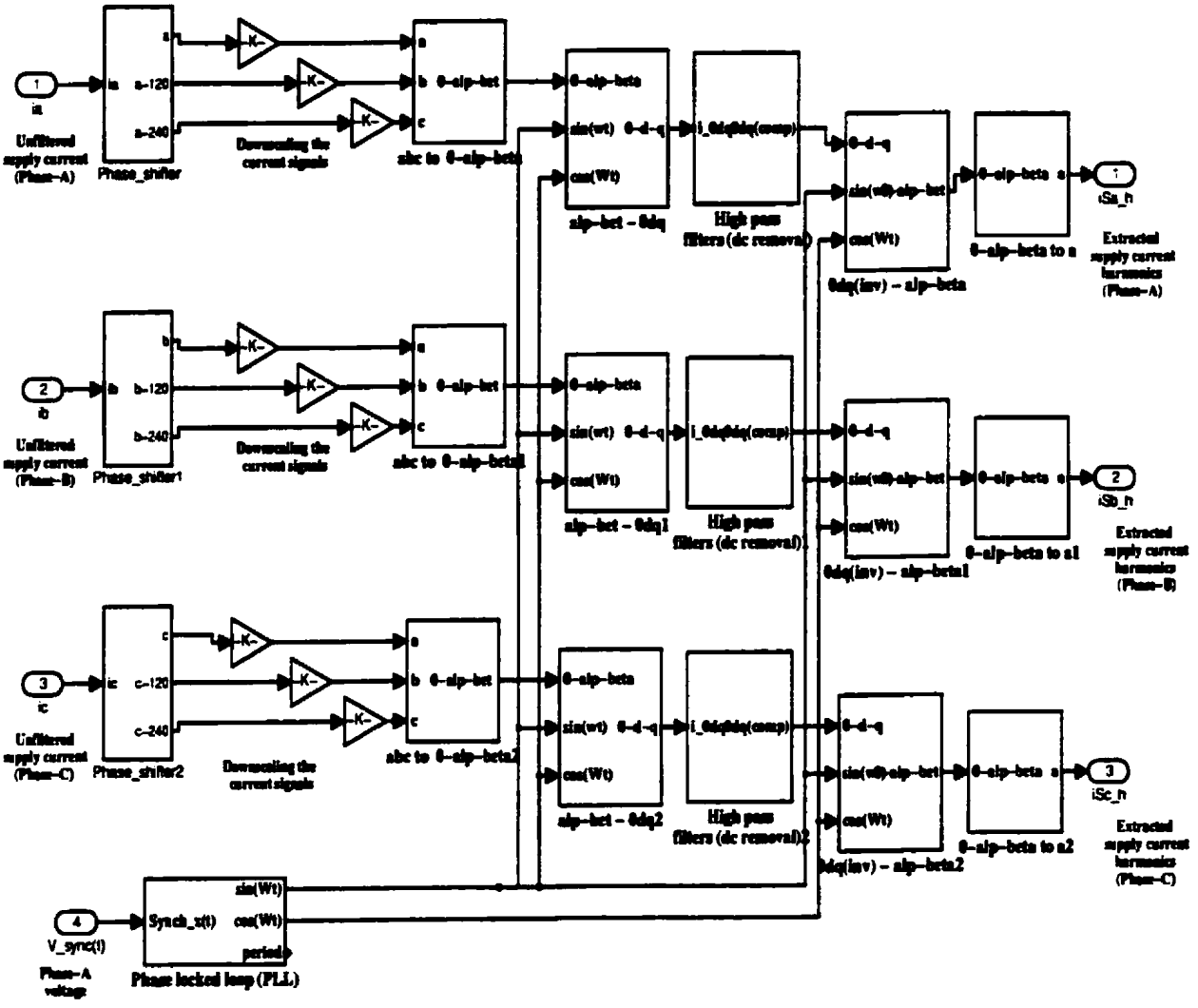

Figure A.4: Simulink diagram of the HCEU

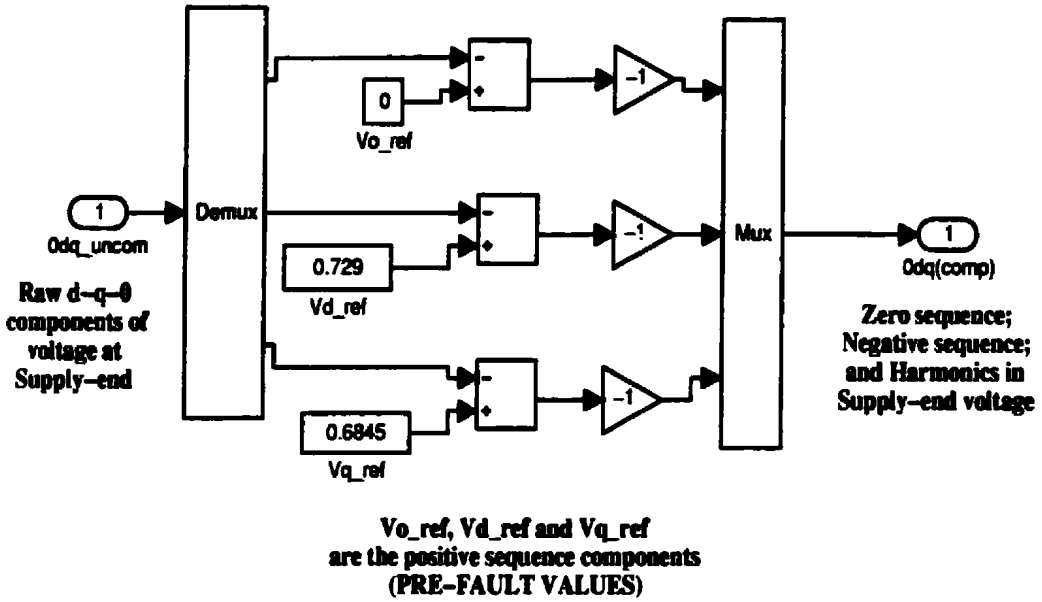

Figure A.5: Block for extracting zero and negative sequence components in the voltages

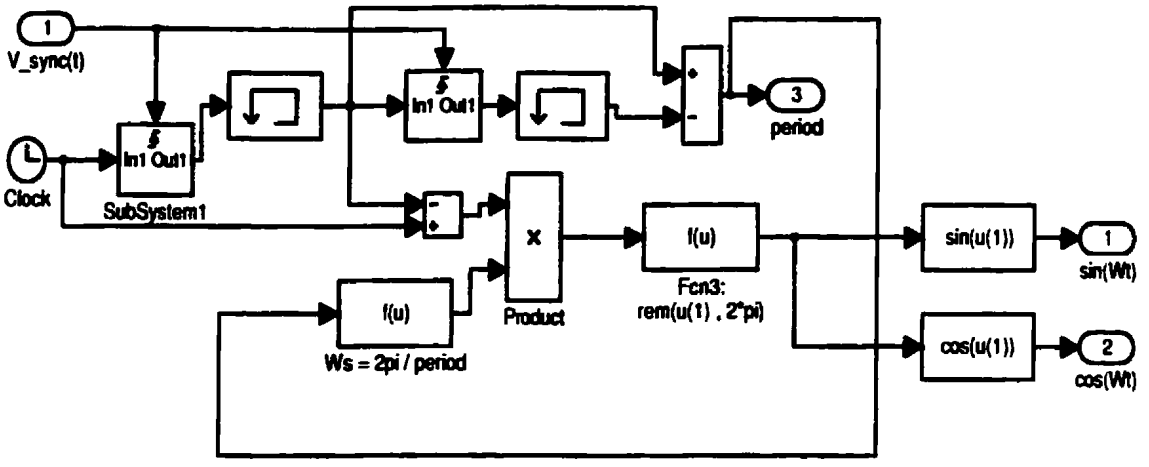

Figure A.6: Phase locked loop block

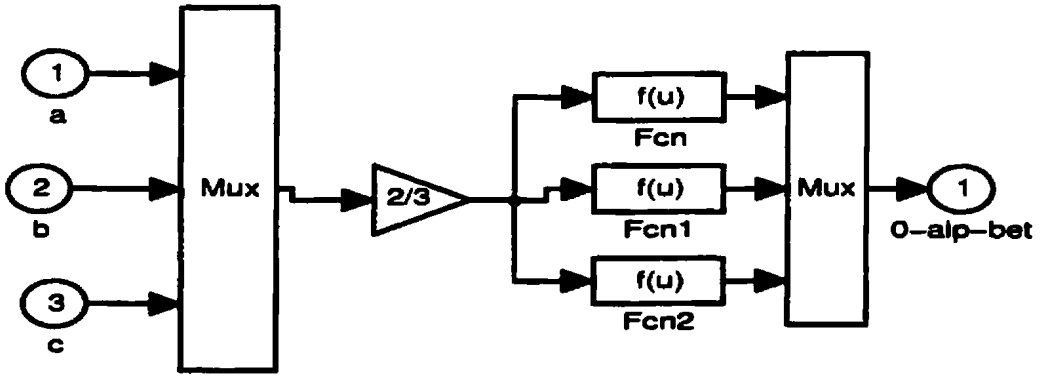

Fcn: **0.5*u(1) + 0.5*u(2) + 0.5*u(3)**
Fcn1: **u(1) -0.5*u(2) - 0.5*u(3)**
Fcn2: **sqrt(3)/2*u(2) - sqrt(3)/2*u(3)**

Figure A.7: Block for the transformation from (a,b,c) to $(0, \alpha, \beta)$

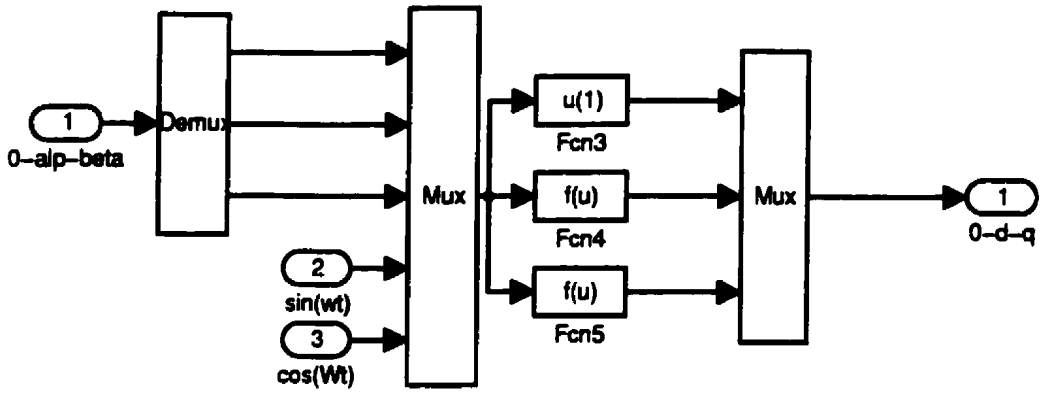

Fcn3: u(1)

Fcn4: u(5)*u(2) + u(4)*u(3)

Fcn5: u(4)*u(2) - u(5)*u(3)

Figure A.8: Block for the transformation from $(0, \alpha, \beta)$ to (0,d,q)

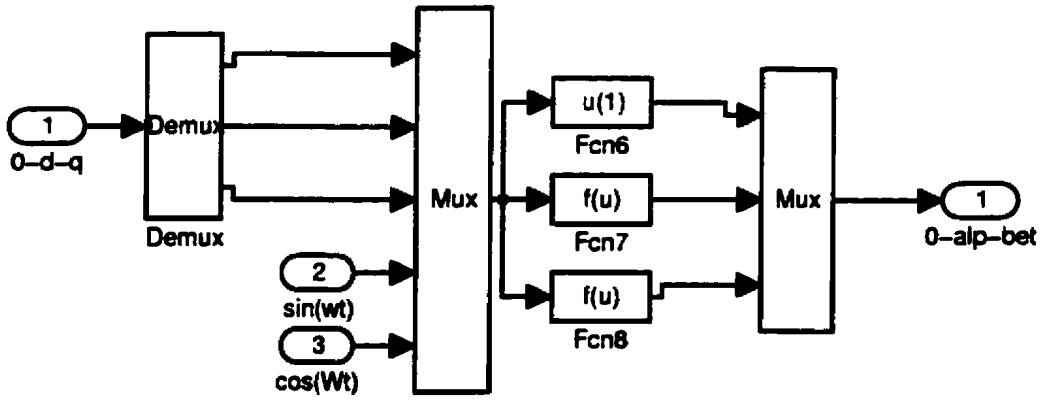

Fcn6 := Fcn3

Fcn7 := Fcn4

Fcn8 := Fcn5

Figure A.9: Block for the transformation from (0,d,q) to $(0, \alpha, \beta)$

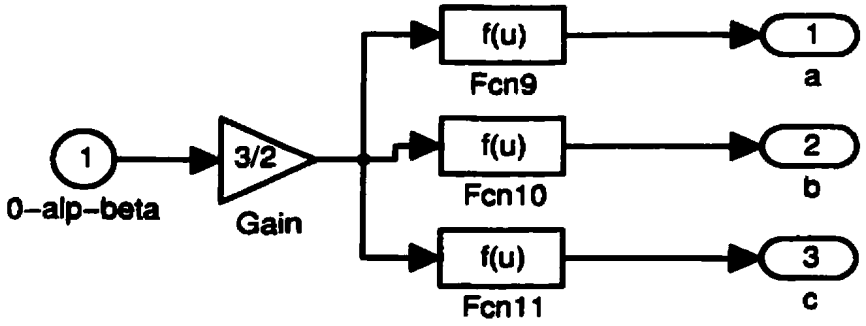

Fcn9: 2/3*u(1) + 2/3*u(2)

Fcn10: 2/3*u(1) - 1/3*u(2) + (1/sqrt(3))*u(3)

Fcn11: 2/3*u(1) - 1/3*u(2) - (1/sqrt(3))*u(3)

Figure A.10: Block for the transformation from $(0, \alpha, \beta)$ to (a,b,c)

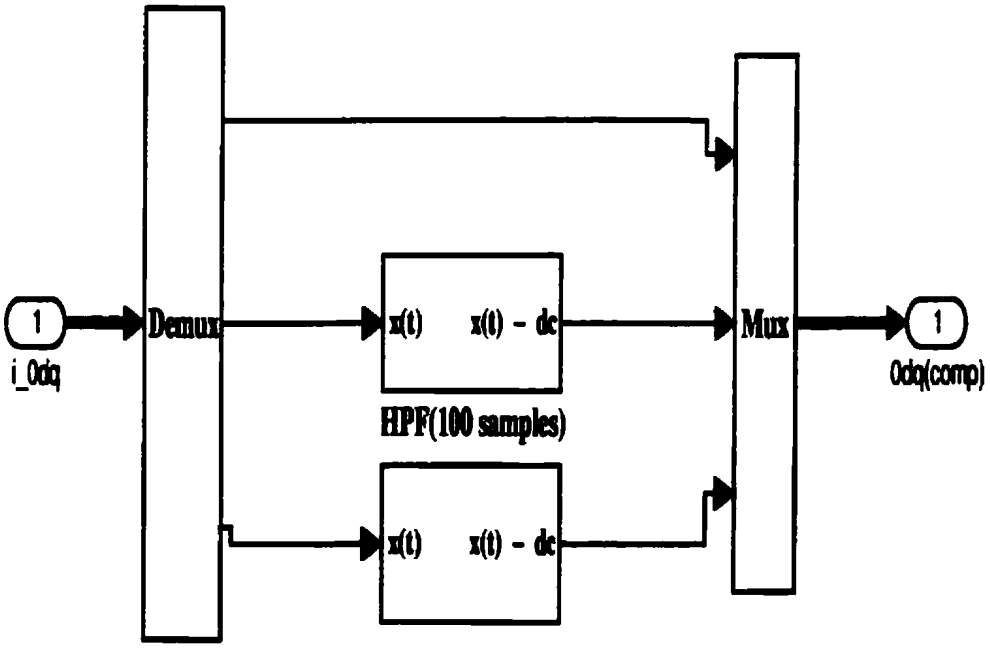

Figure A.11: Block of the filtering unit

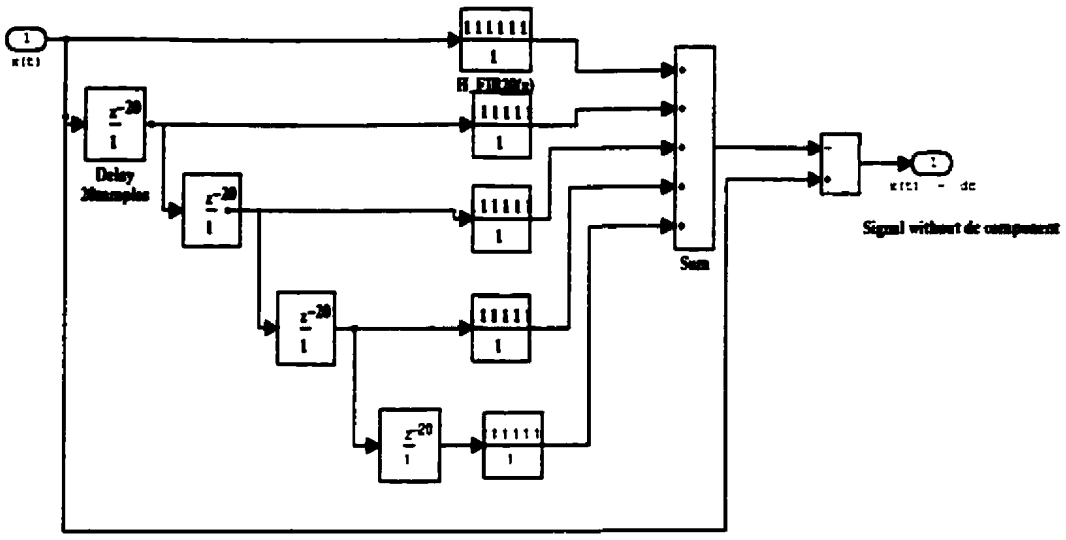

Figure A.12: Block of the high pass filter

A.1.2 Three single-phase modules

The three-phase circuit is constructed using three identical single-phase modules. Due to the similarity in structure, only one single-phase unit (PHASE-A) is shown in Figure A.13. The block inter-connection and their respective transfer functions are based on the signal flow graph developed for the three-phase circuit.

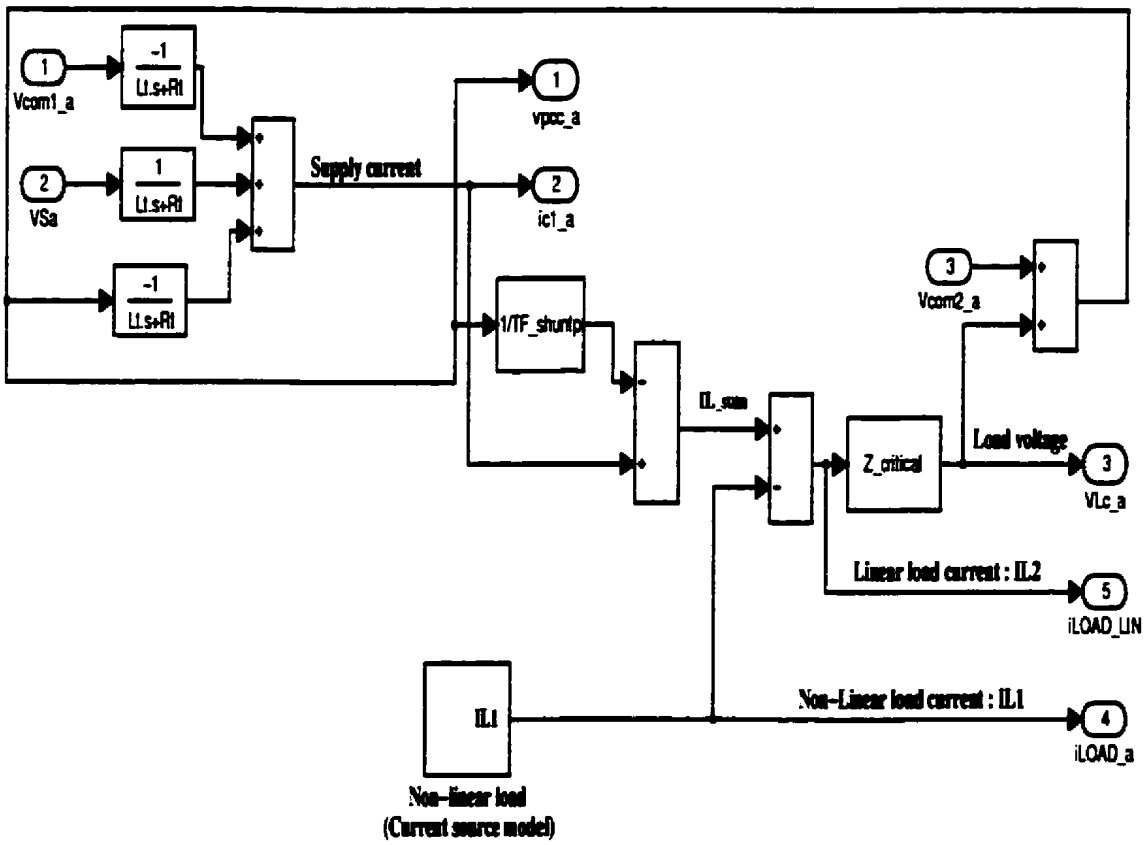

Figure A.13: single-phase module

A.1.3 Three-phase supply

A single-phase sag is introduced in phase-a to simulate an imbalance in the supply voltage. This imbalance in the supply voltage reflects as an imbalance in the load current in the absence of the compensator. A sag of 30% is introduced at a time, t_{sim} = 0.35s using a step function and a multiplier.

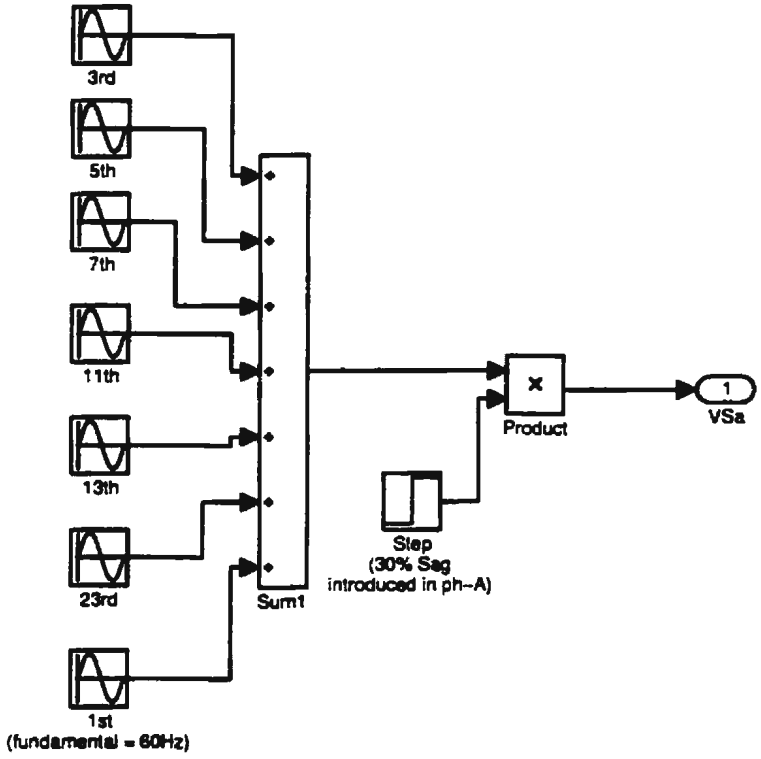

Figure A.14: Supply voltage

A.1.4 Inverter

The inverter is modeled as a gain block.

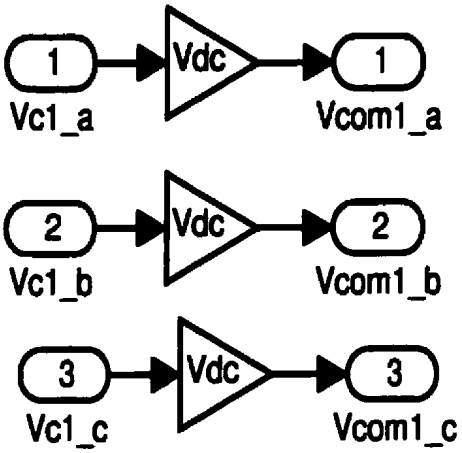

Figure A.15: Inverter block

Appendix B

Matlab Programs

B.1 Matlab Routine for Initialization and Evaluation of Transfer Functions in the Overall Three-phase SIMULINK Model

```
% Program#1

% MATLAB batch program for the three-phaseSIMULINK MODEL (Appendix A.1)

% This Program:

% - Initilizes the controller and system parameters in the

%   SIMULINK model(A.1)

% - Evaluates the transfer funtions for the filter, line and load

%   impedances

 FSUPPLY = 60                          % Supply frequency = 60 Hz

 TSUPPLY = 1/FSUPPLY;

 V_phase_rms = 115.47;

 VPEAK = V_phase_rms * 1.4142;
```

```
 Rt = 0.001;

 Lt = 0.5e-3;

 Zt = tf([Lt,Rt],[.000001,1]);  % Line impedance transfer function

% The SHUNT PASSIVE filter is a parallel combination of

% a 5th harmonic, 7th and a HPF

% Filter Parameters and their transfer functions

% BPF for 5th Harmonic

L5 = 0.82e-3

C5 = 340e-6;

Q5 = 6;

R5 = 1/Q5*sqrt(L5/C5);

TF5 = tf([0,C5,0],[L5*C5,R5*C5,1])

% BPF for 7th Harmonic

L7 = 0.82e-3;

C7 = 170e-6;

Q7 = 6;

R7 = 1/Q7*sqrt(L7/C7);

TF7 = tf([0,C7,0],[L7*C7,R7*C7,1])

% High Pass Filter (for bypassing the higher order harmonics)

LH = 0.26e-3;
```

```
CH = 300e-6;

RH = 2;

TFH = tf([LH*CH,RH*CH,0],[RH*LH*CH,LH,RH])

% Combined Transfer function TF_shuntp = 1/(TF5 + TF7 + TFH)

% Load(Critical) Transfer function

Lc = 2e-3;

Rc = 4;

Z_critical= tf([Lc Rc],[0.00001 1]);

% Equivalent transfer function (load impedance || shunt filter impedance)

ZLeq = Z_critical*TF_shuntp/(Z_critical + TF_shuntp);

% Controller Parameters

Rh = 2.5;        % Gain of HCEU

Kv = 1;          % Gain of VCU

% Derivation of the Transfer function for stability analysis

L1 = -Rh/Zt;

L2 = -ZLeq/Zt;

L3 = Kv;

L4 = -Kv*ZLeq/Zt;

T1 = ZLeq/Zt;

D1 = 1-L3;
```

```
DELTA = 1 -L1-L2-L3-L4 + L2*L3;

TF_VL = (T1*D1)/DELTA;

G1 = Rh/Zt + ZLeq/Zt

% Transformer Parameters

TR = 1;       % Transformer turns ratio

% Filter Parameters (at the output of the inverter)

Lr = 1e-3;

Cr = .33e-6 ;         % For Cr = 100uf, Lr = 100uH Wr = 1/sqrt(Lr*Cr);

                      % Fr = 1.591 kHz Fr = Wr/(2*pi);

                      % Can compensate upto 23rd Harmonic Qr = 20;

TS = TSUPPLY/100;     % Sampling Time

% Supply distortion and nonlinear LOAD specifications

% ( CURRENT SOURCE MODEL)

for i=1:23,

    if  mod(i,2) ~= 0 & mod(i,3) ~= 0

       AMP(i) = (2/pi)*(cos(pi*i/6)/i)*( 1 - (-1)^i);

    end

end;

% Harmonic Voltage magnitudes (Supply voltage distortion)

KL = 0.3;
```

```
Vm = VPEAK;

B1 = AMP(1)*Vm*KL;

B5 = AMP(5)*Vm*KL ;

B7 = AMP(7)*Vm*KL;

B11 = AMP(11)*Vm*KL;

B13 = AMP(13)*Vm*KL;

B17 =AMP(17)*Vm*KL;

B19 = AMP(19)*Vm*KL;

B23 = AMP(23)*Vm*KL;

B3 = Vm/4*KL;

% phases of the supply voltages

pa = 0; pb = -2*pi/3 + pa;  pc = 2*pi/3 + pa;

% LOAD CURRENT HARMONICS

% nonlinear CRITICAL LOAD PARAMETERS

% Modifications on the critical load to account for nonlinearity

% Current source model for critical load % A single-phase bridge

% rectifier feeding a dc motor has been chosen as an % 5th and

% 7th are the dominant harmonics

Im = 50        % Current drawn on dc side of the load

IL_critical_1 = Im*AMP(1);
```

```
IL_critical_7 = Im*AMP(7);

IL_critical_5 = Im*AMP(5);

IL_critical_11= Im*AMP(11);

IL_critical_13= Im*AMP(13);

ph_critical = 0 ;

% Phases of the fundamental components pa_1 = 0 pb_1 = -120 +

pa_1; pc_1 = 120 + pa_1;

% Computation of total harmonic distortion of the supply voltage

% and nonlinear load

THD_supply = sqrt(B3*B3 + B5*B5 + B7*B7 + B11*B11 + B13*B13)/B1

THD_NL_load = sqrt(IL_critical_5^2 + IL_critical_7^2 +

IL_critical_11^2 + IL_critical_13^2)/IL_critical_1
```

B.2 MATLAB Program for Spectral Analysis and Evaluation of THD of some system variables

```
% Program#2

% MATLAB PROGRAM for calculating the FFTs of the SIMULINK waveforms

% The SIMULINK model(Appendix A.1) stores the results (waveform data)

% as a structure WAVEFORMS of two fields TIME and SIGNALS

% The field SIGNALS is an array of 8 sub-structures

% This program:
```

```
% - Extracts a single cycle of waveform information (for FFT computation)
% - The choice of 'start' time is decided based on whether the system has
%   reached steady state operation
% - FFTs of the signals are computed and appropriately scaled
% - Results are plotted
FSUPPLY = 60;
TSUPPLY = 1/FSUPPLY;
t = waveforms.time;              % Extract time vector from SIMULINK model
start = round(length(t)/2);  % Choice is made based on steady state
                                 % operation
N_WAVEFORMS = 8;
for k = 1:N_WAVEFORMS,
    i = 1;
    while (abs(t(start + i) - t(start)) <= TSUPPLY)
       waves(k,i) = waveforms.signals(k).values(start + i);
       i = i + 1;
    end
end
LEN = i-1;          % Number of sample points corresponding to a
                    % single cycle
```

```
freq = 1:LEN/2;
freq = freq -1; % Frequency points on X-axis
for count = 1:N_WAVEFORMS,
    wave_single_cycle = waves(count,1:LEN);       % time domain signal
    V_FFT1 = 2/(LEN)*abs(fft(wave_single_cycle)); % Computation of FFT
    for i = 1:LEN/2,
        V_FFT(i)= V_FFT1(i);  % The first half of the samples
                              % carry the necessary frequency information
                              % The second half is redundant and discarded
    end
    FFTs(count,1:length(V_FFT)) = V_FFT;
end
% Plotting the results
for i=1:N_WAVEFORMS,
    subplot(N_WAVEFORMS,1,i);
    stem(freq,FFTs(i,1:LEN/2));
    grid;
    axis([0 17 0 170]);
end;
xlabel('Harmonic Number - n'); ylabel('FFT');
```

```
% Computation of total harmonic distortions

% Only the odd harmonics are used for FFT computation

THD = zeros(1,5);

for j = 1:4,

    for i = 3:2:23,

        THD(j) = THD(j) + FFTs(j,i+1)*FFTs(j,i+1);

    end

THD(j) = sqrt(THD(j))/FFTs(j,2);

end;

for i = 3:2:19,

    THD(5) = THD(5) + FFTs(8,i+1)*FFTs(8,i+1);

end

THD(5) = sqrt(THD(5))/FFTs(8,2);

Supply_voltage_distortion = THD(1)

Supply_current_distortion = THD(2)

NL_load_distortion = THD(3)

linear_load_distortion = THD(4)

load_voltage_distortion = THD(5)
```

B.3 Matlab Program For Determining The Root Loci For The Two Topologies

```
% Program#3

% This MATLAB program has two parts:

% - Generates root-locus plots for the two topologies

% (SINGLE COMPENSATOR and TWO-COMPENSATOR)

% - The second part generates the stability boundaries for the two

%   topologies based on the critical value of voltage gain Kv for

%   which the system becomes unstable

% The transfer functions are presented in Chapters-4,5 of the thesis

%  System Parameters

 FSUPPLY = 60        % Supply frequency = 60 Hz

 TSUPPLY = 1/FSUPPLY;

 Rt = 0.001;

 Lt = 0.5e-3;

 Zt = tf([Lt,Rt],[.000001,1]);

% The SHUNT PASSIVE filter is a parallel combination of a 5th harmonic

% pass, 7th pass and a HPF

% Filter Parameters and their transfer functions

% BPF for 5th Harmonic
```

```
L5 = 0.82e-3;

C5 = 340e-6;

Q5 = 6;  % (6) (14)

R5 = 1/Q5*sqrt(L5/C5);

TF5 = tf([0,C5,0],[L5*C5,R5*C5,1])

% BPF for 7th Harmonic

L7 = 0.82e-3;

C7 = 170e-6;

Q7 = 6;  % 14

R7 = 1/Q7*sqrt(L7/C7);

TF7 = tf([0,C7,0],[L7*C7,R7*C7,1])

% High Pass Filter

LH = 0.26e-3;

CH = 300e-6;

RH = 2;

TFH = tf([LH*CH,RH*CH,0],[RH*LH*CH,LH,RH])

% Combined Transfer function

TF_shuntp = 1/(TF5 + TF7 + TFH)

% Load(Critical) Transfer function

% Note that Rc = 2 corresponds to 1p.u.
```

```
% Load conditions : 0.5pu, 1pu, 2pu, 4pu

Lc = 1e-3;

Rc = 1;

Z_critical = tf([Lc Rc],[1e-6 1]); % Power Factor

ZLeq = Z_critical*TF_shuntp/(Z_critical + TF_shuntp);

% Controller Parameters

Rh = 2.5;  % Current gain, Nominal = 2.5

Kv = 0.98; % Voltage gain

% Derivation of the Transfer function for stability analysis

L1 = -Rh/Zt;

L2 = -ZLeq/Zt;

T1 = ZLeq/Zt;

L3 = Kv;

L4 = -Kv*ZLeq/Zt;

D1 = 1-L3;

DELTA = 1 -L1-L2-L3-L4 + L2*L3;

TF_VL = (T1*D1)/DELTA;

pole(TF_VL)

% For generating root locus plot : Akagi's scheme

TF_sysplot_akagi = Zt/(Rh + TF_shuntp);
```

```
% Proposed scheme : Two-compensator topology
N1 = 1+(Zt + Rh)/TF_shuntp;
G1 = (Zt + Rh)*TF_shuntp/(Zt + Rh + TF_shuntp);
TF_sysplot_proposed = G1/Z_critical;
K = 0:0.05:2.5;      % Voltage gain Kv, is the controller variable
K = 1-K;
% Based on the type of topology (SINGLE COMPENSATOR OR TWO-COMPENSATOR)
% the appropriate transfer function may be chosen
TF_sysplot = TF_sysplot_proposed;
% TF_sysplot = TF_sysplot_akagi;
rlocus(TF_sysplot,K);
% PART-2
% MATLAB ALGORITHM to determine the stability limits for the
% PROPOSED TWO-COMPENSATOR topology Kv_critical(or KV_MAX) V/S ZLOAD
% - By sweeping Kv over a range [0,3]. The value of Kv, which forces
%   one of the poles to cross over to the Right Half Plane is
%   captured as the critical gain Kv_critical for that particular
%   value of Rh and ZLOAD
% Nominal shunt impendance for the dominant harmonics : 0.1 - 0.3ohms
% for Q = 14 to 6
```

```
% Lt = 0.5mH, Line impedance (0.2ohms for fundamental)
% The load impedance is varied from 0.5 pu to 4pu in steps of 0.1
R_base = 2;
RLOAD = 0.5:0.02:4; % 0.5:0.1:4;
RLOAD = RLOAD * R_base;
% The series resistance is varied from Rh = 3 to Rh = 10
Rh_values = [3,5,7,10];
% For each value of Rh, the system stability is examined for
% Kv ranging from 0-3.
KV = 0:0.1:3;
KV_MAX = zeros(length(Rh_values),length(RLOAD));
Zf = TF_shuntp;
for i = 1:length(Rh_values),
  for j = 1:length(RLOAD),
     % Linear component of the critical load
     Z_critical = tf([Lc RLOAD(j)],[1e-6 1]);  % Load transfer function
     Zeq = Z_critical*Zf/(Z_critical + Zf);
     for m = 1:length(KV),
     % Choose one of the two transfer functions
     TF_proposed =(Z_critical*Zf*(1-KV(m)))/((Rh_values(i)+Zt)*Zf*(1-KV(m))
```

```
                + (Zt + Rh_values(i) + Zf)*Z_critical);
        REAL_POLES = real(pole(TF_proposed));
%%      TF_akagi = Zeq*(1-KV(m))/( Zeq + (1-KV(m))*Zt + Rh_values(i) );
%%      REAL_POLES = real(pole(TF_akagi));
        POLE_TEST = 0;
           for k = 1:length(REAL_POLES),
              if (REAL_POLES(k) > 0),
                 KV_MAX(i,j) =  KV(m);
                 POLE_TEST = 1;
                 break;
              end
           end
           if (POLE_TEST == 1)
              break;
           end
     end
  end
end;
RLOAD = RLOAD/R_base;
% Plotting the results
```

```
for i = 1:length(Rh_values),

    plot(RLOAD, KV_MAX(i,1:length(RLOAD)),'r');

    hold on;

end

grid;

xlabel('ZLOAD (p.u)');

ylabel('Kv_critical (or KV_MAX)');
```

B.4 Program to evaluate the compensator ratings for the two topologies

```
%  Calculation of compensator ratings for both the single and

%  the two-compensator topologies using the single-phase

%  equivalent models described in chapters 4 and 5.

%    System Parameters

Vs = 200/sqrt(3);

FSUPPLY = 60        % Supply frequency = 50 Hz

Ws = 2*pi*60;

TSUPPLY = 1/FSUPPLY;

Rt = 0.001;

Lt = 0.5e-3;

% BPF for 5th Harmonic
```

```
L5 = 0.82e-3;

C5 = 340e-6;

Q5 = 20;  % 14

R5 = 1/Q5*sqrt(L5/C5);

ZF(5) = R5 + j*(5*Ws*L5 - 1/(5*Ws*C5));

% BPF for 7th Harmonic

L7 = 0.82e-3;

C7 = 170e-6;

Q7 = 10;  % 14

R7 = 1/Q7*sqrt(L7/C7);

ZF(7) = R7 + j*(7*Ws*L7 - 1/(7*Ws*C7));

% Load(Critical) Transfer function

L = 1e-4;

RL = 5;

rating_linear = Vs^2/RL;

%% Controller parameters: Rh = 5, Kv = 0.95

Rh = 2.5; Kv = 0.8; % 0.8;

rating = 7000 + rating_linear

% Current source load 7kVA

IL1 = (7000 + rating_linear)/Vs;
```

```
VSH(5) = 0.05*Vs;

VSH(7) = 0.04*Vs;

ILH(5) = 20;

ILH(7) = 15;

K = 0:0.05:6;

SINGLE_RATING = zeros(1,length(K));

TWO_RATING = zeros(1,length(K));

HARMONIC_I = zeros(1,length(K));

HARMONIC_V = zeros(1,length(K));

RATING_C2 = zeros(1,length(K));

RATING_C1 = zeros(1,length(K));

PRODUCT = zeros(1,length(K));

% Compensator ratings for a single compensator topology

for p = 1:length(K),

Rh = K(p);

% Harmonic equivalent circuit model described in Chapter 4

for n=5:2:7,

    ZL(n)  = RL + j*Ws*n*L;

    ZT(n)  = Rt + j*Ws*n*Lt;

    G11(n) = ZF(n)*ZL(n)*(1-Kv)/( (1-Kv)*ZT(n)*(ZF(n) + ZL(n)) +
```

```
            Rh*(ZF(n) + ZL(n)) + ZF(n)*ZL(n));

    G12(n) = -ZF(n)*ZL(n)*( (1-Kv)*ZT(n) + Rh )/( (1-Kv)*ZT(n)*(ZF(n)

            + ZL(n)) + Rh*(ZF(n) + ZL(n)) + ZF(n)*ZL(n));

    VLH(n) = G11(n)*VSH(n) + G12(n)*ILH(n);

    ISH(n) = VLH(n)*(1/ZF(n) + 1/ZL(n)) + ILH(n);

    VFH(n) = VSH(n) - ISH(n)*ZT(n);

    VCH(n) = Rh*ISH(n) + Kv*VFH(n);

    IL_TOT_H(n) = ILH(n)+ VLH(n)/ZL(n); % Load generated harmonics

    HDF(n) = 1-(ZF(n) + ZL(n))*( (1-Kv)*ZT(n) + Rh )/( (1-Kv)*ZT(n)*(ZF(n)

            + ZL(n)) + Rh*(ZF(n) + ZL(n)) + ZF(n)*ZL(n));

end;

VC_harmonics = sqrt(abs(VCH(5)^2) + abs(VCH(7)^2));

VC_sag = 0.3*Vs*Kv;

VCmax = sqrt(VC_sag^2 + VC_harmonics^2);

IS_harmonics = sqrt(abs(ISH(5)^2) + abs(ISH(7)^2));

IL_harmonics = sqrt(abs(IL_TOT_H(5)^2) + abs(IL_TOT_H(7)^2));

harm_dis_fact = sqrt(abs(HDF(5)*IL_TOT_H(5))^2 + abs(HDF(7)*IL_TOT_H(7))^2)/IL_

VL_harmonics = sqrt(abs(VLH(5)^2) + abs(VLH(7)^2));

ICmax = sqrt(IL1^2 + IS_harmonics^2);

IS_singlecomp = ICmax;
```

```
KVA_rating_single_comp = VCmax*ICmax;

SINGLE_RATING(p) = KVA_rating_single_comp;

HARMONIC_I(p) = harm_dis_fact;

HARMONIC_V(p) = VL_harmonics;

end % Kv loop ends here

subplot(3,1,1);

plot(K,SINGLE_RATING);

grid on;

hold on;

subplot(3,1,2);

plot(K,HARMONIC_I*100);

grid on;

hold on;

subplot(3,1,3);

plot(K,HARMONIC_V/Vs*100);

grid on;

hold on;

% Compensator ratings for a two-compensator topology

Rh = 2.5; Kv = 0.99; Kv1 = 0.0;

for i = 1:length(K),
```

```
Rh = K(i);
% Harmonic equivalent circuit model described in Chapter 5
for n=5:2:7,
    ZL(n)  = RL + j*Ws*n*L;
    ZT(n)  = Rt + j*Ws*n*Lt;
    G1(n) = ZF(n)*ZL(n)*(1-Kv)/( ((1-Kv1)*ZT(n) + Rh)*(1-Kv)*ZF(n) +
            ((1-Kv1)*ZT(n) + ZF(n) + Rh)*ZL(n) );
    G2(n) = -ZL(n)*ZF(n)*((1-Kv1)*ZT(n) + Rh)*(1-Kv)/(ZL(n)*(ZF(n) +
            (1-Kv1)*ZT(n) + Rh) + (1-Kv)*ZF(n)*((1-Kv1)*ZT(n) + Rh));
    VLH(n) = G1(n)*(1-Kv1)*VSH(n) + G2(n)*ILH(n);
    ISH(n) = ILH(n) + VLH(n)/ZL(n) + VLH(n)/((1-Kv)*ZF(n));
    VFH(n) = VSH(n) - ISH(n)*ZT(n);
    IL_TOT_H(n) = VLH(n)/ZL(n) + ILH(n);
    HDF(n) = 1 - ((ZL(n) + (1-Kv)*ZF(n))*((1-Kv1)*ZT(n) + Rh))/(ZL(n)*(ZF(n)
             + (1-Kv1)*ZT(n) + Rh) + (1-Kv)*ZF(n)*((1-Kv1)*ZT(n) + Rh));
    VC2H(n) = Kv*(ISH(n) - IL_TOT_H(n))*ZF(n);
    VC1H(n) = Rh*ISH(n) + Kv1*VFH(n);
end;
VC1_harmonics = sqrt(abs(VC1H(5)^2) + abs(VC1H(7)^2));
VC2_harmonics = sqrt(abs(VC2H(5)^2) + abs(VC2H(7)^2));
```

```
VC_sag2 = 0.3*Vs*Kv;

VC_sag1 = 0.3*Vs*Kv1;

VC2max = sqrt(VC_sag2^2 + VC2_harmonics^2);

VC1max = sqrt(VC_sag1^2 + VC1_harmonics^2);

IS_harmonics = sqrt(abs(ISH(5)^2) + abs(ISH(7)^2));

VL_harmonics = sqrt(abs(VLH(5)^2) + abs(VLH(7)^2));

IL_harmonics = sqrt(abs(IL_TOT_H(5)^2) + abs(IL_TOT_H(7)^2));

harm_dis_fact = sqrt(abs(HDF(5)*IL_TOT_H(5))^2 + abs(HDF(7)*IL_TOT_H(7))^2)

                /IL_harmonics;

IC2max = sqrt(IL1^2 + IL_harmonics^2);

IC1max = sqrt(IL1^2 + IS_harmonics^2);

KVA_comp2 = VC2max*IC2max;

KVA_comp1 = VC1max*IC1max

KVA_rating_two_comp = KVA_comp1 + KVA_comp2

TWO_RATING(i) = KVA_rating_two_comp;

RATING_C1(i) = KVA_comp1;

RATING_C2(i) = KVA_comp2;

HARMONIC_I(i) = harm_dis_fact;

HARMONIC_V(i) = VL_harmonics;

end; % Rh loop ends here
```

Appendix C

Additional Results and Discussions

C.1 Effects of Phase Shift Errors on Compensation

In the VCU, the choice of reference voltages play a very crucial role. For a positive voltage sequence, the reference voltage for the zero sequence is zero, while the reference voltages for the d and q axes are constants. There are numerous d-q values which correspond to a nominal peak voltage $V_{L_{peak}}$. If the voltages at the faulted end are synchronized with the compensator voltages, the range of compensation is maximized. What this means is that for a symmetric sag of 30% and no phase imbalance, the maximum compensator voltage that is injected is 0.3p.u. If the voltages are not synchronized for some reason, a 20% sag may require a compensation voltage of 0.3p.u. When there is no phase imbalance, synchronizing the PLL in the control unit with one of the phase voltages (say phase-a) and setting the d-q-0 reference set appropriately serves in synchronizing the voltages at the faulted end with the compensator voltages. In cases where an imbalance in magnitude is followed by an imbalance in

phase, synchronization becomes difficult. The finite delays of the filters, sensors and the latency time of control algorithm also contribute to synchronization errors. In such a case, the choice of d-q-0 reference coefficients is best made based on pre-fault values.

C.2 Additional Simulation Results and Discussions

The nominal gain parameter set chosen in Chapter-6, was $R_h = 2.5$ and $K_V = 1$. However, the supply current distortion is still significant (around 7%). Increasing the value of R_h for a unity K_V leads to system instability. However a value of K_V smaller than unity gives rise to a compensation error due to sags and swells. The effect of increasing R_h and K_V is illustrated through four sets of gain values shown in Table C.1.

Table C.1: Table showing effect of controller gain parameters on current distortion and compensation error (E_r)

Test cases	I_{S_h} [%]	E_r [%]
1) $K_V = 0.3$, $R_h = 3.5$	5.6	22
2) $K_V = 0.0$, $R_h = 5.0$	3.5	30
3) $K_V = 0.3$, $R_h = 2.5$	6.9	23
4) $K_V = 0.7$, $R_h = 2.5$	7.4	12

The compensation error (E_r) is defined as

$$E_r = \frac{V_{L_{nom}} - V_{L_1}}{V_{L_{nom}}} \tag{C.1}$$

where $V_{L_{nom}}$ is the nominal load voltage, measured under pre-fault conditions. The

percentage sag introduced in the simulation is 30%. From the above table, the compensation error for $K_V = 0$ is 30% and the error decreases with increasing K_V. Cases 3 and 4 in Table C.1 along with Figs C.3 and C.4 support the previous statement.

It can be inferred from the results for cases 1 and 2, that the THD of the supply current decreases with increasing R_h. This is shown in Figs C.1 and C.2.

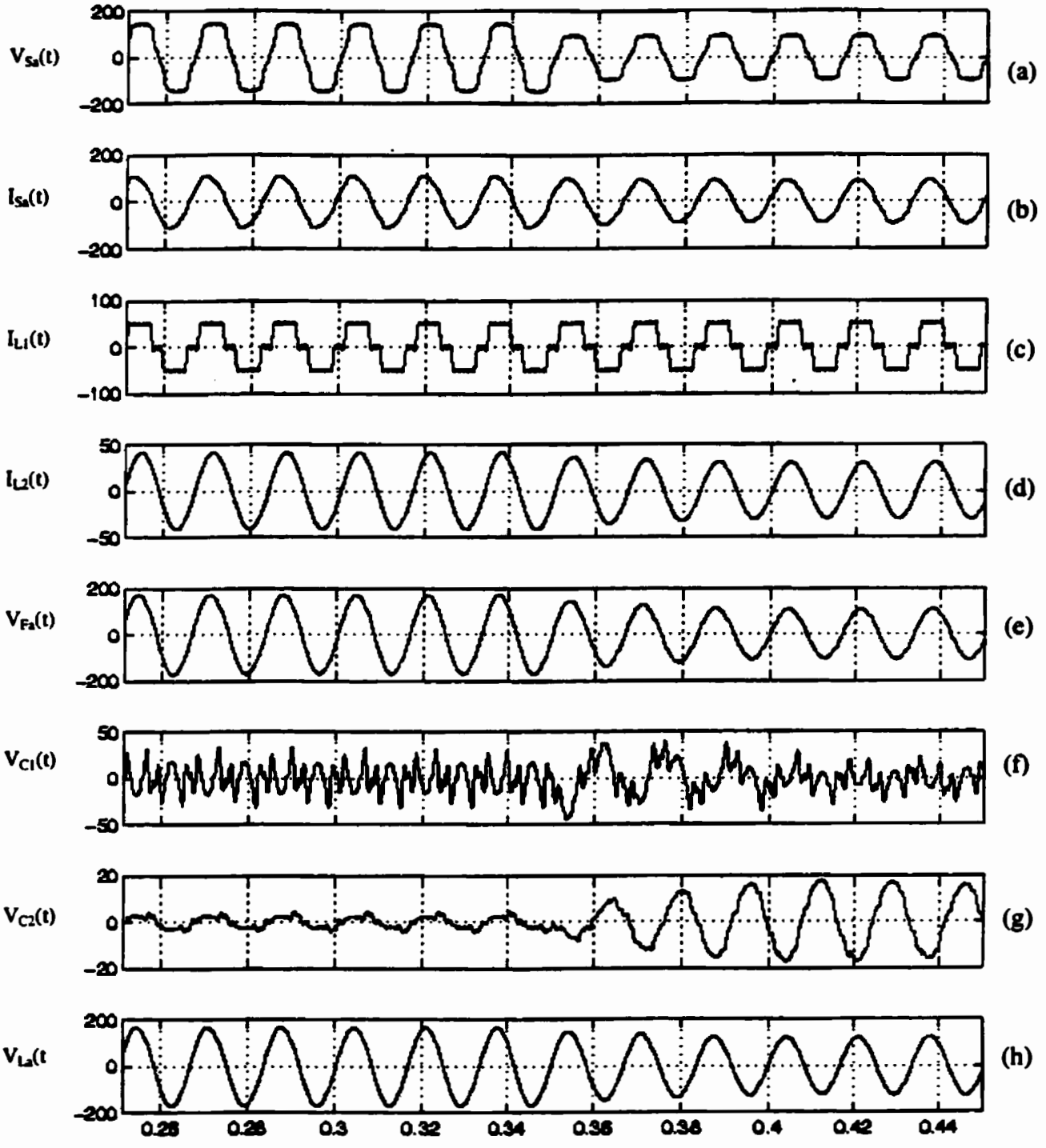

Figure C.1: Simulation waveforms for ($K_V = 0.3$, $R_h = 3.5$).
(a) Supply voltage (phase-a); (b) Supply current, $I_{Sa}(t)$; (c) Non-linear load (L1) current, $I_{L1}(t)$; (d) Linear load (L2) current; (e) Voltage across passive filter; (f) Voltage injected by harmonic isolator (COM1); (g) Voltage injected by COM2; (h) Terminal load voltage, $V_{La}(t)$

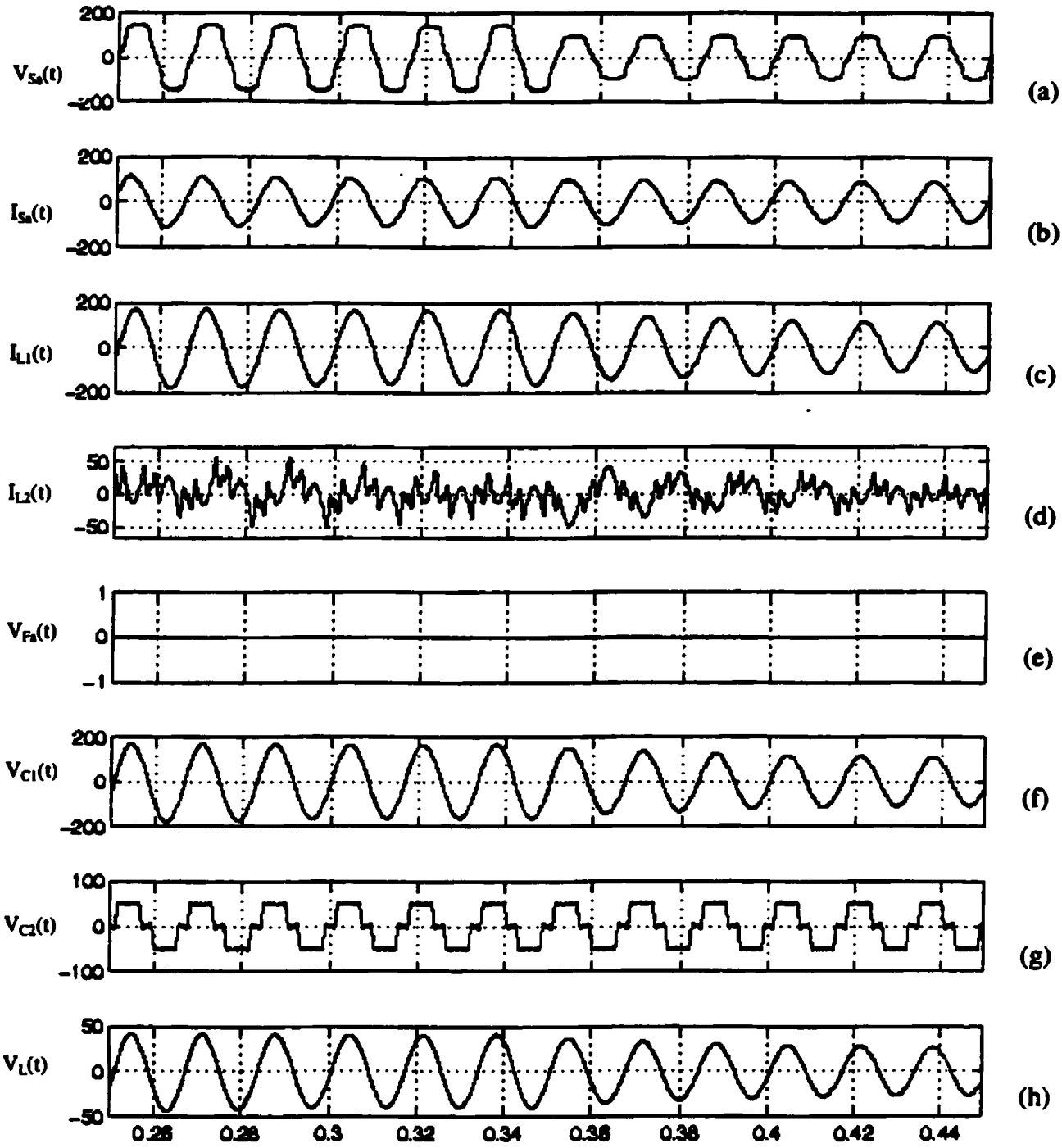

Figure C.2: Simulation waveforms for ($K_V = 0$, $R_h = 5$).
(a) Supply voltage (phase-a); (b) Supply current, $I_{Sa}(t)$; (c) Non-linear load (L1) current, $I_{L1}(t)$; (d) Linear load (L2) current; (e) Voltage across passive filter; (f) Voltage injected by harmonic isolator (COM1); (g) Voltage injected by COM2; (h) Terminal load voltage, $V_{La}(t)$

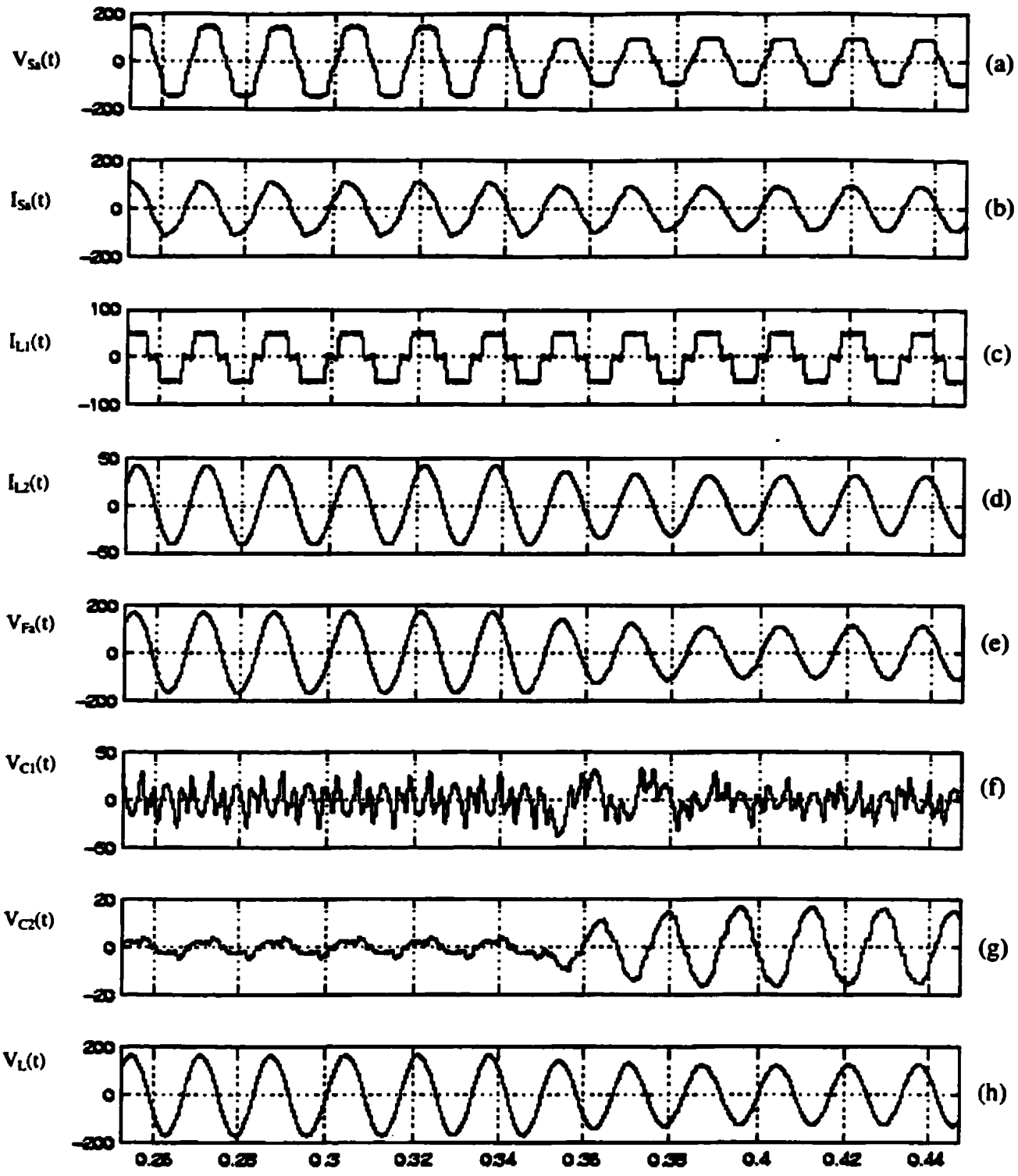

Figure C.3: Simulation waveforms for ($K_V = 0.3$, $R_h = 2.5$).
(a) Supply voltage (phase-a); (b) Supply current, $I_{Sa}(t)$; (c) Non-linear load (L1) current, $I_{L1}(t)$; (d) Linear load (L2) current; (e) Voltage across passive filter; (f) Voltage injected by harmonic isolator (COM1); (g) Voltage injected by COM2; (h) Terminal load voltage, $V_{La}(t)$

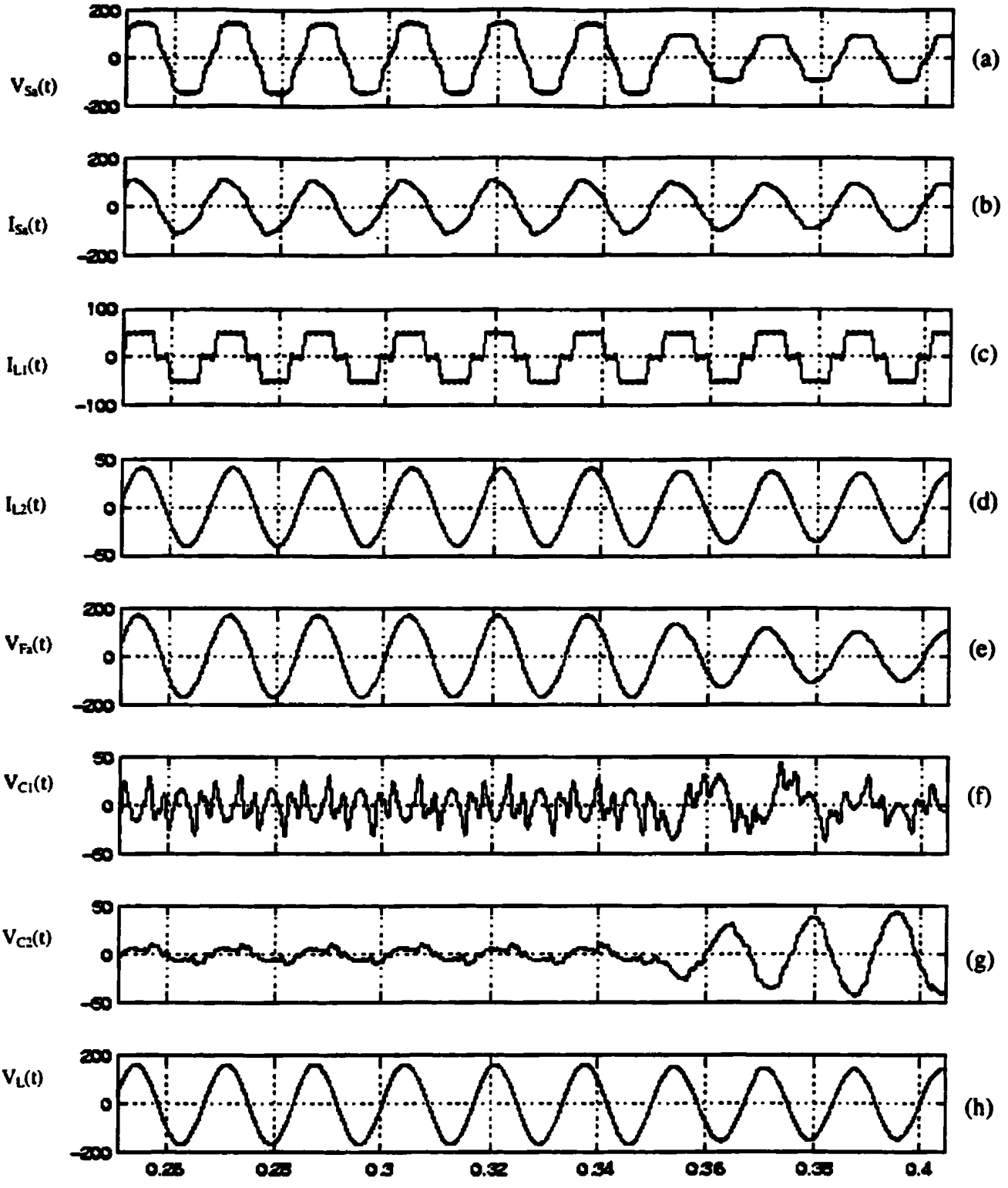

Figure C.4: Simulation waveforms for ($K_V = 0.7$, $R_h = 2.5$).
(a) Supply voltage (phase-a); (b) Supply current, $I_{Sa}(t)$; (c) Non-linear load (L1) current, $I_{L1}(t)$; (d) Linear load (L2) current; (e) Voltage across passive filter; (f) Voltage injected by harmonic isolator (COM1); (g) Voltage injected by COM2; (h) Terminal load voltage, $V_{La}(t)$